C.3

SAND94-1884
Printed December 1994

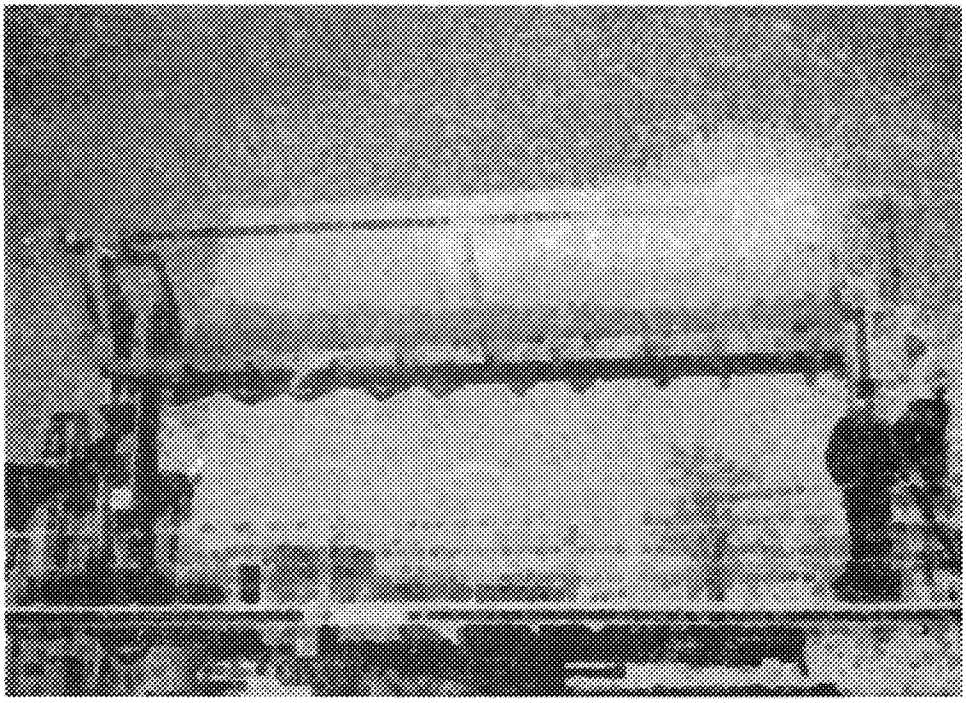

Test Results

SEGS LS-2 Solar Collector

Vernon E. Dudley
EG&G Special Projects
Albuquerque, New Mexico 87119

Gregory J. Kolb
A. Roderick Mahoney
Thomas R. Mancini
Chauncey W. Matthews
Sandia National Laboratories
Albuquerque, New Mexico 87185

Michael Sloan
Sloan Solar Engineering
Austin, Texas 78756

David Kearney
Kearney and Associates
Del Mar, California 92014

Distribution
Categories UC-1302, 1303

Issued by Sandia National Laboratories, operated for the United States Department of Energy by Sandia Corporation.

Available to DOE and DOE contractors from
Office of Scientific and Technical Information
PO Box 62
Oak Ridge, TN 37831

Prices available from (615) 576-8401, FTS 626-8401

Available to the public from
National Technical Information Service
US Department of Commerce
5285 Port Royal Rd
Springfield, VA 22161

NTIS price codes
Printed copy: A16
Microfiche copy: A01

SAND94-1884
Unlimited Release
Printed December 1994

Distribution
Categories UC-1302, 1303

Test Results

SEGS LS-2 Solar Collector

Vernon E. Dudley
E G & G Special Projects
Albuquerque, New Mexico 87119

Gregory J. Kolb
A. Roderick Mahoney
Thomas R. Mancini
Chauncey W. Matthews
Sandia National Laboratories
Albuquerque, New Mexico 87185

Michael Sloan
Sloan Solar Engineering
Austin, Texas 78756

David Kearney
Kearney and Associates
Del Mar, California 92014

ABSTRACT

A SEGS LS-2 parabolic trough solar collector was tested to determine the collector efficiency and thermal losses with two types of receiver selective coatings, combined with three different receiver configurations: glass envelope with either vacuum or air in the receiver annulus, and glass envelope removed from the receiver. As expected, collector performance was significantly affected by each variation in receiver configuration. Performance decreased when the cermet selective coating was changed to a black chrome coating, and progressively degraded as air was introduced into the vacuum annulus, and again when the glass envelope was removed from the receiver. For each receiver configuration, performance equations were derived relating collector efficiency and thermal losses to the operating temperature. For the bare receiver (no glass envelope) efficiency and thermal losses are shown as a function of wind speed. An incident angle modifier equation was also developed for each receiver case. Finally, equations were derived showing collector performance as a function of input insolation value, incident angle, and operating temperature. Results from the experiments were compared with predictions from a one-dimensional analytical model of the solar receiver. Differences between the model and experiment were generally within the band of experimental uncertainty.

H. Price

SAND94-1884
Unlimited Release
Printed December 1994

Distribution
Categories UC-1302, 1303

Test Results

SEGS LS-2 Solar Collector

Vernon E. Dudley
E G & G Special Projects
Albuquerque, New Mexico 87119

Gregory J. Kolb
A. Roderick Mahoney
Thomas R. Mancini
Chauncey W. Matthews
Sandia National Laboratories
Albuquerque, New Mexico 87185

Michael Sloan
Sloan Solar Engineering
Austin, Texas 78756

David Kearney
Kearney and Associates
Del Mar, California 92014

ABSTRACT

A SEGS LS-2 parabolic trough solar collector was tested to determine the collector efficiency and thermal losses with two types of receiver selective coatings, combined with three different receiver configurations: glass envelope with either vacuum or air in the receiver annulus, and glass envelope removed from the receiver. As expected, collector performance was significantly affected by each variation in receiver configuration. Performance decreased when the cermet selective coating was changed to a black chrome coating, and progressively degraded as air was introduced into the vacuum annulus, and again when the glass envelope was removed from the receiver. For each receiver configuration, performance equations were derived relating collector efficiency and thermal losses to the operating temperature. For the bare receiver (no glass envelope) efficiency and thermal losses are shown as a function of wind speed. An incident angle modifier equation was also developed for each receiver case. Finally, equations were derived showing collector performance as a function of input insolation value, incident angle, and operating temperature. Results from the experiments were compared with predictions from a one-dimensional analytical model of the solar receiver. Differences between the model and experiment were generally within the band of experimental uncertainty.

ACKNOWLEDGEMENTS

The authors would like to thank several individuals who helped on this project. Construction and test support were provided by Gilbert Cohen and Harvey Stephens from KJC Operating Company, as well as John Kelton and Al Heckes from Sandia. We also appreciate the review comments we received from Lindsey Evans (Ewing) and Frank Lippke (ZSW, Germany).

TABLE OF CONTENTS

FIGURES

Testing of SEGS LS-2 Parabolic Solar Collector

Introduction

The Sandia National Laboratories and the KJC Operating Company are involved in a cost-shared program to identify various means of reducing operating and maintenance (O&M) costs for solar thermal power plants. As a part of this program, KJC provided Sandia a module of the SEGS LS-2 parabolic trough concentrator for thermal testing. The purpose of the testing was to gain a thorough understanding of the efficiency of the collector given a variety of operating conditions. This information could then be used in studies by the O&M staffs at Solar Electric Generating System (SEGS) plants to help them optimize operation of the plants.

The LS-2 collector is one of three generations of parabolic troughs installed in the nine SEGS built by LUZ in the desert near Barstow, CA. The LS-2 design accounts for about 65% of the collectors installed. Together, the nine SEGS plants produce 354 MW of electric power; more than 90% of the world's grid-connected solar generating capacity. Total installed LS-2 mirror aperture is more than a million sq. meters. The SEGS plants use large fields of SEGS parabolic trough collectors to supply thermal energy to boilers producing steam to drive a conventional Rankine steam turbine/generator system. Figure 1 is a view of the SEGS solar plants at Kramer Junction, CA.

The LS-2 module tested at Sandia was the smallest portion of the complete solar collector assembly (SCA) that could be operated independently, and was also the largest piece that could be installed on the rotating test platform. As tested, the mirror aperture was 5 m and the length was 7.8 m. A complete LS-2 SCA consists of six collector modules and is 49 m long. Two different receiver selective coatings - black chrome and cermet - were tested. Both types are currently in use at the SEGS plants. Figure 2 shows the LS-2 collector as installed on the rotating platform at Sandia for test.

The solar collector receivers, known as heat collection elements (HCEs, Figure 3), were tested in three configurations: with vacuum in the annulus between the receiver surface and the glass envelope, with air in the annulus, and with the glass envelope completely removed. The design of the HCE calls for the vacuum level to be 10^{-4} torr. At this level, convective heat losses are essentially eliminated. However, due to a variety of mishaps during operation, the vacuum can be lost or the glass envelope can be broken. KJC wanted to quantify how much collection efficiency degraded given these mishaps to help them decide when it became cost-effective to replace a degraded HCE.

Selective surface coatings are used on the HCEs because they provide a high absorptivity (about 95%) for incoming light from the sun, while reducing (by 10-20%) the infrared heat emitted by the hot receiver surfaces. For comparison, common black paint might have an absorptivity near 90%, but would also have an emissivity of 90%. Cermet is a graded ceramic/metal selective surface coating applied to the steel receiver tube by a vacuum sputtering process. Black chrome selective coatings have been used for a number of years on both concentrating and non-concentrating solar collectors. The coating is applied by an elecroplating process, which must be very carefully done for a reasonable coating lifetime. Black chrome is also limited to lower maximum operating temperatures than those possible with cermet coatings.

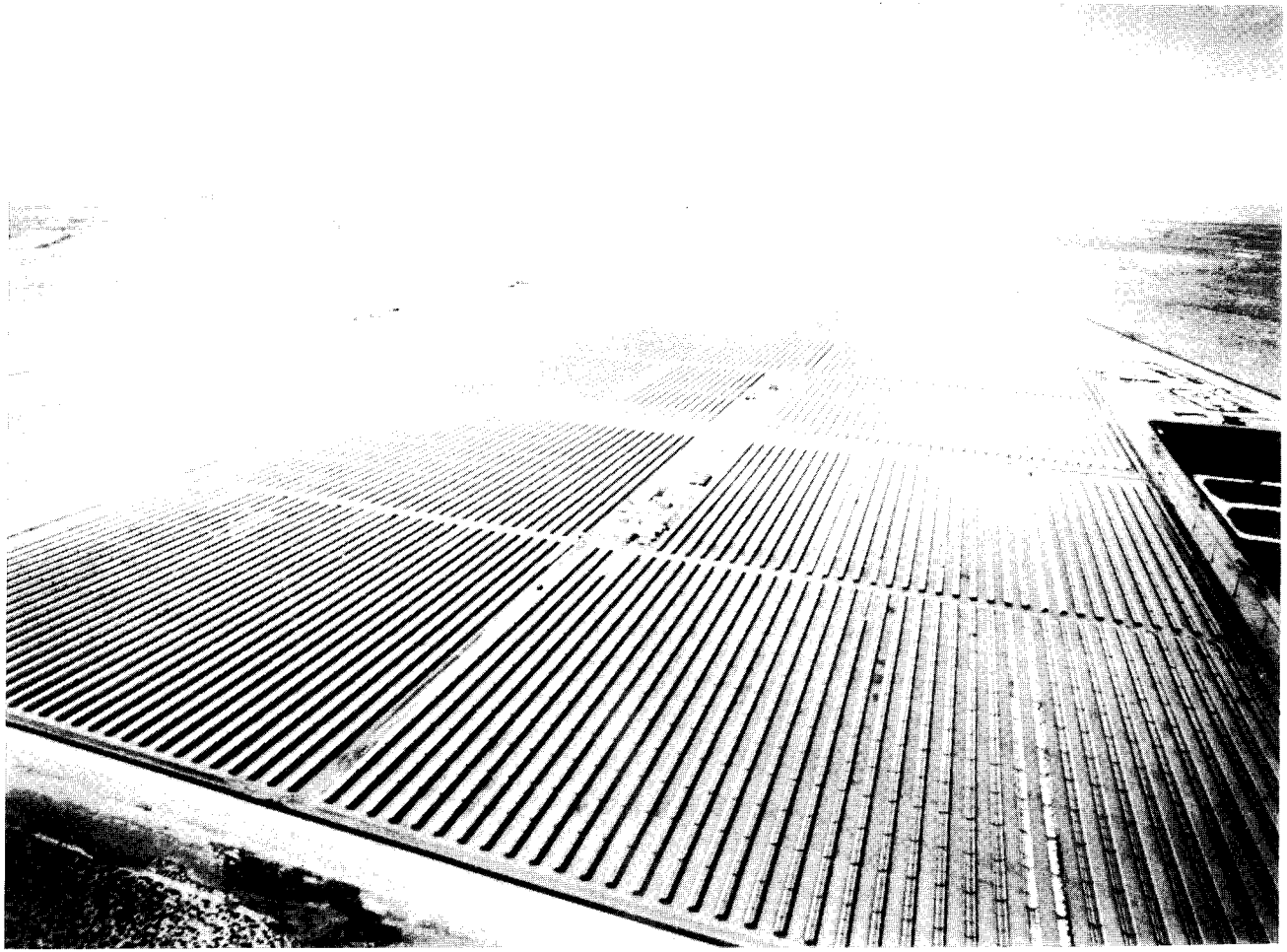

Figure 1. Aerial view of SEGS plants at Kramer Junction, California.

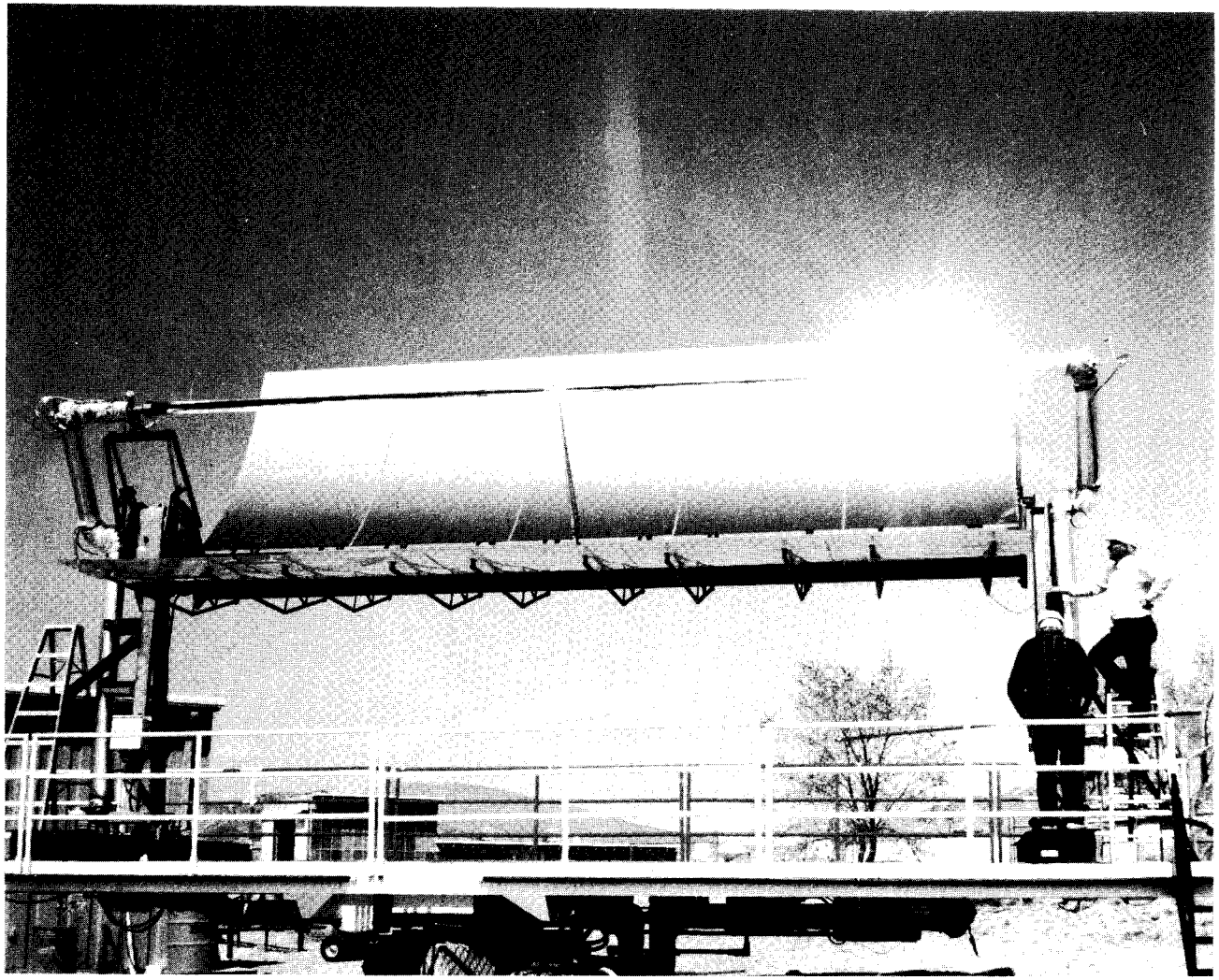

Figure 2. Rotating test platform at Sandia National Laboratories.

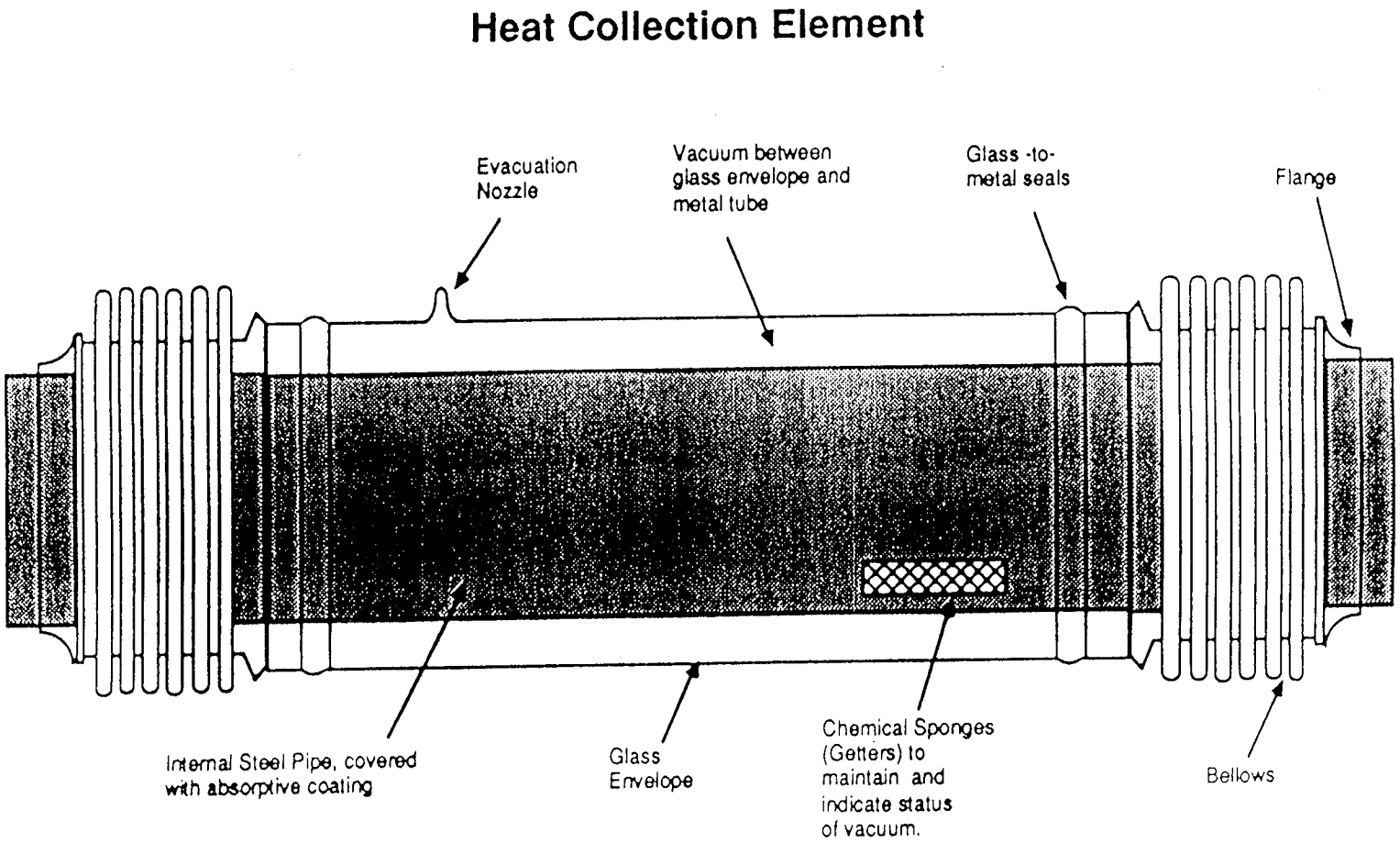

Figure 3. Heat collection element.

Test Results

Figure 4 summarizes the efficiency test results with the cermet receiver. When air is introduced into the receiver annulus, efficiency falls as thermal losses increase because of increased conduction and convection in the air transferring heat from the receiver surface to the glass. In still air, efficiency decreases by a comparable amount when the glass is removed from the receiver. As wind speed increases, efficiency can be seen to fall to unacceptable levels. The equations shown in Figure 4 were obtained from a least-squares regression analysis of the measured data points. Note that these equations apply only at the insolation values present during the test, and should not be used for other levels of insolation. The complete set of measured data is contained in Tables 1, 2, and 3 of Appendix D. The error bars on the data points are the expected worst-case errors caused by the measuring instruments. A discussion of the test errors is shown in Appendix E. Error bars are not included for the bare tube test case, because errors due to temperature instability (caused by variable winds) could not be quantified. The expected uncertainty in the data is certainly larger, but the magnitude is unknown.

Figure 5 shows thermal loss data from tests at approximately the same operating temperatures as in Figure 4. The thermal loss curves reflect the same phenomena as the efficiency test data: increasing losses as the receiver is degraded by allowing air into the vacuum annulus, and significantly worse losses with increasing wind-driven convection and conduction. The complete data sets are in Tables 6, 7, and 10 of Appendix D.

After exchanging the cermet receiver for the black chrome version, all of the tests except for glass removal were repeated. Figure 6 shows the efficiency test results, and Figure 7 shows results of thermal loss testing. The efficiencies are slightly lower at high temperatures, and losses slightly higher, both probably due to higher emissivity of the black chrome selective surface. Emissivity of black chrome is about 0.24 at 300°C, compared to about 0.14 for cermet coatings at 350°C. In Appendix D, efficiency data are contained in Tables 4 and 5; thermal loss data are contained in Tables 8 and 9.

Figures 8 and 9 compare efficiency and thermal loss curves for black chrome and cermet selective coatings, for both the vacuum and air test cases. Cermet is better than black chrome at the 350-400°C temperatures used for normal operations in the SEGS collector fields, but the difference is not great. The biggest advantage of cermet may be a better lifetime at high temperatures. But an evacuated tube is clearly a significant advantage for either selective coating. The bare HCE case was not included in this comparison, because the performance degradation with a bare tube completely swamps the smaller differences due to selective coatings.

Figure 10 summarizes the cermet HCE test data collected to determine the performance degradation due to increasing solar beam incident angle. All these tests were done with cold water as the heat-transfer fluid, with the receiver operating at near-ambient-air temperatures, so there were no discernible thermal losses, even with a bare receiver tube. We expected to see relatively small differences when the glass was removed, due to removal of any glass reflections. None were found, indicating that the antireflective coatings on both inside and outside of the glass envelopes were very effective.

An incomplete set of incident angle data for the black chrome receiver was obtained (not shown here). No significant differences from the cermet data were noted.

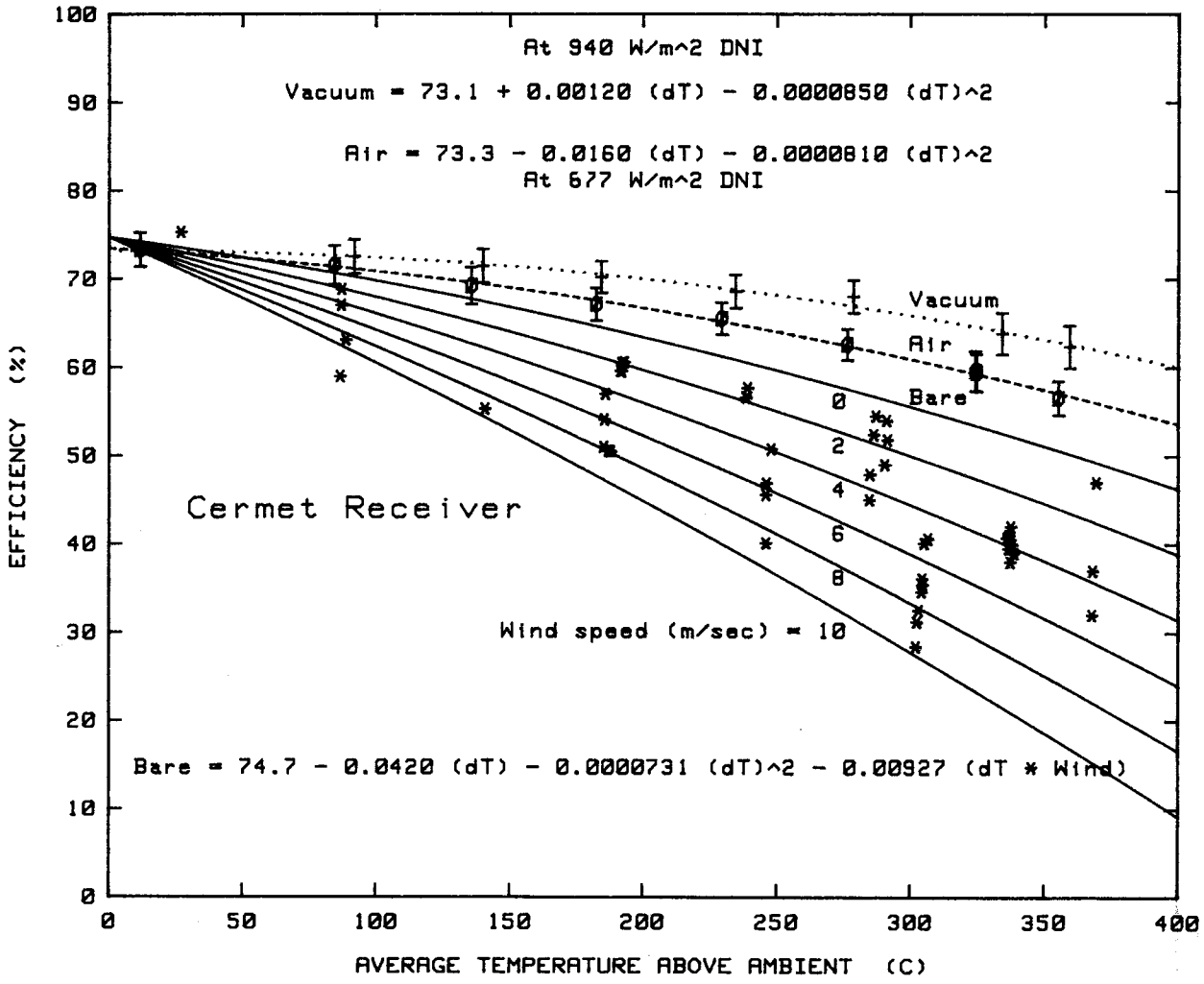

Figure 4. SEGS LS-2 Efficiency vs. Temperature Above Ambient (dT) and Wind - Cermet Receiver.

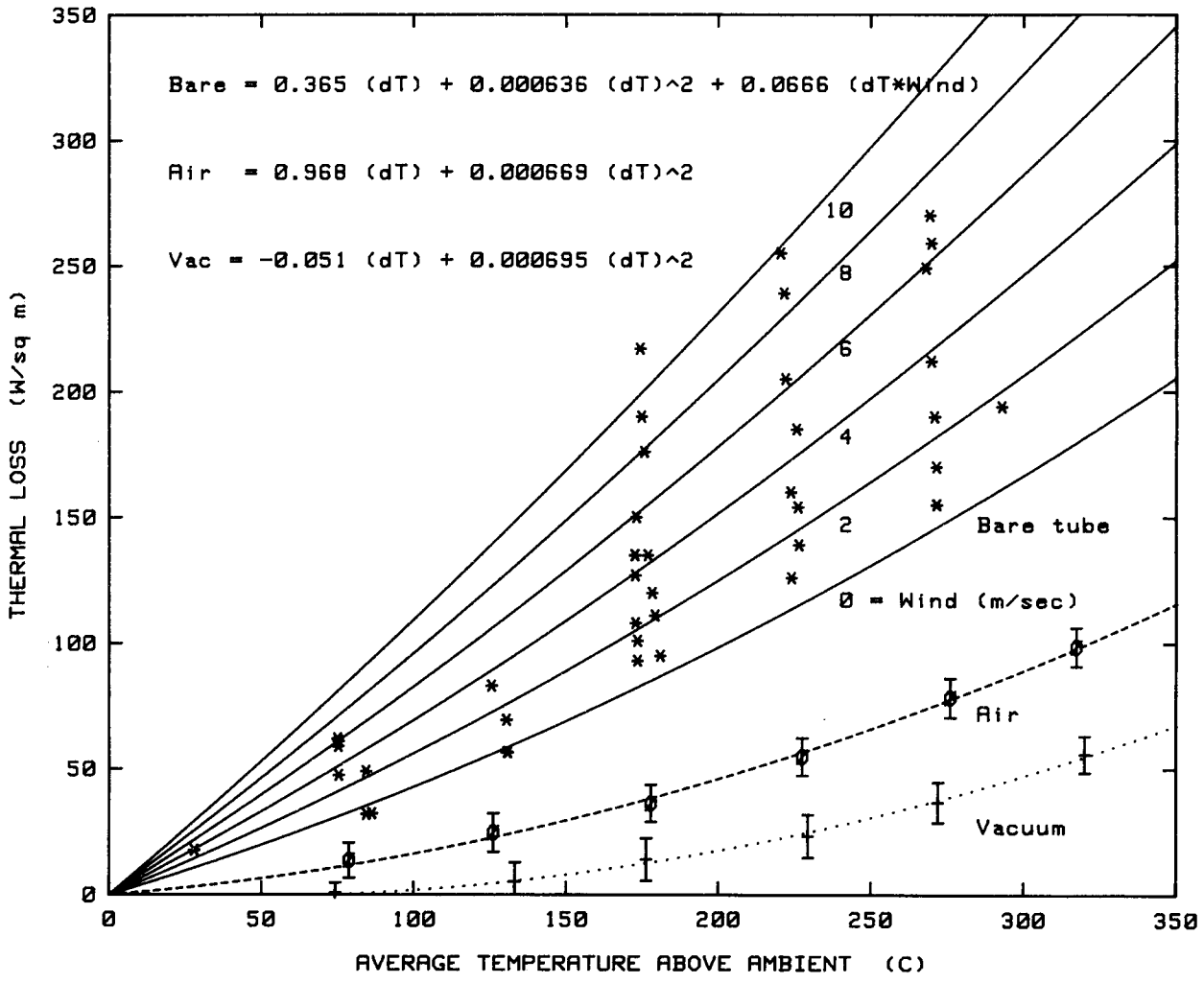

Figure 5. SEGS LS-2 Thermal Loss vs. Temperature Above Ambient (dT) and Wind - Cermet Receiver.

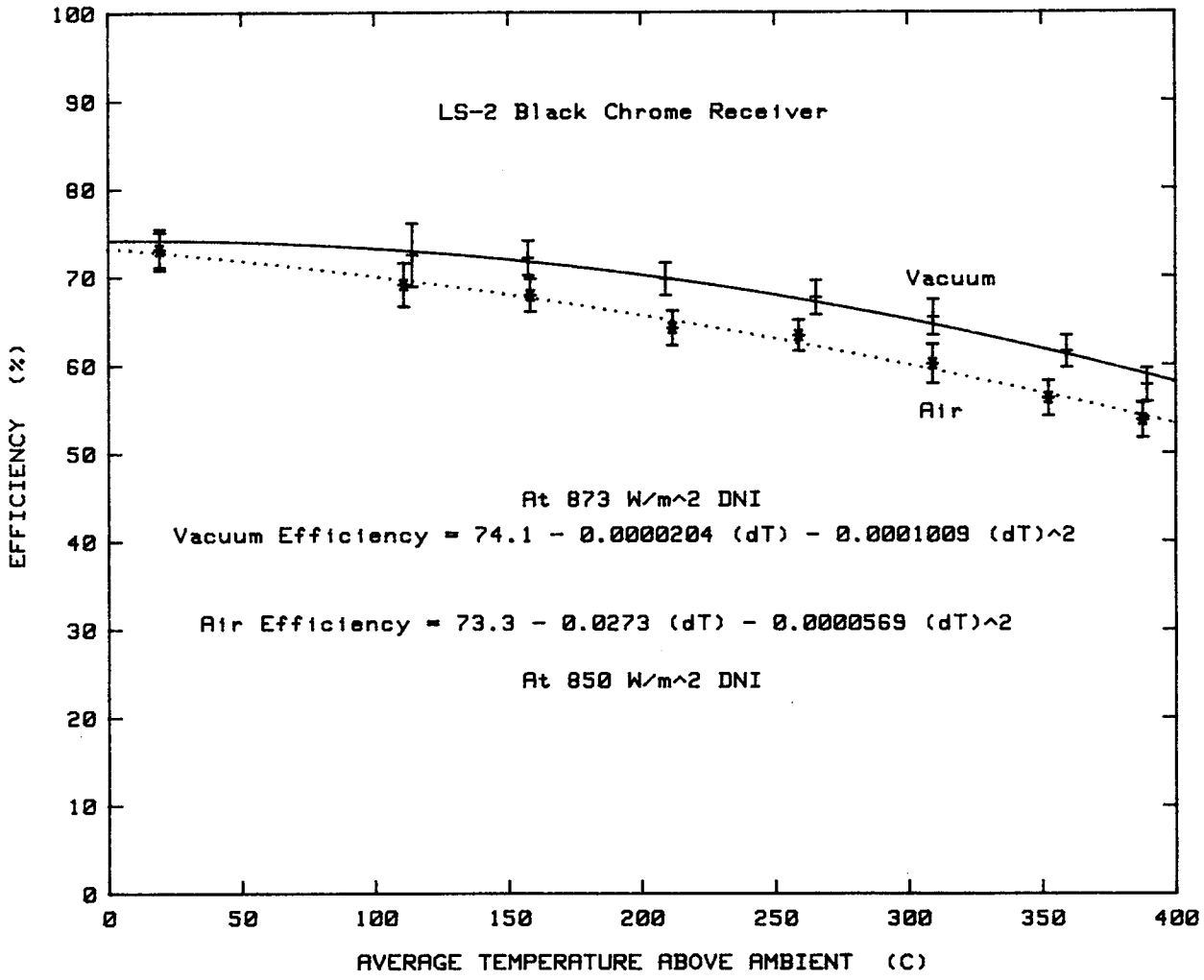

Figure 6. Black Chrome Efficiency Comparison - Air vs. Vacuum.

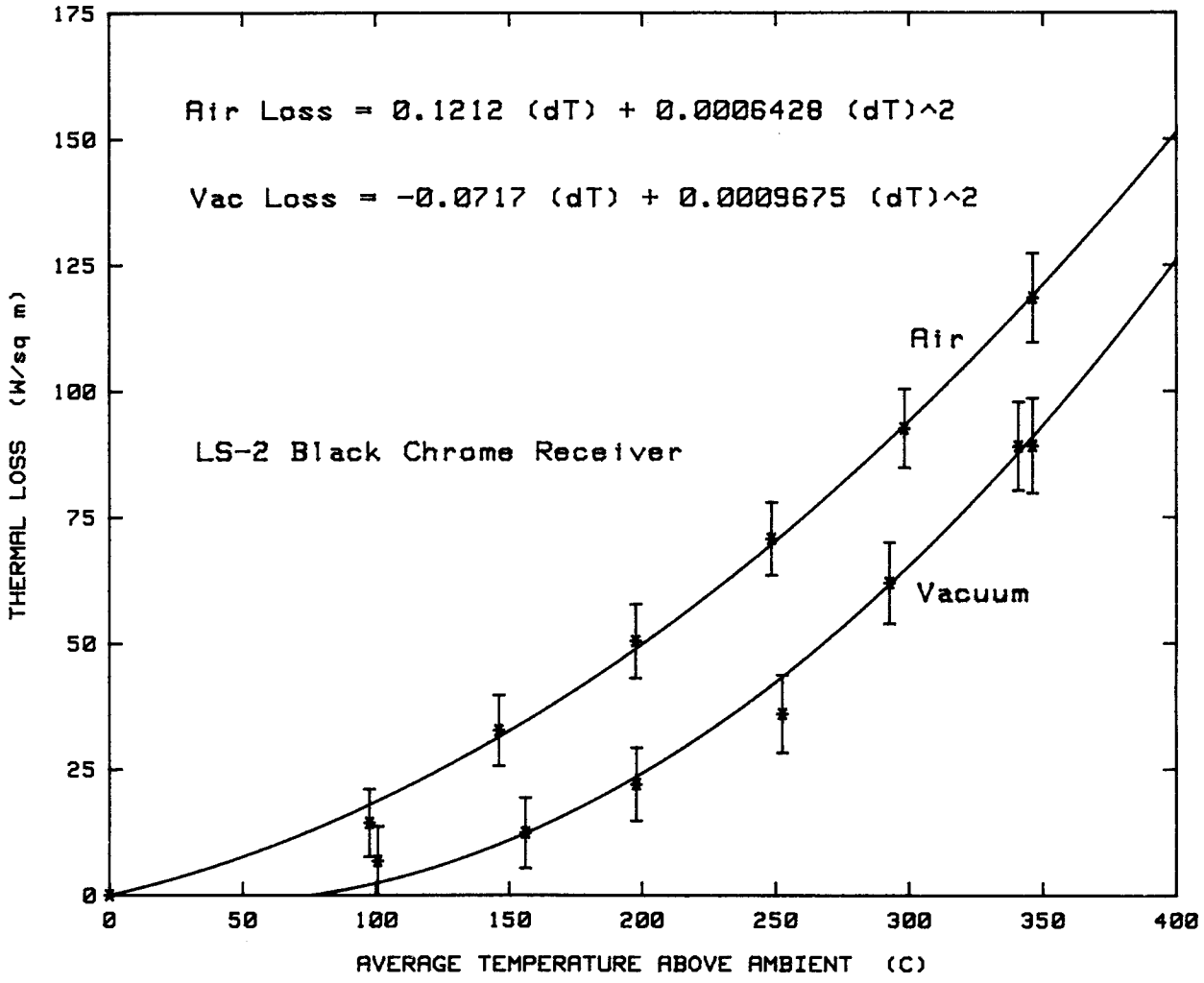

Figure 7. Black Chrome Thermal Losses with Air and Vacuum.

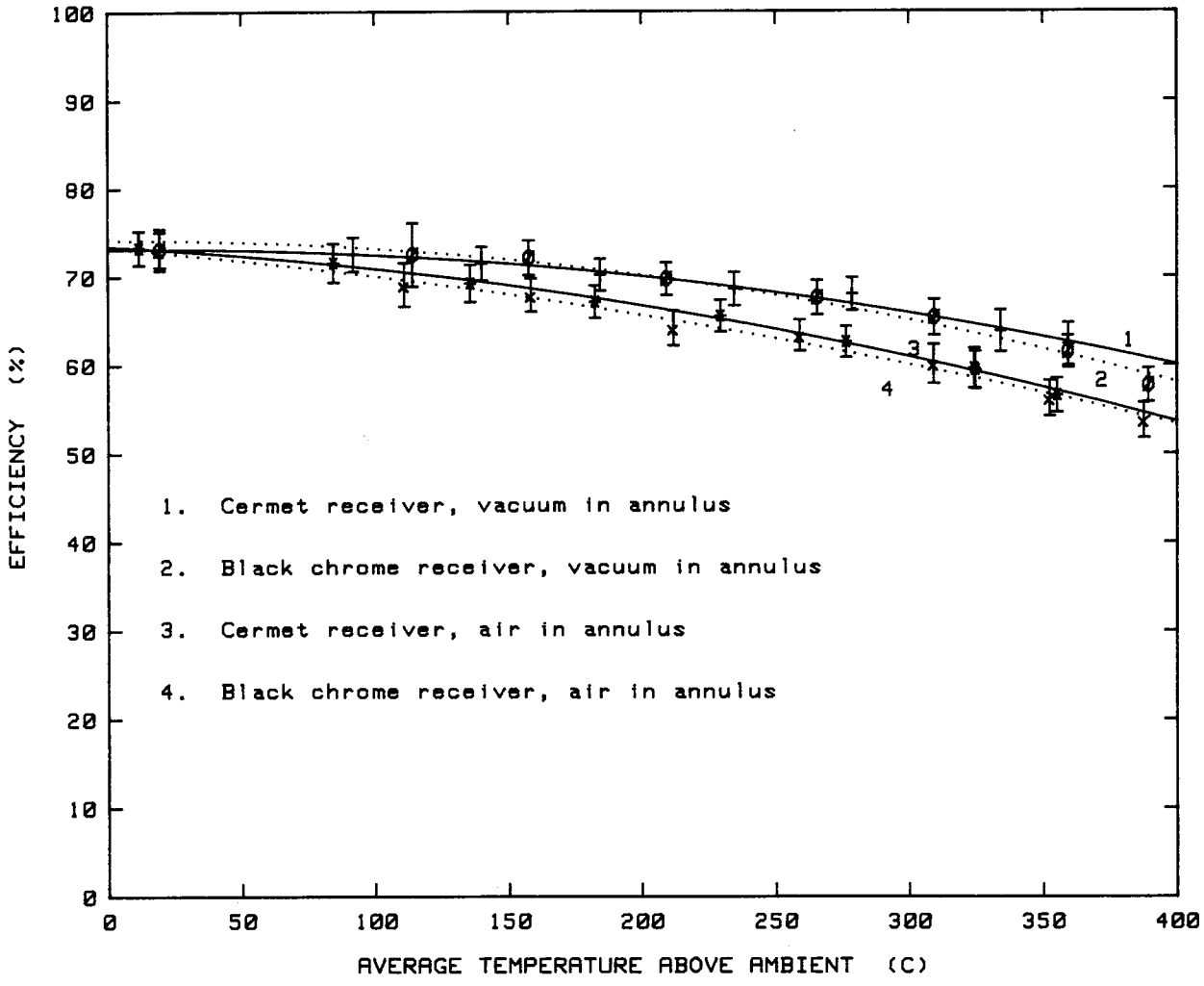

Figure 8. Efficiency Comparison of LS-2 Black Chrome and Cermet Receivers.

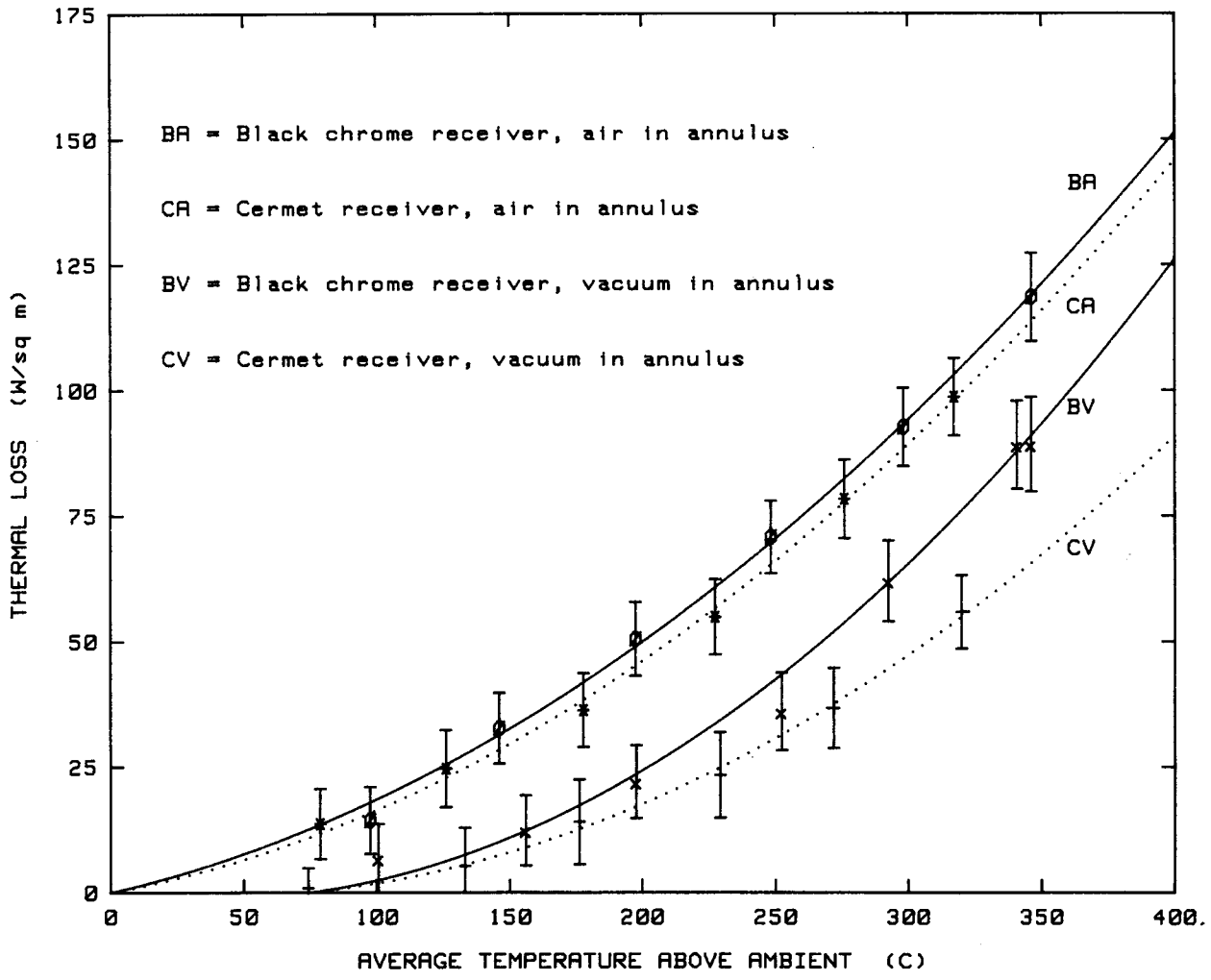

Figure 9. Thermal Loss Comparison of LS-2 Black Chrome and Cermet Receivers.

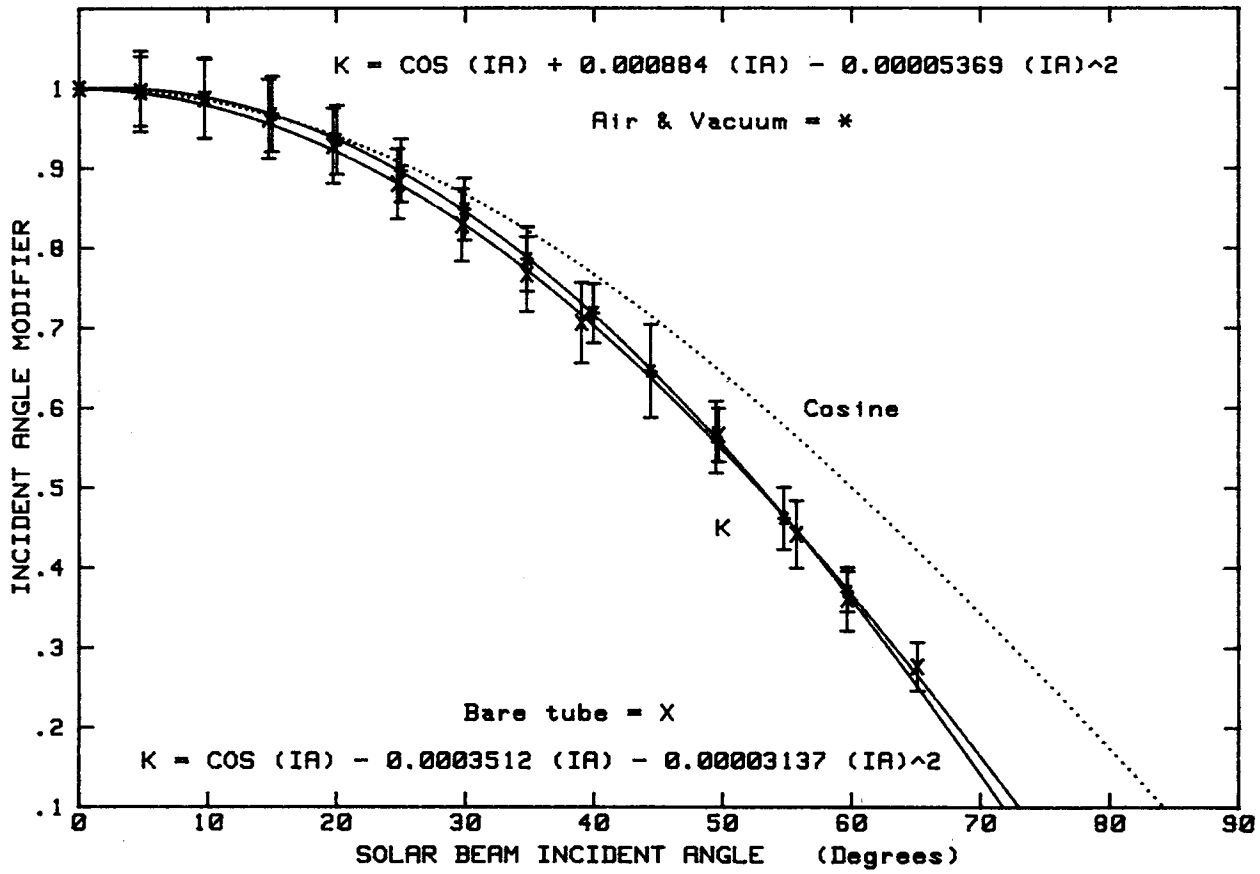

Figure 10. Incident Angle Modifier - SEGS LS-2 Receiver.

Performance Equations

The operating efficiency data and equations shown in the previous figures are valid only for a narrow range of insolation values near those existing during the tests. The thermal losses shown are valid only for an essentially zero value of incident direct insolation on the receiver. These equations will not correctly predict collector performance when insolation differs by hundreds of W/m^2 from the Sandia test conditions, as happens daily in an operational solar field such as the SEGS. The performance equation can be extended as outlined in Appendix C to cover the complete range of expected solar irradiance. The resulting performance equation for the cermet/vacuum receiver is shown in Figure 11. Incident angle is also included as a factor in the equation. A performance equation in this form has been shown to correctly predict the all-day, steady-state output from a single collector module, and from a small collector field (Ref. 1 and 2). We believe the equation can also be successfully used with large solar installations such as the SEGS plants[1].

The general shape of Figure 11, and the equation used to draw the figure, show that collector efficiency varies in a hyperbolic fashion with changing values of insolation; and as a quadratic polynomial with changes in operating temperature. The performance equations shown for efficiency and incident angle modifier are not exact physical models of the collector, but are instead empirical fits to the experimental test data. The first term in the performance equation (e.g., 73.3) represents the approximate optical efficiency of the collector. Some experience with the Acurex collector (Ref. 2) indicates that the optical efficiency term can be varied slightly to account for accumulated soiling of the collector mirrors and receiver glass.

It is possible to read a collector efficiency from a graph such as Figure 11, but not very accurately, and a new graph would be needed for each different incident angle. A more practical way to use this data is to solve the equations (1) to (5) shown below for each operating parameter set of interest. Note that the incident angle modifier K is the same for all the receiver variations. Also note that the equations are valid only for steady-state conditions. If the collector field is increasing or decreasing in temperature, a separate calculation is necessary to account for heat stored in, or removed from, the mass of oil and pipe in the field.

The equations below summarize the test performance of the SEGS LS-2 collector, and should apply to any temperature between ambient and 400°C, at any insolation level from 100 to 1100 W/m^2, and at any incident angle from 0 to 60 degrees.

Cermet with vacuum annulus

$$\eta = K\,[73.3 - 0.007276\,(\Delta T)] - 0.496\,(\Delta T/I) - 0.0691\,(\Delta T^2/I) \qquad (1)$$

Cermet with air in annulus

$$\eta = K\,[73.4 - 0.00803\,(\Delta T)] - 9.68\,(\Delta T/I) - 0.0669\,(\Delta T^2/I) \qquad (2)$$

[1]Before applying the equation to a SEGS plant, the reader should understand that differences exist between the flow conditions in the experiment and in a SEGS plant. These differences cause the experiment to overpredict losses by approximately 10% at a given fluid temperature. This subject is described in detail in the report section that describes validation of the analytical model.

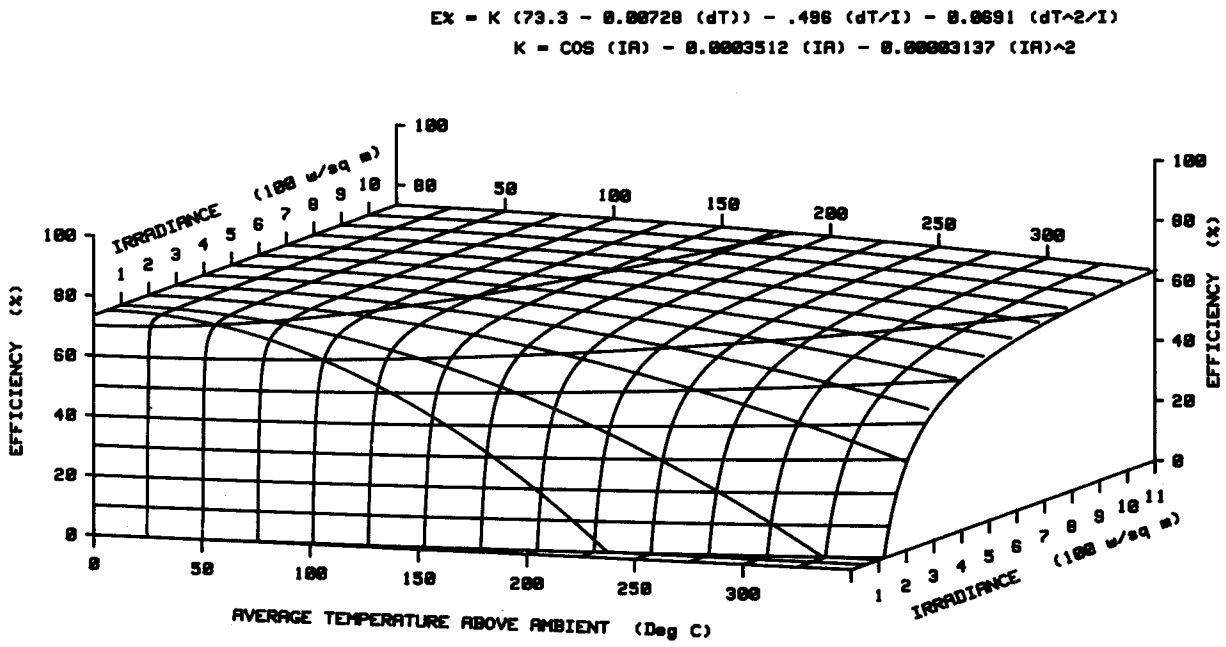

Figure 11. SEGS LS-2 Cermet/Vacuum Efficiency at Zero Incident Angle.

Black chrome with vacuum annulus

$$\eta = K\,[73.6 - 0.004206\,(\Delta T)] + 7.44\,(\Delta T/I) - 0.0958\,(\Delta T^2/I) \quad (3)$$

Black chrome with air in annulus

$$\eta = K\,[73.8 - 0.006460\,(\Delta T)] - 12.16\,(\Delta T/I) - 0.0641\,(\Delta T^2/I) \quad (4)$$

Incident Angle Modifier, K

$$K = \cos(Ia) - 0.0003512\,(Ia) - 0.00003137\,(Ia)^2 \quad (5)$$

In performance equations (1) through (5):

η = Collector efficiency, in percent
K = Incident angle modifier
ΔT = Receiver fluid temperature above ambient air temperature, °C
Ia = Solar beam incident angle, in degrees

References:

1. Dudley, V. E., and Workhoven, R. M., 1982. SAND81-0984, *Performance Testing of the Solar Kinetics T-700 Solar Collector.* Albuquerque, N.M.: Sandia National Laboratories.

2. Cameron, C. P., and Dudley, V. E., 1985. SAND85-2316, *Acurex Solar Corporation Modular Industrial Solar Retrofit Qualification Test Results.* Albuquerque, N. M.: Sandia National Laboratories.

Analytical Modeling of SEGS LS-2 Parabolic Solar Collector

In order to gain a detailed understanding of the heat transfer phenomena that have a significant influence on the performance of an LS-2 collector, an analytical model was developed and compared to the results of the Sandia tests. In this section we describe the analytical model and compare model predictions with test results. This validated model will be used by KJC Operating Company to do trade studies to determine optimum replacement intervals for degraded HCEs. The model can also be readily adapted to study troughs significantly different than the LS-2 (Dudley, draft).

Model Description

The thermal loss model for the heat collection element is one-dimensional and assumes steady-state heat transfer. It is based on the following thermal-resistance network:

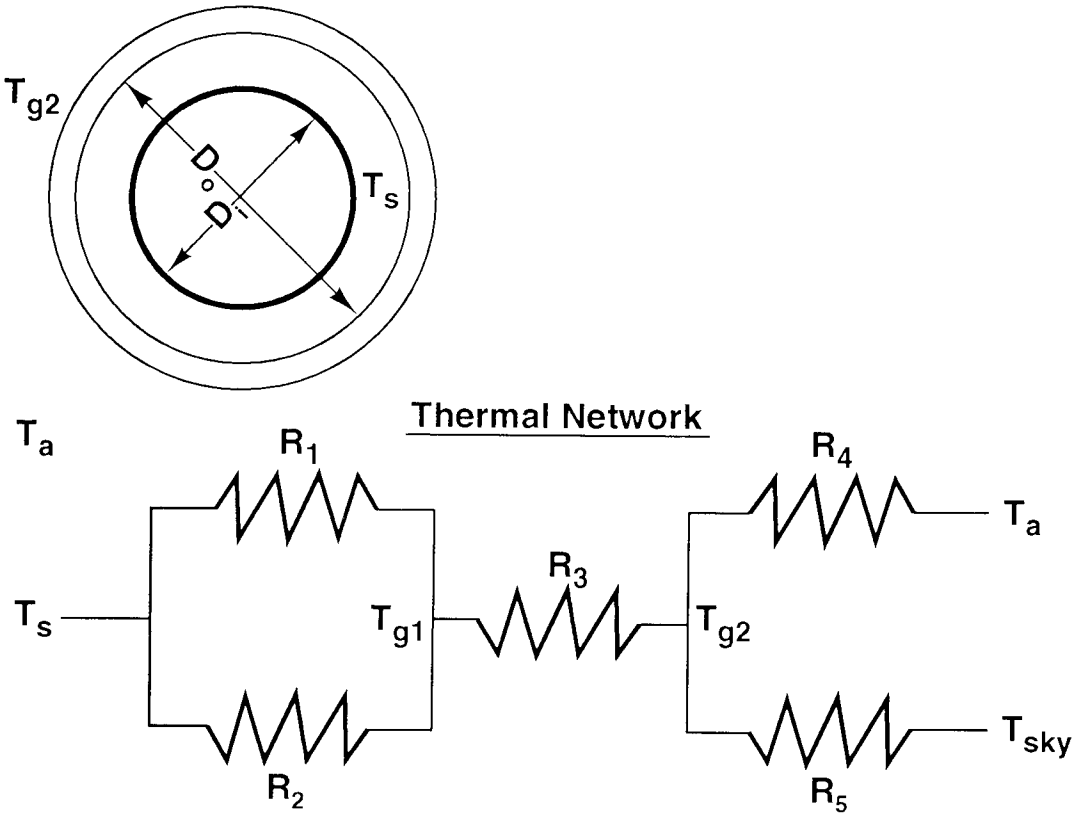

Figure 12. Thermal Resistance Network for Heat Collection Element.

Nomenclature

A = area [m^2]
D = diameter [m]
h = heat transfer coefficient [$W/m^2°K$]
K = thermal conductivity [$W/m°K$]
K_{eff} = effective thermal conductivity [$W/m°K$]
Q = heat flow per unit length of tube [W/m]
R = thermal resistance [°Km/W]

T_a = ambient temperature [°K]
T_{g1} = inside glass temperature [°K]
T_{g2} = outside glass temperature [°K]
T_s = tube surface temperature [°K]
T_{sky} = sky temperature [°K]

α = absorptivity
ε = emissivity
γ = intercept factor
ρ = reflectivity
σ = Stefan-Boltzmann Constant, $5.67\ 10^{-8}\ W/m^2°K^4$

N_u = Nusselt Number, the ratio of convective to conduction heat transfer
P_r = Prandtl Number, the ratio of viscous to thermal diffusion through a fluid boundary layer
R_a = Rayleigh Number, the ratio of the buoyant to viscous forces within a fluid field

General Modeling Approach

R_1 is the resistance between the receiver tube at T_s and the inner surface of the glass envelope at T_{g1}.

The model for R_1 in the annular space at reduced pressures. It is based on the theory of conduction heat transfer and kinetic theory. The model is shown schematically in Figure 13 over the range of pressures from atmospheric to 10^{-4} torr. In this figure the temperatures of the receiver tube and glass envelope are assumed to be held constant and the only variable is the pressure in annular region. Descriptions of the heat transfer mechanisms in each of the regions identified in Figure 13 are presented below.

In region (a), the gas in the annular region is circulating by laminar natural convection. In laminar flow, the fluid does not mix and the heat transfer mechanism is molecular conduction. The region previously described by equations 1, 2, and 3 and applies when $100 < Ra_c < 10^7$.

The heat transfer in region (b) is also molecular conduction. The thermal conductivity of the gas is a function of temperature and not pressure in this region. As the pressure decreases, over nearly three decades from near 100 torr to 10^{-1} torr, the density of the gas also decreases. However, there

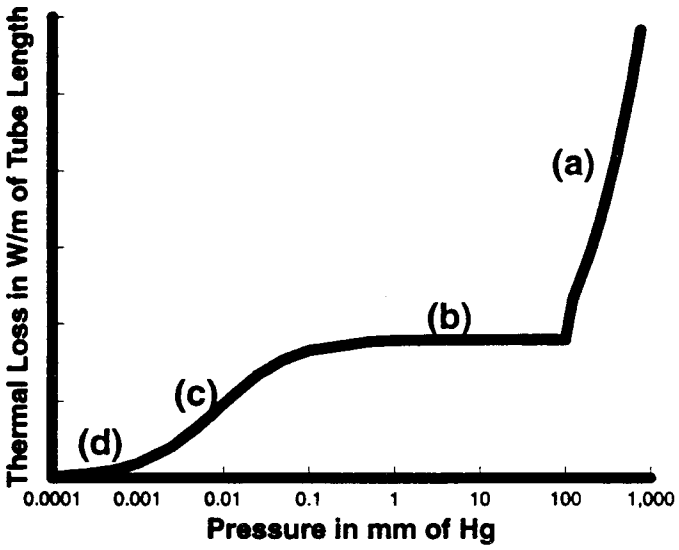

Figure 13. Annular Conduction and Convection Heat Loss Model

are still many molecules and the mean-free path between molecular collisions is very small. Therefore, since the geometry, temperatures, and thermal conductivity are all constant, the thermal loss is also constant.

In region (c), the density of the gas continues to decrease. With the reduction in pressure, the mean-free path between molecular collisions is starting to increase. As the mean-free path increases, the apparent thermal conductivity of the gas decreases. Mechanistically, the molecular transport is reduced because there are not enough molecules to transfer energy one to the other. Therefore, the mean-free-path term in the heat-transfer coefficient starts to dominate, and the conduction losses decrease further.

In region (d), the conduction is very small and of little consequence to the heat-loss calculation. In this region, intermolecular collisions almost never occur and the only transport is from the molecules that travel across the gap between the receiver tube and the glass envelope. Therefore, in region (d), R_1 becomes very large and heat loss is radiation dominated.

Calculating the reduced pressure conduction heat loss requires only knowing the gas that is in the annulus, the pressure, and the temperature. The first step is to calculate the mean-free path between molecules. This is calculated using the following dimensional equation.

$$\lambda = 2.331 \times 10^{-20} \frac{T}{P\delta^2} \tag{1}$$

In this equation,

λ = mean-free-path between collisions of a molecule in cm.
T = average temperature of the gas in the annular space in degrees K.
P = pressure of the gas in the annular space in mm of Hg.

δ = molecular diameter of the gas in cm. Air and hydrogen have molecular diameters of 3.53 $\times 10^{-8}$ and 2.32 $\times 10^{-8}$ cm, respectively.

A second, intermediate coefficient is a function of the gas and the interaction between the gas and the walls of the enclosure. It is calculated as shown in Equation (2) below.

$$b = \frac{2-a}{a} \times \frac{9\gamma - 5}{2(\gamma + 1)} \tag{2}$$

In Equation (2), "b" is a non-dimensional coefficient, "a" is the accommodation coefficient, also non-dimensional, and γ is the ratio of specific heats for the gas inside the annulus (for air and hydrogen γ = 1.4 and 1.41, respectively).

The accommodation coefficient is defined as *the ratio of the energy actually transferred between impinging gas molecules and a surface and the energy which would be theoretically transferred if the impinging molecules reached complete thermal equilibrium with the surface.* The accommodation coefficient is not well characterized for glass-air surfaces and, not surprisingly, no data could be found for selective surfaces. However, several references noted that for normal surface-gas interactions "a" is near unity. One experimental study for several surfaces and gases determined that a = 1 unless the surfaces were *extremely* well cleaned. This is what was assumed here.

Once the quantities λ and "b" are calculated, Equations (1) and (2), the next step is to calculate the effective heat-transfer coefficient using Equation (3).

$$H = \frac{K}{r_i \ln \frac{r_o}{r_i} + b\lambda\left(\frac{r_i}{r_o} + 1\right)} \tag{3}$$

where,

H = heat-transfer coefficient in W/m^2K
K = thermal conductivity of the gas at standard temperature and pressure in W/mK
r_i and r_o = inner and outer radii, respectively, of the annulus in meters
b = coefficient calculated using Equation (2); it is non-dimensional
λ = mean-free path between molecular collisions as calculated using Equation (1). Its units should be in meters for use in Equation (3).

The first term in the denominator of Equation (3) represents the molecular conduction through the evacuated, cylindrical region. In Figure 13, this term dominates the heat transfer in region (b) from 100 to 10^{-1} torr. As the pressure decreases further, the mean-free path between molecules increases and the second term in the denominator increases to the point that is starts to reduce the value of the heat-transfer coefficient. This is represented by region (c) in Figure 13, i.e., from about 10^{-1} to 10^{-3} torr. As the pressure decreases further, the mean-free path between molecules becomes very large, as in region (d). In fact, molecules in region (d) are not likely to collide with one another at all, but rather *bounce* back and forth between the receiver tube and the glass

envelope. It is not clear that this correlation applies in this pressure regime. However, since the conduction heat transfer is small, it is a reasonable assumption to apply the model in region (d).

The heat transfer by conduction for a unit length of the HCE can now be calculated using Equation (4).

$$Q = 2\pi r_i H(T_i - T_o) \tag{4}$$

where,

Q = conduction heat loss per unit length of the HCE in W/m
r_i = inner radius of the annulus in meters
H = heat-transfer coefficient in W/m^2K as calculated using Equation (3)
T_i and T_o = temperatures of the inner and outer surfaces of the annulus in degrees K

Sample Calculations

To gain additional insights, the model just described was applied to a very simple case for the SEGS HCE. The geometry of the annulus was fixed to an outer diameter of 10.9 cm and an inner diameter of 7.0 cm. The outer temperature was chosen to be 112°C and the inner one 349°C. Air was assumed to be inside the annulus and only the pressure of the air was allowed to change. The heat transfer by conduction using the annular convection model described by Equations (1), (2), and (3) was compounded with the kinetic theory model described in the previous section. The results of this analysis are shown in Figure 14.

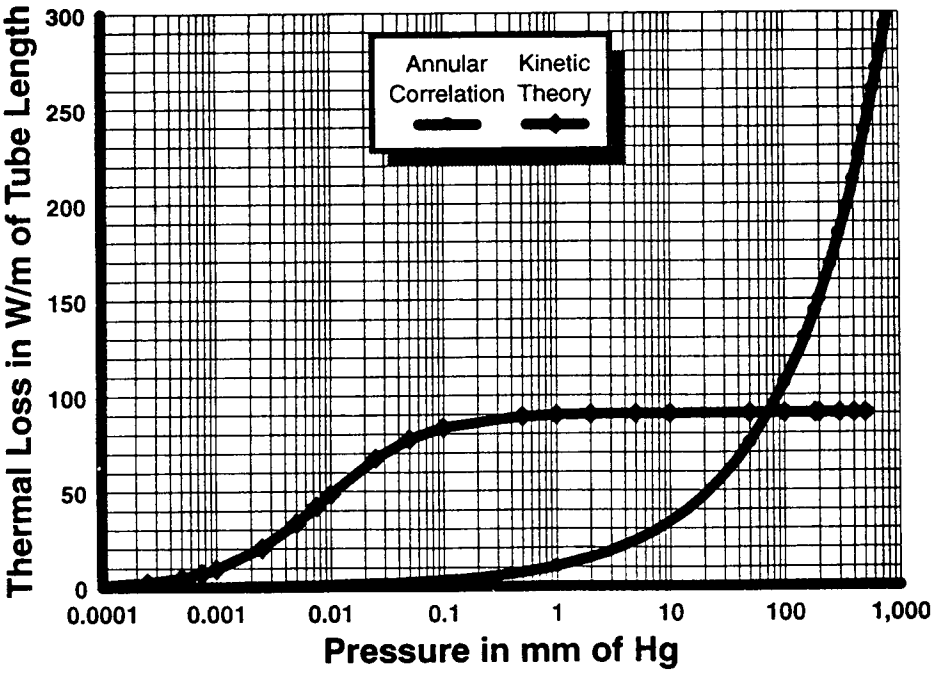

Figure 14. Heat Loss with Convection and Kinetic Theory Models.

Figure 14 clearly demonstrates that applying the annular convection model for low pressures under predicts the thermal losses from the HCE. This was found when comparing the model with data from the experiment, described below.

It is recommended that the annular convection model be used down to a lower limit of $Ra_c = 100$. For lower values of the Ra_c, the kinetic theory method for calculating the heat losses should be used. While the critical Rayleigh number is the appropriate criterion for determining when to use the annular convection model and the kinetic theory model, the pressure in the annulus can also be used as an indicator. For the case modeled, the pressure that corresponds to $Ra_c = 100$ is about 180 torr.

$$Q_1 = \frac{2\pi K_{eff}}{ln(D_o / D_i)}\left[T_s - T_{g1}\right] \tag{5}$$

$$K_{eff} = K(0.386)\left[\frac{P_r}{0.861 + P_r}\right]^{.25} {}^{*\,.25} R_{ac} \tag{6}$$

$$R^{*}_{ac} = \frac{\left[\ln(D_o / D_i)\right]^4}{L^3\left[D_i^{-0.6} + D_o^{-0.6}\right]^5} R_{a1} \tag{7}$$

R_2 is the radiant resistance between the receiver tube and the inner surface of the glass envelope. The glass tube is modeled as a "black" surface in the thermal spectrum, i.e., $\alpha = \varepsilon = 1.0$.

$$Q_2 = \varepsilon_s \sigma A_s\left[T_s^4 - T_{g1}^4\right] \tag{8}$$

R_3 is the conduction resistance between the inner and outer surfaces of the glass envelope.

$$Q_3 = \frac{2\pi K}{\ln(D_o D_i)g}\left[T_{g1} - T_{g2}\right] \tag{9}$$

R_4 is the convective resistance from the outside of the glass envelope to the ambient.

$$Q_4 = \bar{h}\, A_g\left[T_{g2} - T_a\right] \tag{10}$$

For Natural Convection

$$Nu_D = \frac{\bar{h}D}{K} = 0.48\, R_{aD}^{.25} \tag{11}$$

For Forced Convection

$$Nu_D = \frac{\bar{h}D}{K} = 0.193\,\mathrm{Re}_D^{.618}\,P_r^{.33} \tag{12}$$

R_5 is the radiation heat loss to the sky and surroundings.

$$Q_5 = \varepsilon_g \sigma A_g \left[T_{g2}^4 - T_{sky}^4 \right] \tag{13}$$

Since the fluid properties vary with temperature and, in some cases, pressure, this model gives rise to a highly nonlinear set of equations. Therefore, an iterative solution technique was used based on the following energy balance.

$$Q1 + Q2 = Q4 + Q5 \tag{14}$$

In Figure 14, only conduction heat losses were modeled. The total heat loss from the HCE can also be calculated and are shown in Figures 15 and 16. Figure 15 shows the conduction, radiation, and total heat losses as a function of pressure. Figure 16 shows the fraction of the total heat loss resulting from conduction and radiation also as a function of the annulus pressure.

Air Versus Hydrogen

Since one of the concerns of the KJC Operating Company is the influx of hydrogen from the ambient air and from the circulating oil into the annular space, the conduction heat transfer for hydrogen at the same conditions established for the earlier examples was also calculated. The results are shown in Figure 17 below.

Figure 17 clearly demonstrates that the thermal losses with hydrogen in the annular region can be as much as six times the conduction losses with air. The total thermal losses with air at atmospheric pressure, shown in Figure 15, are 540 W/m of tube length. If the annulus contained hydrogen at a pressure of 10^{-2} torr, the same total thermal losses as with air at atmospheric pressure would be calculated.

In summary, the annular convection model [Equations (11), (12), and (13)] should be used down to a lower limit of $Ra_c = 100$. For lower values of Ra_c, the kinetic method for calculating heat losses should be used.

References

Ratzel, A., C. Hickox, and D. Gartling, Techniques for Reducing Thermal Conduction and Natural Convection Heat Losses in Annular Receiver Geometries, Journal of Heat Transfer, Vol. 101, No. 1, February 1979.

Handbook of Vacuum Physics, Volume 1: Gases and Vacua, A.H. Beck, ed., Pergamon Press, London, 1966.

Holkeboer, D., D. Hones, F. Pagano, and D. Santeler, *Vacuum Engineering*, Boston Technical Publishers, Cambridge, 1967.

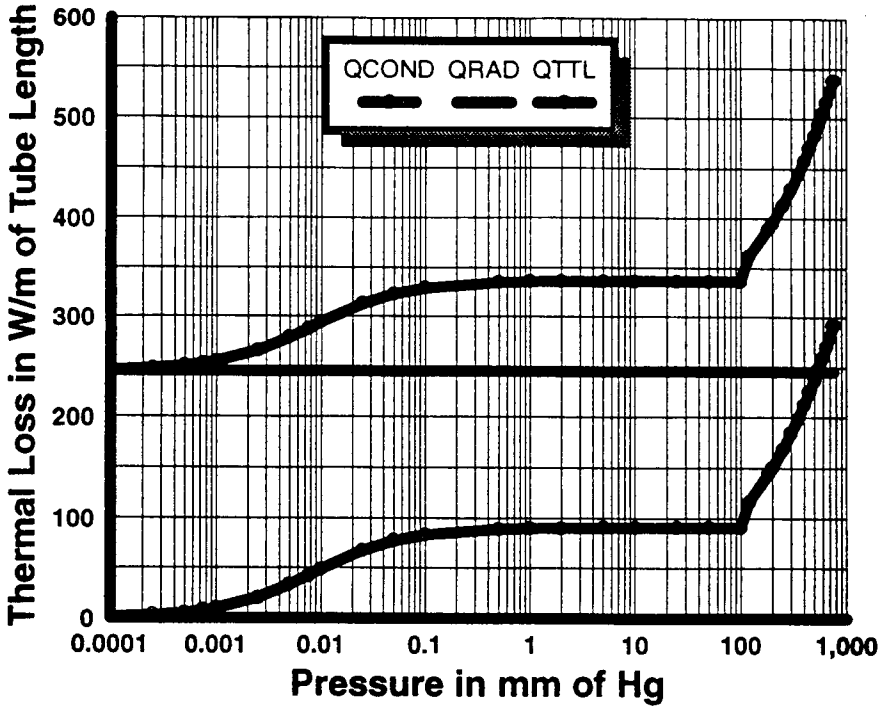

Figure 15. Thermal Losses from a SEGS HCE.

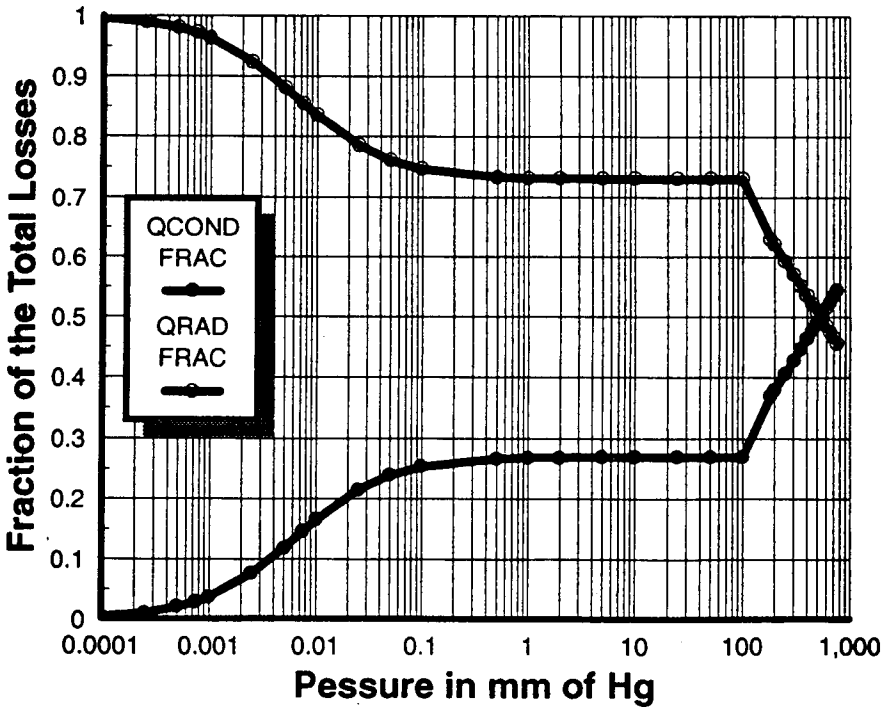

Figure 16. Fraction of Losses—Conduction and Radiation.

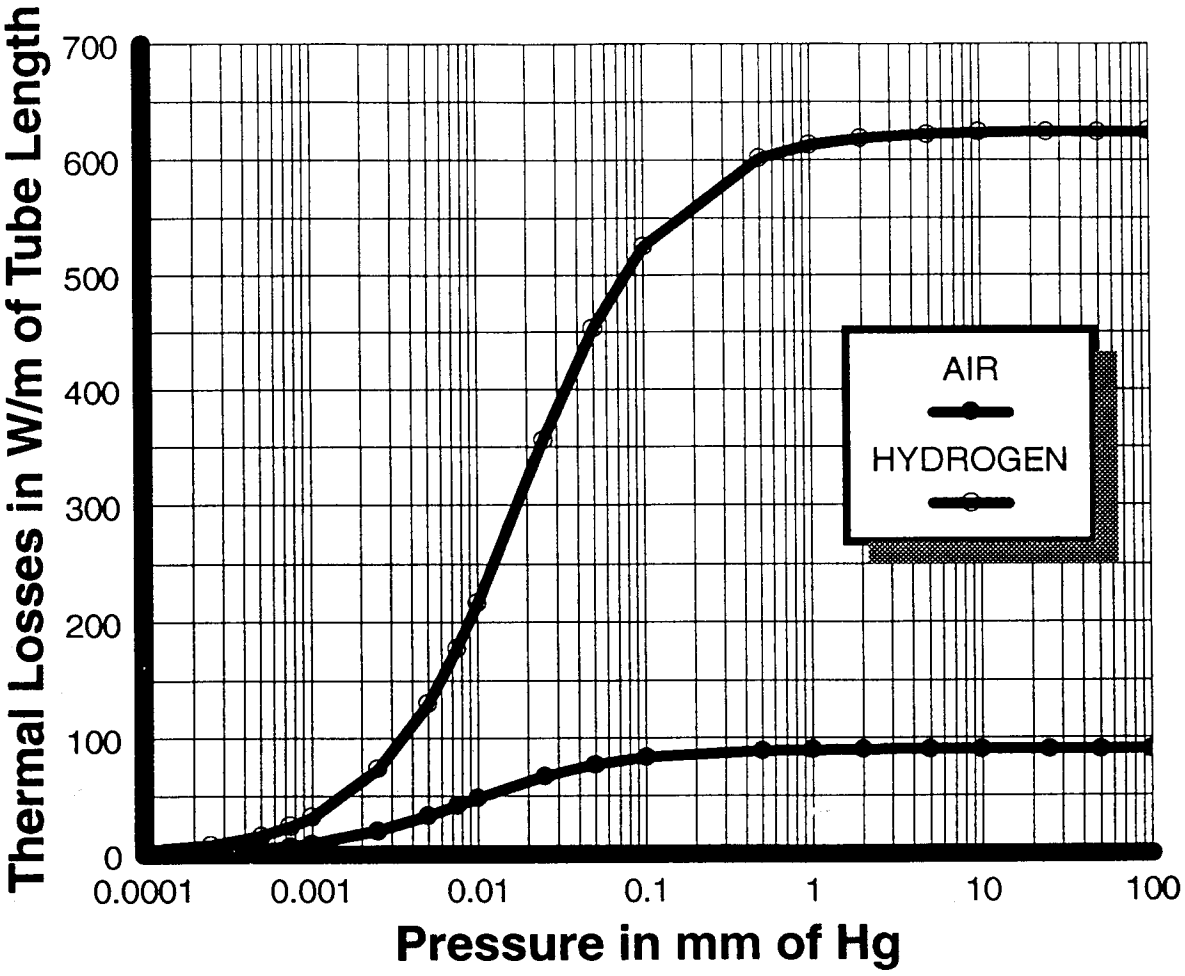

Figure 17. Conduction with Air and Hydrogen in the Annulus.

Handbook of Heat Transfer, W.M. Rohsenow and J.P. Harnett, McGraw-Hill Book Company, New York, 1973.

Incropera, F.P., and D.P. DeWitt, *Fundamentals of Heat and Mass Transfer*, John Wiley & Sons, New York, 1985.

Fox, R.W., and A.T. McDonald, *Introduction to Fluid Mechanics*, John Wiley & Sons, New York, 1978.

Dudley, V.E., and Lindsey R. Evans, "Test Results: Industrial Solar Technology Solar Collector," Draft report, to be published.

Computer Model of LS-2 Collector

The heat transfer methodology described in the previous section was incorporated within a QuickBasic computer program called HCE-HTX. The program calculates the one-dimensional, steady-state heat losses and HTF heat gain per unit length (meter) of an HCE. The principal model parameters include fractional HTF flow rate, HTF bulk temperature, ambient solar and weather conditions, and a detailed specification of the HCE. The model accommodates several conditions of the HCE annulus: vacuum intact, lost vacuum (air in annulus), and broken annulus cover (bare tube). A detailed description of the program can be found within the HCE-HTX User's Manual (Appendix F).

Comparisons of Model Predictions With Experimental Data for the Cermet HCEs

The following section compares output from the HCE-HTX code with experimental data collected by Sandia. The comparisons are made graphically and each plot is discussed, including comments on potential sources of deviation. Much of these data have been verified through selected hand calculations of subroutine calculations and property look-ups.

Sandia performed tests for both full sun and no sun conditions using cermet HCEs in conditions: 1) as new with vacuum intact, 2) annulus filled with ambient air, and 3) with the glass cover completely removed such that the bare absorber is directly exposed to ambient conditions. Data were also collected to evaluate the sensitivity of the HCE heat loss to wind speed.

Several conditions specific to the SNL test procedure differ from normal SEGS operating conditions. These conditions are summarized below:

- While existing SEGS plants utilize a diphenyl/biphenyl-oxide heat transfer fluid (Therminol VP-1 or Dowtherm A), the SNL test utilized a silicone-based fluid (Syltherm 800). Though the two synthetic oils have different material properties, the appropriate properties were used when comparing the model with the experiment.

- At full solar power, a typical flow rate in an LS-2 collector operating in a 30 MW SEGS plant is about 140 gpm. However, because of limitations in the test loop, typical flow rates for the Sandia tests were about 14 gpm, or 10% of the design flow of a SEGS plant. To achieve an increased flow velocity in the test loop (approximately 3 times higher), a 2-inch diameter flow restriction device (solid plug) was centered in the 2.6 inch (66 mm) inside diameter HCE absorber tube. With the plug the fluid velocity at 14 gpm of Syltherm in the test loop was 0.63 m/s at a Reynolds number of $1.8\ 10^4$, compared to 2.58 m/s and a Reynolds number of $7.9\ 10^5$ at 140 gpm of Therminol VP-1 in an operating SEGS plant. However, the wall-to-fluid ΔT in the test loop is five times higher than in a SEGS HCE, i.e., 20°C vs. 4°C. Hence, the comparable products of $h\Delta T$ for these two cases, which are equivalent to the heat flow to the fluid, are 16,400 W/m^2 in the test loop and 16,625 W/m^2 in a SEGS HCE at full flow. The effect that the higher ΔT has on the predicted thermal losses in an operating SEGS plant is discussed at the end of this section.

The validation presented here consists of a set of direct comparisons between measured and modeled data. Each comparison contains a plot of heat loss versus temperature difference

(between HTF and ambient). The tests described earlier consisted of a series without insolation (no-sun case) to measure the thermal loss, and a series with insolation to measure collector efficiency. Within these series, tests were conducted with full vacuum, loss of vacuum but with mechanical integrity of the glass envelope, and with the glass envelope removed.

The first validation plot, Figure 18, shows the heat loss for the no-sun case with vacuum intact. A similar plot for the no-sun case with ambient air in the annulus (i.e., bad seal condition resulting in lost vacuum) is presented as Figure 19. No-sun and full-sun cases for all annulus conditions - vacuum, air, and bare - are summarized in Figure 20 and 21, respectively.

All of the validation runs presented in Figs. 18-21 are based on the following assumptions: cermet absorber coating, Syltherm 800 HTF; restricted flow (2 inch diameter concentric plug), 14 gpm flow rate, no wind, ambient atmospheric air pressure at 0.83 atm., ambient temperature at 22°C, and effective sky temperature at 14°C. For the full-sun cases (Figure 21), direct normal irradiance was 940 W/m2; for the vacuum cases (Figs. 18, 20, and 21), the evacuated annulus pressure was 10^{-4} torr.

Detailed output from the HCE-HTX validation runs can be found in Appendix F.

Figure 18 - No sun with vacuum intact

The most simple case available for comparing predicted performance from the model with empirically-derived data is the case with no-sun on the HCE with vacuum intact, Figure 18. With vacuum intact, heat loss from the absorber is almost entirely by radiation. Since the heat transfer is between the fluid and the absorber is relatively small, the absorber temperature is almost the same as the HTF temperature. Since the HTF and ambient temperature were measured during the experiment, the only significant uncertainty stems from proper characterization of the emissivity of the absorber. Predicted radiation loss is directly proportional to the value of emissivity. Accordingly, proper characterization of the emissivity of the absorber is very important. The cermet emissivity data currently used in the code as the baseline is a linear fit to two data points taken from the actual tubes that were tested on the platform at Sandia. (The effect that the uncertainty in emissivity measurement has on the comparison of the model with the experiment is discussed later under Figure 22.) The agreement between the model and SNL test data is reasonably good for Figure 18. At normal operating temperatures (about 300°C above ambient) modeled performance, using the baseline emissivity, is very close to the uncertainty attributed to the experiment.

Figure 19 - No sun with air in annulus

The case defined by no-sun with air in the annulus is presented in Figure 19. The agreement here is very good; the model and test data essentially agree, within the bounds of experimental uncertainty, over the entire temperature range. The conditions of Figure 19 deviate from those of Figure 18 in that convection within the annulus is of the same order of magnitude as the radiation. It is noted that air in the annulus was modeled at 0.83 atm rather than 1 atm due to Albuquerque's high altitude (> 5,000 ft above sea level).

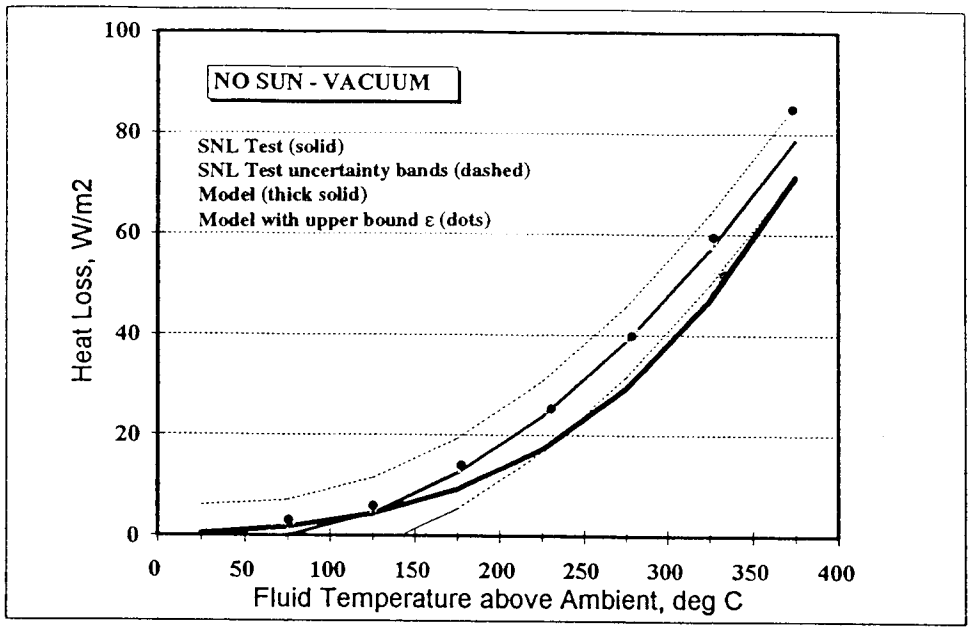

Figure 18. HCE Heat Loss: Vacuum Intact case.

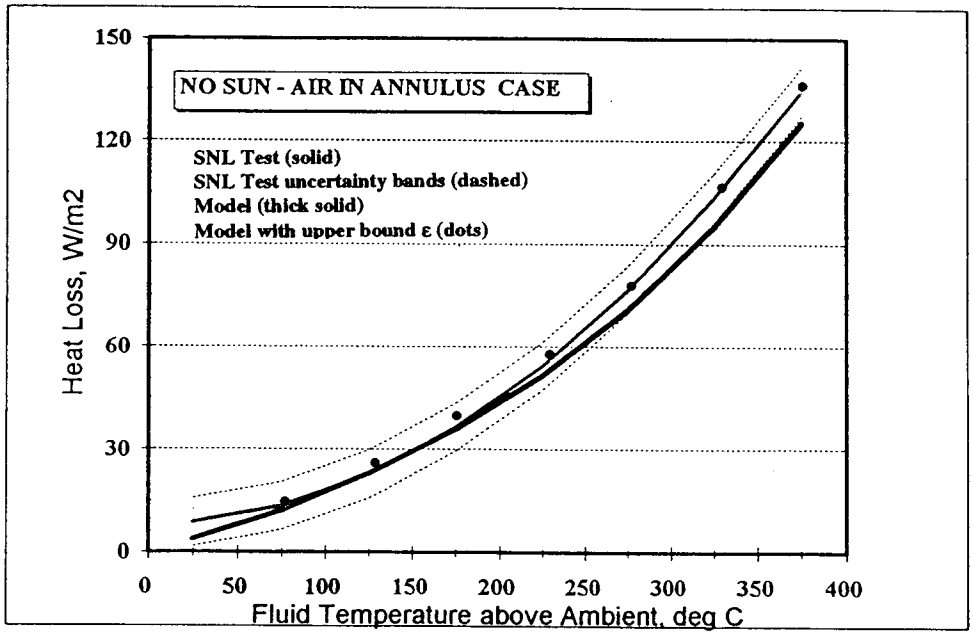

Figure 19. HCE Heat Loss: Air in Annulus case.

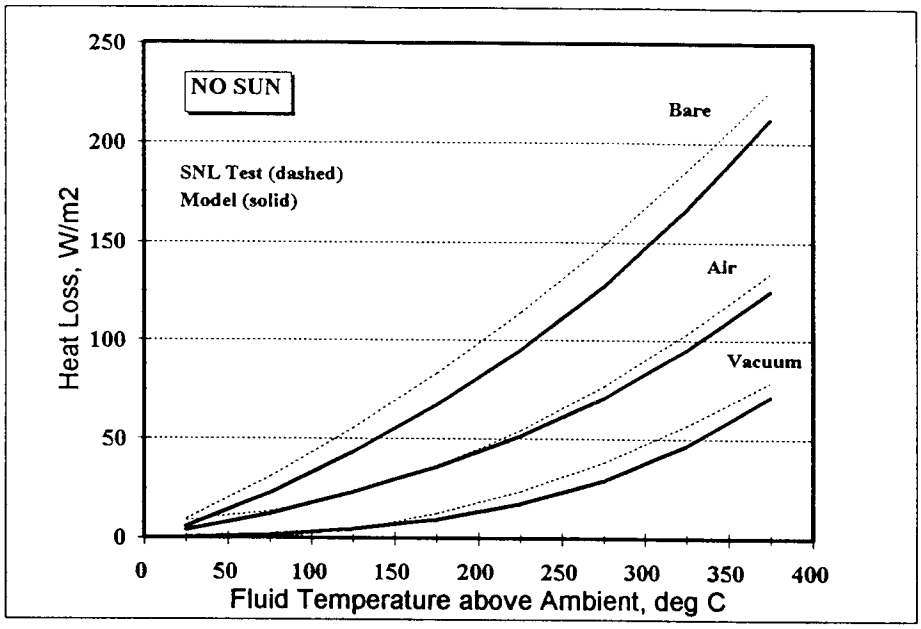

Figure 20. HCE Heat Loss: No-Sun cases.

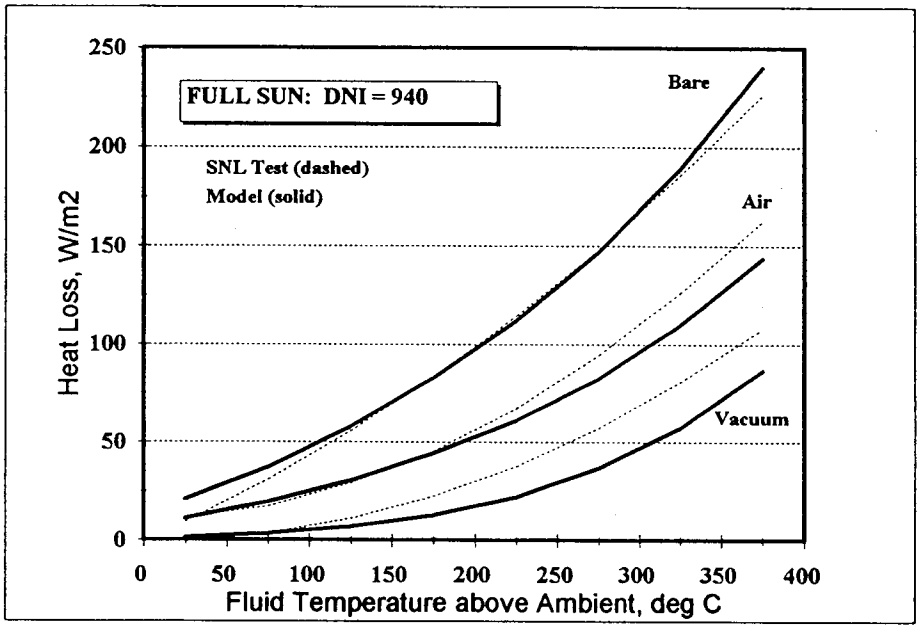

Figure 21. HCE Heat Loss: Full-Sun cases (DNI = 940 W/m^2).

Comparison of Figures 18 and 19

One reason the agreement between model and data may be better for Figure 19 than Figure 18 is because there is less uncertainty regarding the condition within the annulus for the case depicted in Figure 19. In Figure 18 it was assumed that a good vacuum existed (i.e., 10^{-4} torr). Sandia was unable to measure the actual vacuum level. As indicated in Figure 13, thermal loss is a strong function of vacuum level. If actual vacuum level was significantly worse than the assumed level, the model would underpredict losses.

Figure 20 - HCE heat losses with no sun

Figure 20 contains the information in Figures 18 and 19 supplemented by additional information for the bare annulus case. Agreement for the bare annulus case is not quite as good as for the vacuum and air cases. The bare-annulus convective heat losses are modeled as pure natural convection. Under test conditions, any wind would increase the convective losses.

Figure 21 - HCE heat losses with full sun

Figure 21 contains information analogous to Figure 20 except that the direct normal irradiance is 940 W/m^2 rather than zero. It can be seen that the vacuum/full sun case shows the greatest deviation between measured and modeled data of any of the cases presented. This case (vacuum/full sun) is particularly relevant, since it is the typical operating condition for SEGS plants.

The presence of high insolation increases the significance of proper modeling of the HTF flow internal convection. For no-sun cases, HTF temperatures are generally only a few degrees greater than absorber temperatures. The low ΔT greatly lessens the influence of HTF internal convection and its relative contribution to the overall solution to the heat loss problem. Over the range of temperatures considered in full-sun cases, HTF temperatures are about 15-50°C less than absorber temperatures - adequate to significantly influence the resulting heat loss solution. The concentric-cylinder forced-flow correlation used in the model (Dittus-Boelter equation with appropriate hydraulic diameter) is reported by Incropera and DeWitt to be valid "to a first approximation." The appropriateness and adequacy of this model is thought to contribute to the difference reflected in the vacuum case of Figure 21. The apparent agreement for bare annulus and air cases, while quite good, may stem from compensating modeling conditions rather than precise determination.

Figure 22 - Cermet emissivity measurements and associated uncertainty

Emittance Measurements in the Field

Field emittance measurements were done on the actual cermet receiver tubes tested on the rotating platform using a portable infrared reflectometer, Model DB-100, manufactured by Gier-Dunkle, Inc. This reflectometer is designed to measure the normal infrared reflectance/emittance of flat opaque samples placed over the measurement port for 100°C and 300°C blackbody radiation. Non-flat sample surfaces can be accurately measured by calibrating the instrument using a reference material and following measurement techniques detailed in reference 1. The DB-100 determines the infrared reflectance, R_{GD}(100°C or 300°C), by viewing the sample with a single thermopile detector while the surface is alternately irradiated with blackbody radiation from a

rotating split-cavity at differing temperatures. To obtain a measured value, the difference in the detector ac signal is integrated and weighted for either a 100°C or 300°C blackbody. A 300°C blackbody is approximated by placing a filter into the detector optical path. When calibrated to a known standard and correcting for the non-flat surface geometry, the measurement uncertainty should be within ±0.05 reflectance units for non-flat samples, see reference 2 (see Figure 22). For opaque surfaces, the normal DB-100 measured emittance, $\varepsilon_{N\text{-}GD}$(100°C or 300°C) is

$$\varepsilon_{N\text{-}GD}(100°C \text{ or } 300°C) = 1\ 000 - R_{GD}(100°C \text{ or } 300°C).$$

Emittance Measurements in the Laboratory

In addition to the tubes tested on the rotating platform, Sandia measured the emittance of several cermet tube sections provided by KJC. The normal emittance was determined in the laboratory with two spectrophotometers. The hemispherical reflectance properties, covering the wavelength range from 0.265μm to 2.4μm, were measured using a Beckman 5270 spectrophotometer equipped with an integrating sphere accessory. All data obtained using this instrument were referenced to NIST calibrated standard materials and corrected for the non-flat sample surface geometry. For the optical properties covering the wavelength range from 2.4μm to 22.4μm, a Perkin-Elmer Model 1800 FTIR (Fourier Transform Infrared) spectrophotometer equipped with an integrating sphere was used. By merging the reflectance spectra from the two laboratory instruments, material properties can be optically characterized over the combined wavelength range to within a measurement uncertainty of ±0.02 units for non-flat sample surfaces. Using the spectral information obtained by this method, blackbody averaged reflectance values, $R_{BB}(T)$, as a function of temperature were calculated using the expression

$$R_{BB}(T) = \frac{\int_{\lambda_{min}}^{\lambda_{max}} BB_\lambda(T)\rho_\lambda(2\pi)d\lambda}{\int_{\lambda_{min}}^{\lambda_{max}} BB_\lambda(T)d\lambda},$$

where λ_{min} = 0.265 μm, λ_{max} = 22.4 μm, $BB_\lambda(T)$ is the Planck distribution value for temperature T(°K) and wavelength λ, and $\rho_\lambda(2\pi)$ is the measured and corrected hemispherical reflectance value at wavelength λ.

Since the sample measured were opaque, the blackbody averaged normal emittance value, $\varepsilon_N(T)$ was calculated using

$$\varepsilon_N(T) = 1.000 - R_{BB}(T).$$

The calculated $\varepsilon_N(T)$ values are characterized by the "normal" designation because both laboratory instruments utilize optical arrangements that allow the measurement of the reflectance properties at near normal incident angles.

Effect of Emissivity Uncertainty on Model Validation

To gauge the effect that uncertainty in cermet emissivity has on the comparison of the model with the experimental data, the model was rerun using the upper-bound emissivity curve shown in

Figure 22. Model predictions given this upper-bound curve are indicated with dots on Figures 18 and 19. As can be seen, agreement using the upper-bound emissivity is excellent.

References

1. Pettit, R. B., "Optical Measurement Techniques Applied to Solar Selective Coatings," SAND77-0421, August 1977.

2. Pettit, R. B. and Mahoney, A. R., "Portable Instrumentation for Solar Absorptance and Emittance Measurements," SAND80-1541C, Proc Line Focus Solar Thermal Energy Tech. Dev. Conf. USDOE, Albuquerque, NM, 1980, pp 437-447.

Figure 23 - Comparison between experiment and actual SEGS conditions

Earlier in this section it was stated that the wall-to-fluid ΔT in the test loop was five times higher than in a SEGS HCE, i.e., 20°C vs. 4°C. Since the tube wall was hotter in the experiment than in an actual SEGS HCE, the thermal losses would be higher in the experiment at a given fluid temperature. To estimate how much higher, the model was rerun assuming the flow conditions in an actual SEGS plant, i.e., 140 gpm, no restricting annulus, Therminol heat transfer fluid. The results of this analysis are presented in Figure 22. By comparing the model for the experiment and the model of actual plant condition it can be seen that losses would be about 10% lower in an actual SEGS plant at a given fluid temperature than was measured in the experiment.

Comparisons of Model Predictions with Experimental Data for the Black Chrome HCEs

The experimental data was also compared with model predictions for the black chrome HCEs. Like the cermet cases, model predictions were generally within the uncertainty bands of the experiment. However, use of the base case emissivity value[2] for the black chrome (0.26 @ 300°C), gave closer agreement between model and experiment than was achieved for the cermet cases shown in Figures 18 and 19. We attribute the better agreement to the fact that the current technique we use to measure emissivity is more accurate with diffuse surfaces such as black chrome; cermet surfaces tend to be much more specular.

[2]Emissivity data presented in "Efficiency Testing of SEGS Parabolic Trough Collector," G. Cohen, et al., Proceedings of American Solar Energy Society, April 25-28, 1993, Washington, D.C.

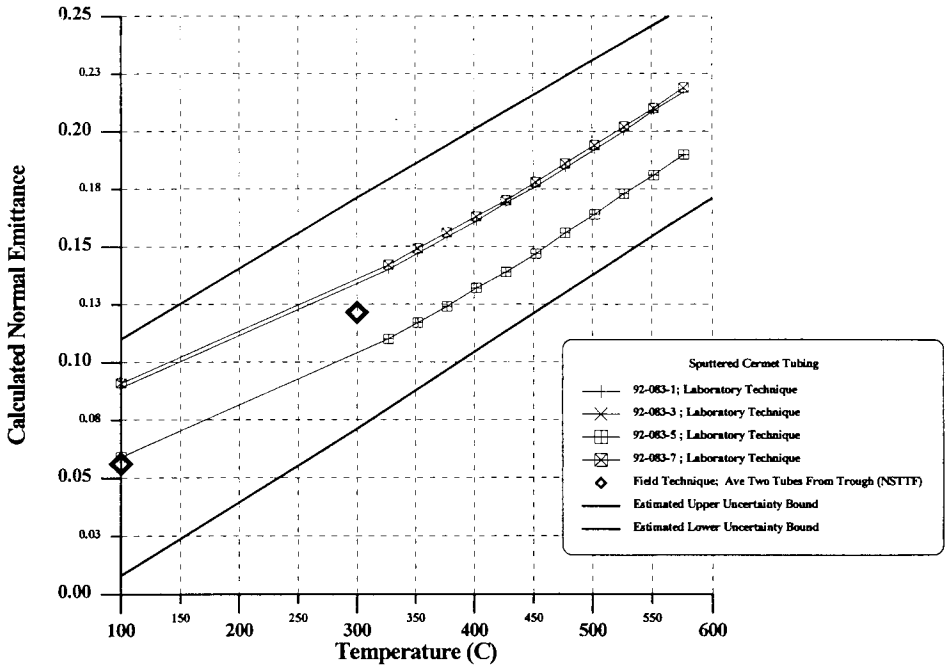

Figure 22. Cermet Emissivity Measurements and Associated Uncertainty.

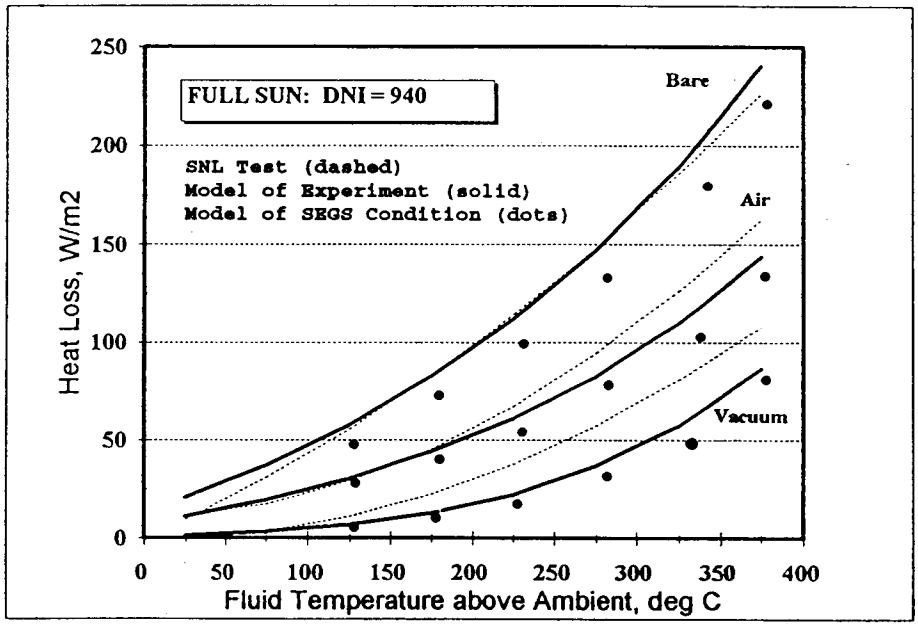

Figure 23. HCE Heat Loss: Comparison between Experiment and SEGS Conditions.

APPENDIX A

SEGS LS-2 TEST ARTICLE

Contents for Appendix A

Table

APPENDIX A: SEGS LS-2 PARABOLIC TROUGH SOLAR COLLECTOR TEST ARTICLE

A complete SEGS LS-2 solar collector assembly (SCA) module, as installed at one of the Solar Electric Generating Systems (SEGS) was much too long to fit on the AZTRAK rotating platform at Sandia Laboratories for testing. A smaller portion of one module was selected for test, consisting of a drive pylon with drive motor and computer control, one group of mirror facets, and an end support pylon. As installed at Sandia, the collector was about 8 m long, with an aperture of 39.2 m^2. A complete SCA is made up of six groups of mirror facets on each side of the drive pylon, for a total length of 47.1 m and 235 m^2 aperture. A total of 4670 LS-2 SCAs (1.097×10^6 m^2) are currently installed in several SEGS. Some SCA data are summarized in Table A-1.

Each SCA tracks the sun independently from the others in a solar field. A central computer controls startup, stow, and on initial startup, directs the SCA to move to the approximate sun position to begin optical tracking. On loss of sun or mistracking, the central computer must again direct the SCA to the calculated sun position to resume optical tracking. Each SCA reports it's current position, operating mode, and local heat-transfer fluid temperature to the central control computer.

Concentrated light from the mirror assemblies is focused on an evacuated receiver, or heat collection element (HCE). The LS-2 HCE consists of a steel tube with a black selective surface coating, surrounded by an evacuated glass tube. Glass-to-metal seals at each end of the glass envelope provide a vacuum seal. Metal bellows at each end allow for differences in thermal expansion between the glass and inner steel tube. The glass envelope has an anti-reflective coating on both surfaces; the glass protects the selective surface coating, and also serves to reduce convection and conduction thermal losses from the heated tube. The space inside the glass envelope is evacuated to further reduce thermal losses. Because hydrogen tends to migrate into the vacuum space from the heat transfer oil, special hydrogen removal devices are installed to prevent gas accumulation in the envelope.

Two different selective coatings are in use in the SEGS solar fields: black chrome and cermet. Black chrome is an electroplated coating, which is not recommended for long term use much above about 300°C, and which sometimes changes color and selective properties while in use. Cermet is a graded ceramic/metal coating developed by LUZ; it is applied by a sputtering process, and can be used up to 400°C. Cermet has superior emissive characteristics at high temperatures, and does not oxidize if HCE vacuum is lost.

Each HCE is 4 m long; two were required for the test collector installed at Sandia. Twelve are required in a normal field SCA; more than 55,000 are installed in the five SEGS fields at Kramer Junction.

Table A-1. SEGS LS-2 Parabolic Trough Solar Collector

Manufacturer:	LUZ Industries, Inc. Israel
Operating Temperature:	100-400°C
Module size:	7.8 m x 5 m (as tested at Sandia) 47.1 m x 5 m (in SEGS solar fields)
Rim Angle:	70 degrees
Reflectors:	12 thermally sagged glass panels (as tested at Sandia) 72 glass panels in SEGS solar field SCA Second-surface silvered Low Iron glass Typical reflectivity : 0.93
Aperture Area:	39.2 m^2 (as tested at Sandia) 235 m^2 (in SEGS solar fields)
Focal Length:	1.84 m
Concentration Ratio:	71
Receiver: (HCE)	Evacuated tube design, metal bellows at each end Absorber diameter: 70 mm length: 4 m (2 per module at Sandia (12 per SCA in SEGS solar fields) Pyrex glass envelope: 115 mm diameter Anti-reflective coated Transmittance: 0.95 Cermet selective surface Absorptance: 0.96 Emmitance: 0.14 @ 350°C Black chrome selective surface Absorptance: 0.95 Emittance: 0.24 @ 300°C
Sun Tracking:	Optical, restricted by computer to ±5° of sun position
Tracking Drive System:	120 vac stepping motor Direct gear box drive

APPENDIX B

TEST FACILITY DESCRIPTION

Contents for Appendix B

Figure

Table

APPENDIX B: TEST FACILITY DESCRIPTION

AZTRAK Azimuth Tracking Platform

During testing of a linear-cylindrical parabolic trough solar collector, one of the performance parameters that must be measured is the peak efficiency of the collector at zero incident angle. When the collector is mounted with a fixed East-West orientation of the trough rotational axis, zero incident angle occurs only once each day, at solar noon. If the trough rotational axis has some other orientation, such as North-South, a zero incident angle may not occur at all on some days of the year.

Because of the limited times that zero incident angles are available, completing a test series with a fixed collector orientation can be a frustrating experience. Some past tests have dragged on for months while waiting for a few days when no clouds were present during the times zero incident angles were also available. Since each test must be repeated at several different temperatures (usually 4-6) to define the operating curve, considerable wasted time is inevitable.

Another important operating parameter is the collector's performance over a range of incident angles, usually 0-60 degrees. Sufficient data to define this parameter can be even more frustrating than peak performance, since clear skies and stable insolation must be available over at least an entire half-day in order to complete the test.

The remaining parameter which must be measured is thermal loss from the collector's receiver as a function of operating temperature. Thermal loss should be measured with zero insolation incident on the receiver. Even though the collector is defocused so that no concentrated light from the reflector assembly falls on the receiver, some heat gain will still result if the direct beam from the sun can reach the receiver surface. The heat gain from unconcentrated sunlight is small, but can significantly change measured heat loss. To obtain a true measure of receiver thermal loss, the receiver must be shaded from direct sunlight.

Because the receiver exchanges infra-red energy with any object in view, it is also not possible to aim the reflector assembly at the ground in order to shade the receiver from sunlight, since the ground temperature is considerably higher than the sky temperature to which the receiver is normally exposed, and would again lead to an error in a thermal loss measurement. For the same reason, it is not possible to cover the receiver with some sort of shadow shield without changing the thermal loss properties of the receiver.

Zero incident insolation is easy if the test is done at night; otherwise it is usually difficult or impossible to accomplish during daylight hours when the test collector has a fixed orientation. The reflector structure never seems to be in the right place to shadow the receiver from incident sunlight.

All the test difficulties mentioned above can be avoided if the solar collector is on a two-axis sun-tracking mount. Since linear-cylindrical parabolic trough concentrating collectors already have a solar elevation tracking capability, only a azimuth-tracking platform is needed to complete a two-axis system. The AZTRAK rotating platform, located at the Solar Thermal Test Facility, Sandia National Laboratories, is an azimuth-tracking platform with unique capabilities for testing solar collectors.

The AZTRAK platform is microcomputer controlled, and can position a collector at zero incident angle at any hour of any day of the year. In addition, the platform can track any given incident angle from 0-90 degrees, and can be maintained for as long as necessary to obtain test data. During thermal loss testing, the collector can be aimed at the sky away from the sun, shading the receiver, while the platform tracks the sun to maintain the receiver shading.

The AZTRAK platform incorporates provisions for electrical power to an installed collector, heat-transfer fluid flow to and from the receiver, and a large variety of instrumentation lines for test instrumentation. The platform is hydraulically driven from local or remote manual control stations, or by the tracking

microcomputer. Provisions are included for automatic defocusing of the test collector and rotation away from the sun upon an overtemperature condition or if heat-transfer fluid flow is lost.

The platform construction uses large square steel beams, welded into a rectangular assembly. The platform's collector mounting surface is 4m (13.1 ft) wide and 13m (42.6ft) long. It is designed to support a collector weighing up to 3600 kg (8000 lbs) with a mirror aperture up to 50 sq m (538 sq. ft), and a center of pressure 1.8m (6ft) above the top surface of the platform. Sun tracking operation is possible in winds up to 13.4 m/sec (30 mph), and the platform is designed to support the collector in winds up to 40 m/sec (90 mph). Platform rotation is 115 degrees in either direction from true South.

Heat Transfer Fluid Supply System

Two heat-transfer fluid supply systems are available for solar collector testing on the AZTRAK platform. Domestic cold water is used for optical efficiency and incident angle testing; a specially designed hot-oil supply system is used for the elevated temperature tests.

Domestic cold water has often been used directly into the collector inlet, with only a flow-control valve needed. During the present test series, we found that the water supply pressure varied randomly due to unknown causes, producing variations in fluid flow rates, and subsequent unacceptable receiver temperature changes. The water supply also contained numerous air bubbles, which contributed to unstable flow measurements. The automatic flow-control valve was unable to maintain a constant flow rate, so a portable pump cart was moved up to supply water to the collector.

Essential components of the water pump cart are a 300 gallon water tank, a multi-stage centrifugal-flow pump, and a pressure-control valve. Water was delivered from the pump at 250 psi, and was throttled to about 100 psi at 6 gpm into the collector. Water flow from the collector was regulated by an automatic flow-control valve, then dumped to the surface; a garden hose served to keep the water tank filled. The large water tank allowed the air bubbles to separate from the water before reaching the pump. This simple system delivered extremely stable water flow rates and temperatures and was largely responsible for the excellent optical efficiency and incident angle data obtained.

The hot-oil fluid system was specifically designed for solar collector testing after considerable experience with the shortcomings of other oil systems. Vital components are a 50 gallon oil tank, centrifugal pump and drive motor, a 40 kW electric oil heater, a water-cooled heat exchanger, an oil filter, flow meters, and several control valves. Operation of the oil system is remotely controlled from the nearby data-acquisition trailer. At present, the system uses Dow Corning's Syltherm® 800 silicone-based heat-transfer fluid; other heat-transfer oils are compatible with the system and could be used if desired. Water cannot be used in this fluid-supply system.

In operation, the oil system pumps oil from the supply tank through the heater and heat-exchanger, out through the solar collector being tested, and return to the supply tank. Both automatic and manual temperature and flow control systems are provided, as well as local and remote temperature and pressure indicators. Oil is supplied to the collector inlet at temperatures from 50 to 400°C, as selected by the operator. Oil pressure at the pump outlet is about 150 psi, and is throttled to about 100 psi at the system outlet. Fluid flow rates from 1 gpm to 15 gpm are available. Figure B-1 shows a flow diagram of the high-temperature fluid loop.

Several of the fluid system's operating characteristics may appear excessive to those not familiar with the problems of solar collector testing. For example, the 20 hp fluid pump is quite large, considering that only 10-15 gpm fluid flow is needed through the collector under test. The pump actually pumps about 60 gpm at a pressure approaching 150 psi. Most of the fluid flow does not go out to the test collector, but is returned to the supply tank after passing through the heating and cooling heat exchangers. One objective of the high flow-rate through the heater, cooling heat-exchanger, and supply tank is to keep the fluid

supply extremely well stirred and uniform in bulk fluid temperature. Close temperature control is also facilitated; since the fluid temperature seen by the heater controller is always an accurate measure of fluid temperature throughout the system. Collector input temperature regulation to 0.1°C is routinely achieved.

Another objective of the large fluid pump is obtaining a highly stable fluid flow-rate through the collector. The fluid flow-control valves throttle the 150 psi pump pressure to about 20 psi at the collector inlet. Fluid flow stability to 0.1 gpm is normally achieved. Constant fluid flow is ultimately a major factor in temperature stability of the test collector.

Fluid temperature control over a wide temperature range by using either a fluid heater or cooler alone is inherently less precise than using both together. For example, at a low operating temperature, the temperature controller will have difficulty getting small amounts of heat from the large electric heater. Thermal losses will be low, resulting in very slow correction rates is the temperature setpoint is overshot by the controller. The problem is a very high rate of response to a temperature below the setpoint, and a very slow rate of response to a temperature above the setpoint.

At the highest operating temperatures, the control problem is exactly reversed. Only a very small amount of cooling will be needed, as thermal losses from the entire heated system may dissipate most of the heat input. The cooling controller may find it impossible to open the cooling water valve by a small enough amount to achieve the required small amount of fluid cooling.

The temperature control scheme incorporated into this high temperature fluid loop is the nearly continuous use of simultaneous heating and cooling. For a given operating temperature, the fluid loop and the collector are first allowed to reach a rough state of temperature equilibrium under automatic control. The control system is set such that the cooling heat exchanger is always dissipating slightly more heat than is produced by the collector being tested. The cooling control is then placed under manual control so that the amount of cooling cannot change. The fluid flow-rate controller is also switched to manual control to improve flow stability. This procedure leaves the heater temperature as the only variable in the system. The heater is thus forced to always operate near the middle of its control range, with a continuous requirement for added heat. Some experience with the fluid loop is needed by the test operator, in order to judge the amount of cooling to use at various operating temperatures.

Examples of the fluid flow and temperature stability achieved can be seen in the test results section of this report.

References

Solar Thermal Test Facility, 1992. NSSTF OP #038, *Operating Procedure for AZTRAK Rotating Platform.* Albuquerque, N.M.: Sandia National Laboratories.

Solar Thermal Test Facility, 1992. NSSTF OP #039 *Operating Procedure for High Temperature Fluid Loop.* Albuquerque, N.M.: Sandia National Laboratories.

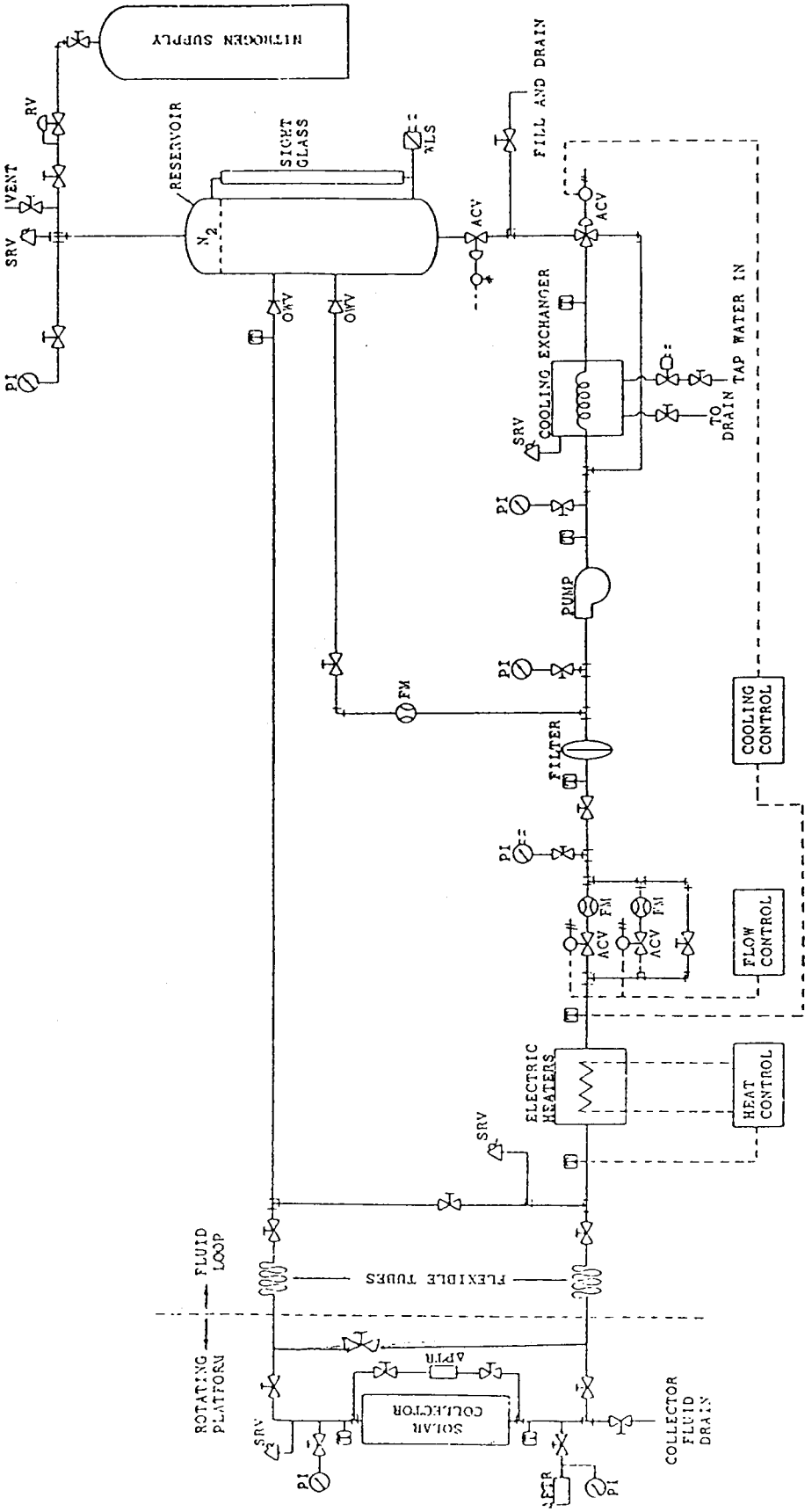

Figure B-1. Schematic of High Temperature Fluid Supply Loop.

Test Instrumentation

Data Acquisition System

The data acquisition system used was based upon a Hewlett Packard 9845B desktop computer. Instrumentation channels were scanned with an HP3497A data acquisition unit, and the analog signals were then measured with an HP3526A digital voltmeter. The accuracy of the voltmeter is better than 0.01%. Voltage measurements were converted to engineering units, recorded on a hard disk, and selected data items were printed and displayed for the test operator. Each day's data file was later transferred to floppy disk for permanent archive. Data was normally measured and recorded at 15-20 second intervals during a test.

Table B-1 lists the test data items included in the data files, the transducer used to measure the item and the data acquisition system channel numbers used for the measurement. Many of the recorded data items are calculated from other measured data.

Heat Transfer Fluid Flow

Both domestic water and Dow Corning's Syltherm-800® were used as heat transfer fluids. Fluid flow was measured by two Flow Technology turbine flow meters installed near the collector fluid inlet. Flow Technology Pulse Rate Converters were used to convert the voltage pulses from the flow meters to a 0-5 volt signal, which was then read by the data acquisition system. When high temperature Syltherm-800® oil was being used, an additional two flow meters measured the oil flow leaving the fluid loop skid. Calibration of these flow meters was performed by Flow Technology immediately before beginning the test series, and their calibration was confirmed to be within 1% by using a bucket and stopwatch during the water tests.

Fluid Property Calculations

Equations for the properties of water were obtained by polynomial fits to data from Keenan & Keyes (Ref. 1). Sufficient terms were included to provide agreement within 0.2% over the range of temperatures used.

Equations for the properties of Syltherm-800® heat transfer fluid were supplied by Dow Corning (Ref. 2). Accuracy of these equations is not specified. Density, specific heat, viscosity, and Reynolds number were calculated for each flow measurement data point. All the calculated data was recorded as part of the collected test data.

Temperature

Temperature data was measured using type T thermocouples. Some additional illuminated surface temperatures were measured using type K. To obtain the best accuracy possible, a number of type T thermocouples were compared by Sandia's Standards Lab; two pairs were selected from the lot which were within 0.1-0.2°C over the temperature range 0-400°C. These two pairs were used to determine the input and output temperatures of the heat transfer fluid. An additional thermocouple was installed at the flow meters for temperature input to fluid property calculations.

Tracking Angle

Collector elevation tracking angle was measured with a Humphrey model CP-49 pendulum potentiometer mounted on the collector. The resolution of the potentiometer is 0.1 degrees. Linearity of the instrument is 1%, with a hysteresis of 0.4 degrees. The accuracy of this potentiometer is not sufficient to exactly

quantify the tracking accuracy of the collector, but it can show mistracking and any large errors. A six-wire voltage ratio measurement was made to prevent any temperature related inaccuracies.

The azimuth tracking angle of the AZTRAK platform (which determines the azimuth angle of the collector rotational axis) is controlled by a microcomputer as required by an individual test objective. The angle was measured by a 10-bit BEI optical shaft encoder, which has a resolution of 0.35 degrees. Calculated azimuth and elevation of the sun, calculated tracking and incident angles, and measured collector positions were included in the data files.

Weather Data

Solar energy input to the collector was measured with an Eppley Normal Incidence Pyrheliometer calibrated against a Kendall secondary standard, active cavity radiometer. Accuracy of the pyrheliometer is 2% of reading, including uncorrected temperature effects. Wind speed and direction at the test site was measured by a Weathertronics instrument, located at 10 m elevation about 30 m west of the installed collector. Ambient air temperature was measured with a type T thermocouple in a shaded enclosure.

References

Keenan, J H., Keys, F. G., Hill, J. G., Moore, J. G. 1978. *Steam Tables.* New York: Wiley-Interscience.

Dow Corning Corporation, 1985. *Properties of Syltherm 800 Heat Transfer Liquid.* Midland, Michigan.

Table B-1. Data Menu For SEGS LS-2 on AZTRAK Platform

Menu #	Chan #	Slot #	Transdu	Description			(Units)
401				Test system number	(#4, SEGS LS-2 trough on Aztrak)		
402			Clock	Date of test	(Menu revised 29 Jun 92)		
403			Clock	Mountain Standard Time			(HH:MM:SS)
404			Calc	Site Solar time			(HH:MM:SS)
405			Calc	Collector solar time			(HH:MM:SS)
406	021	S01	NIP	Direct normal insolation			(W/m^2)
407	372	S23	TCamb	Ambient air temperature			(Deg C)
408	023	S01	WS100	Wind speed			(m/s)
409	024	S01	WD100	Wind direction			(degrees CW from North)
410	305	S20	AZ100	Platform Azimuth	(Degrees from South, +East, -West)		
411	306	S20	FT100	Collector flow #1			(L/min)
412	307	S20	FT101	Collector flow #2			(L/min)
413	308	S20	FIC 1A	Fluid loop high flow			(L/min)
414	309	S20	FIC 1B	Fluid loop Low flow			(L/min)
415	310	S20	IN100	Inclinometer Voltage Ratio			
416	311	S20	IN100	Collector elevation Inclinometer			(Deg above horizon)
417	312	S20	PDI 6	Collector delta pressure			(kPa)
418	313	S20	PI3	Collector Inlet pressure			(kPa)
419	314	S20	Manual	Water / Oil Test?		1 = Water,	0 = Oil
420	315	S20	Spare				
421	316	S20	Spare				
422	317	S20	Spare				
423	318	S20	TC1/10	Collector Diff. Delta-T Volts #1		(TC 01/TC 10)	(mv)
424	319	S20	TC2/09	Collector Diff. Delta-T Volts #2		(TC 02/TC 09)	(mv)
425	360	S23	TC001	Collector inlet temperature #1			(Deg C)
426	361	S23	TC002	Collector inlet temperature #2			(Deg C)
427	362	S23	TC003	Spare T-Type Thermocouple #3			(Deg C)
428	363	S23	TC004	Spare T-Type Thermocouple #4			(Deg C)
429	364	S23	TC005	Spare T-Type Thermocouple #5			(Deg C)
430	365	S23	TC006	Spare T-Type Thermocouple #6			(Deg C)
431	366	S23	TC007	Spare T-Type Thermocouple #7			(Deg C)
432	367	S23	TC008	Flowmeter temperature			(Deg C)
433	368	S23	TC009	Collector Outlet temperature #2			(Deg C)
434	369	S23	TC010	Collector Outlet temperature #1			(Deg C)
435			Calc.	Average Receiver Temperature		(TC #1)	(Deg C)
436			Calc.	Average Receiver Temp above ambient		(TC #1)	(Deg C)
437			Calc.	Solar azimuth	(Degrees from South, +East, -West)		
438			Calc.	Solar elevation			(degrees above horizon)
439			Calc.	Solar Incident angle			(degrees from normal)
440			Calc.	Solar tracking angle			(degrees above horizon)
441			Calc.	Collector delta-T	(Diff. dT #1)	(TC 01/10)	(Deg C)
442			Calc.	Collector delta-T	(Sub. dT #1)	(TC 01/10)	(Deg C)
443			Calc.	Mass flow		(Flowmeter temp)	kg/hr)
444			Calc.	Heat gain	(Diff. dT #1)	(TC 01/10)	(W/m^2)
445			Calc.	Heat gain	(Sub. dT #1)	(TC 01/10)	(W/m^2)

Table B-1. Data Menu for SEGS LS-2 on AZTRAK Platform (Concluded)

Menu #	Chan #	Slot #	Transdu	Description	(Units)
446			Calc.	Efficiency (Diff. dT #1) (TC 01/10)	(%)
447			Calc.	Efficiency (Sub. dT #1) (TC 01/10)	(%)
448			Calc	Density of Heat Transfer Fluid	kg/m^3)
449			Calc.	Specific Heat of Heat Transfer Fluid	(J/kg °C)
450			Calc.	Viscosity of Heat Transfer Fluid	(N sec/m^2)
451			Calc.	Reynolds Number, Collector HTF flow	(Thousands)
452			Calc.	Mirror Aperture of Collector under test	(m^2)
453	380	S24	TC011	Receiver K Thermocouple #1	(Deg C)
454	381	S24	TC012	Receiver K Thermocouple #2	(Deg C)
455	382	S24	TC013	Receiver K Thermocouple #3	(Deg C)
456	383	S24	TC014	Receiver K Thermocouple #4	(Deg C)
457	384	S24	TC015	Receiver K Thermocouple #5	(Deg C)
458	385	S24	TC016	Receiver K Thermocouple #6	(Deg C)
459	386	S24	TC017	Receiver K Thermocouple #7	(Deg C)
460	387	S24	TC018	Receiver K Thermocouple #8	(Deg C)
461	388	S24	TC019	Collector Outlet Temp - K TC # 9	(Deg C)
462	389	S24	TC020	Syltherm tank Sight Gage TC - Bottom	(Deg C)
463	390	S24	TC021	Syltherm tank Sight Gage TC - Mid	(Deg C)
464	391	S24	TC022	Loop Cooling Water - Output temp	(Deg C)
465			Calc.	Collector delta-T (Diff. dT #2) (TC 02/09)	(Deg C)
466			Calc.	Collector delta-T (Sub. dT #2) (TC 02/09)	(Deg C)
467			Calc.	Heat gain (Diff. dT #2) (TC 02/09)	(W/m^2)
468			Calc.	Heat gain (Sub. dT #2) (TC 02/09)	(W/m^2
469			Calc.	Efficiency (Diff. dT #2) (TC 02/09)	(%)
470			Calc.	Efficiency (Sub. dT #2) (TC 02/09)	(%)
471			Calc.	Tracking Error - (#440 - # 416)	(Deg)
472			Calc.	Efficiency (#447, corrected for end loss)	(%)

APPENDIX C

TEST PLAN

Contents for Appendix C

Figures

APPENDIX C: TEST PLAN

The operating characteristics of a concentrating parabolic trough solar collector can be determined with only a few selected tests. These are:

- Measure peak efficiency at several elevated temperatures.
- Measure peak efficiency at near-ambient-air temperature.
- Measure receiver thermal loss as a function of temperature.
- Measure collector performance as a function of incident angle.

Peak efficiency of a concentrating solar collector can be determined only when the solar beam incident angle is zero. For single-axis tracking devices such as the LS-2 parabolic trough collector, zero incident angles usually occur only once per day if the rotational axis is oriented East-West; or twice per day if the axis is oriented North-South, as it is in the Solar Electric Generating Stations (SEGS). To allow continuous testing at any desired incident angle, the test collector was mounted on the AZTRAK rotating platform. For details on this device, see Appendix B.

All the calculations for heat gain or loss from an operating hot fluid system assume that the system is in equilibrium -- constant fluid flow-rate, and constant input and output temperatures. If equilibrium has not been established, then heat is either being stored in the system, or heat is being extracted from the system. In either case, calculations of heat gain or loss will not be correct. Because of the absolute necessity for highly stable flow and temperatures, a special hot-fluid supply source was used for the SEGS collector tests. For details on the Sandia high-temperature fluid loop, see Appendix B.

Even with a stable temperature source, long operating times are still necessary before all parts of the heated system are at their equilibrium temperatures. A time-constant test was performed to determine the time necessary to achieve temperature stability (see Figure D-2, Appendix D). Time to reach temperature stability was longer than normal for the SEGS LS-2 collector as installed for testing because an inner plug tube had to be inserted inside the receiver tube. The internal plug was necessary to restrict flow to a small annulus in order to achieve acceptable Reynolds numbers with the fluid flow-rates available from the test fluid loop. The internal plug was filled with the heat transfer fluid, but was closed at one end; so the internal fluid mass was heated only by conduction from the outer annulus. After nearly an hour at a given temperature setpoint, the system would settle down to variations on the order of 0.1°C. Heat gain/loss measurements were then deemed stable enough to be believed, and a data set was recorded for a time equal to about three collector time-constants.

Peak Efficiency Measurements

Measurements of zero-incident-angle efficiency were made with the heat-transfer fluid at approximately ambient-air temperature, and at approximately 50°C intervals up to 400°C. Data was continuously recorded at 15-20 sec intervals while the system was in operation. Each data point listed in the data tables in Appendix D, and shown in the performance figures is the mean of all data measured over a time span of about three collector time-constants. Objective of each data set was stability of all variables that could cause significant changes in the desired measurements. Stability objectives for the three-time-constant data collection interval were:

- Fluid temperatures constant to about 0.1°C (±0.05°C).
- Fluid flow-rate constant to about 0.2 L/min. (± 0.1 L/min)
- Insolation constant to about 1%.

Performance measurements made within the system stability limits listed above produce data that is repeatable from day to day, with stability induced errors that are within the combined measurement errors of the instruments in the data acquisition system. The same stability criterion was applied to all data measurements made on the collector under test.

The near-ambient-air temperature measurement was used to define the approximate optical efficiency of the collector. The higher-temperature efficiency measurements document the decrease in efficiency caused by increasing thermal losses as the operating temperature is increased. Data from all the efficiency measurements were used in a least-squares curve fit to obtain a performance equation of efficiency vs temperature under bright sunshine, zero incident angle, stable temperature and flow conditions.

Procedure for Efficiency Measurement (Elevated Temperature)

Inlet temperature to the collector was set to a constant value, such that the output temperature would approximate the desired test temperature. The exact temperature achieved was not important; but temperature stability was extremely important during these tests.

Heat-transfer fluid flow was set to a constant value (usually the maximum obtainable for these tests). As for temperature, the exact flow-rate value was not very important; but flow stability was extremely important, because any change in fluid flow-rate would also cause changes in collector temperatures.

For the series of peak efficiency measurements, it is highly desirable for all the measurements to be made at the same level of solar irradiance. If the individual efficiency test points are obtained with a solar irradiance that differs more than about 100 W/sq.m between points, data extrapolation to other operational conditions will be less accurate. The solar irradiance levels during the efficiency tests should also be as high as are available at the test site. This last requirement essentially eliminates very-early-morning and late-afternoon efficiency tests. These hours are more profitably used for thermal loss testing.

Procedure for Efficiency Measurement (Near-Ambient-Air Temperature)

The objective of this test was to determine approximate optical efficiency for the SEGS collector. True optical efficiency could be measured only if thermal losses from the collector system could be reduced to zero.

Zero thermal loss cannot be achieved during an in-focus test of a real solar collector, but a close approach can be made by operating the system at a low temperature as close as possible to the ambient air temperature.

Since the oil supply fluid loop could not be operated at temperatures much below 60°C, another source of heat-transfer fluid was needed. City water direct from local supply mains was used; see Appendix B for a description of the water supply system. Note that water flow was restricted to the collector only; no water was introduced into the oil supply system.

Ideally, water flow through the system would be adjusted such that the average temperature of the collector's receiver was approximately equal to local ambient air temperature. Because of the limited flow-rates and temperatures of the available water, this was not always possible. We used the closest approximation obtainable.

Two test results were needed from the tests performed with cool water:

1. Peak efficiency at zero incident angle.

2. Efficiency variation with incident angles up to about 60 deg.

Given a cloud-free sky, data satisfying both test criteria were usually obtainable during a single test day.

Incident Angle Modifier Tests

Measured efficiency of a parabolic trough collector decreases as the solar beam incident angle increases. Collector efficiency is at a maximum only when the incident angle is zero. The decrease in collector efficiency with increasing incident angle is caused by cosine foreshortening of the collector aperture as well as other effects, such as the transmissivity of the glass envelope or the absorption of the selective surface as a function of incidence angle. Losses caused by the finite length of the collector (i.e., end losses) were eliminated from the test results; in effect, the results presented here assume a collector with infinite length.

The object of the incident angle modifier test was documenting efficiency as a function of incident angle. Efficiency data was usually measured at 5 degree intervals from zero to 60 degrees incident angle. The AZTRAK rotating platform was used to maintain each selected constant incident angle for as long as necessary to obtain stable data. The incident angle modifier K is defined as the efficiency at any given angle divided by the efficiency at zero incident angle. A regression analysis of the data was then used to obtain an equation of the form:

$$K = \cos(A) - B(A) - C(A)^2 \quad (1)$$

Where:

K = Incident angle modifier; value ranges from 0 to 1
A = Solar beam incident angle (0 to 60 degrees)
B = Coefficient for linear term
C = Coefficient for nonlinear term

As noted in the previous section, incident angle data was measured with cold water as the heat-transfer fluid, in conjuction with testing for optical efficiency. Equation (2) above is not intended as a physical model of incident angle effects; instead it is an empirical fit from test data that successfully characterizes the collector.

If the collector and it's sun-tracking system were perfectly symmetrical, the incident angle modifier would be the same for both positive and negative incident angles. As installed at Sandia for testing, the SEGS LS-2 collector module was not exactly symmetrical because of a small shadowed area at one end of the receiver at zero incident angle. With positive incident angles, the shadow moved off the receiver within a few degrees; but at negative incident angles, the shadow became a larger and larger fraction of the illuminated receiver length as the angle increased. This nonsymmetrical behavior was peculiar to the test installation, and was not representative of the full collector field at the SEGS power plants. Also, except for a short time just after sunrise and just before sunset during mid-summer, incident angles at the SEGS collector fields are always positive.

The SEGS collectors are normally installed with the rotational axis oriented North-South in order to maximize power production during the summer months. In such an installation, collector rotation to follow the sun is always clockwise (as seen from North end of collector row). As a result, the tracking system was not designed to track the sun with a counter-clockwise rotation, as would be required for sun tracking during the afternoon (and at negative incident angles) in our test installation. This tracking problem could be fixed with the proper software changes to the tracking computer, but was not considered very important, since it would never occur in a normal field installation.

For the reasons outlined above, only positive incident angle test results are shown in this report. Test data obtained is shown in Tables 12 and 13 in Appendix D.

Thermal Loss Tests

Objective of the thermal loss test series was determination of steady-state heat losses from the collector receiver as a function of operating temperature. Losses were expected to be significantly different for each of the receiver configurations. Loss tests were therefore repeated with a vacuum in the receiver annulus, with air in the annulus, and again with the receiver cover glass completely removed. Since the black chrome and cermet receiver selective coatings had different emissivity values, all of the tests (except bare receiver tube) were also repeated for each of the two coatings.

Good thermal loss data is more difficult to obtain than heat gain (efficiency) data, because the temperature change across the collector receiver is smaller by as much as an order of magnitude. But the measuring instrument errors, temperature instabilities and flow variations remain about the same; therefore the possible errors in the loss measurements are larger.

The three components of thermal loss (conduction, convection and radiation losses) are changed in different ways depending on the receiver's configuration and operating conditions. When a vacuum is present in the annulus between the receiver surface and the glass envelope, conduction and convection across the annulus is effectively eliminated. When air is introduced into the vacuum space, we expected the measured losses to increase significantly as conduction and convection begin to transfer heat to the glass envelope. Radiation loss from the heated receiver surface to the glass envelope is not changed very much by the presence of air in the annulus. Since the glass is opaque to the infrared radiation, all three loss components serve to transfer heat from the receiver surface to the glass envelope. A second loss series then transfers heat by convection and conduction from the glass to the ambient air, and by radiation to the sky.

Surface temperature of the glass is significantly lower than the receiver's metal surface. If the glass envelope is removed, conduction and convection losses to the ambient air will be greatly enhanced, and wind effects will be much larger. Radiation losses will also increase when the glass is removed because of the higher temperature radiating surfaces.

Thermal loss from radiation effects is a problem for solar collector testing, because radiation loss is not necessarily dependent on ambient air temperature in the same way as conduction and convection losses. Some of the heat radiated by the collector's receiver is focused back in the direction the reflector is aimed, so temperature of the aim point becomes a factor in the radiation loss.

Temperature of the ground surface or other nearby objects is certain to be different (usually higher) than the sky temperature. Since the collector is always aimed at the sky when in operation, only a sky aim-point is suitable for reasonably accurate test results. Effective sky temperature is also changed by the presence of clouds; thermal loss tests made with an overcast sky show lower losses than those made with a clear sky. For our test purposes, the sky temperature was unknown, but is probably always lower than the ambient air temperature around the collector. A true measure of receiver thermal loss with zero contribution due to direct or scattered light absorption by the receiver can be obtained by aiming the reflector at a clear sky, at night. Other tests have also shown that an equivalent loss value occurs during more normal daylight hours when the receiver is shaded from direct sunlight and the reflector is aimed at a clear sky. (See Ref. 1, SAND 83-0984).

The receiver must be shaded from direct sunlight because the receiver surface would absorb energy equivalent to that from a non-concentrating collector with an aperture area equal to that of the receiver surface. This small amount of absorbed energy is not negligible when compared to the receiver thermal loss.

Since the measured temperature drop across the receiver can be quite small during some loss tests (less than 1°C), a test operator may wish to reduce fluid flow rates from normal in-focus flow values in order to increase the delta-temperature. But changing fluid flow will introduce another error, because fluid pressure drop across the receiver is converted to heat, which tends to cancel some part of the thermal loss. Therefore, for minimum thermal loss error, the same fluid flow rates used for efficiency testing must also be used during loss tests. In this respect, the LS-2 tests at Sandia do not exactly reproduce thermal losses of this collector in a field installation, because fluid flow rate was not the same, and receiver configuration was not the same (added plug tube inside the receiver). Both these receiver changes could change fluid pressure drop through the receiver.

Thermal loss from the SEGS collector receiver was measured at approximately the same temperatures used for peak efficiency measurements. As in all the tests, an exact value of temperature was not important; stability of fluid temperature and flow rate were the most important criteria for the test. The following test conditions were established for the loss tests:

- Clear or nearly clear sky.
- Collector defocused.
- Receiver shaded, reflector aimed at the sky.
- Losses measured at approx. 50°C intervals, 100-350°C.
- At each temperature, the system was operated until temperatures were stable to within about 0.1 °C over a measurement period equal to about three receiver time constants. At least one hour was usually required to achieve temperature stability.
- Tests were repeated for each receiver configuration:

  Cermet selective coating:

  Vacuum in annulus
  Air in annulus
  Bare receiver

  Black chrome selective coating:

  Vacuum in annulus
  Air in annulus

Test Data Analysis

Figure C-1 illustrates some of the factors that result in the operating heat gain (or efficiency) of a solar collector. By measuring collector efficiency at a low enough temperature, thermal losses will be reduced to zero (or at least a very small value), and we can determine the approximate optical efficiency. At any given higher operating temperature, we should be able to measure total thermal losses, subtract these losses from the heat gain at optical efficiency, and end up with the operating heat gain at the new temperature. Or alternatively, we should be able to measure heat gain (efficiency) at some high temperature, and derive the losses by the decrease in heat gain from that expected at optical efficiency. We will soon find out that the real collector is not that simple.

Figure C-2 shows what actually happens when we make some loss measurements. Measured thermal loss in Figure C-2 is that measured with the receiver shaded, at approximately zero incident sunlight. The "in-focus" curve is derived by calculating the heat gain difference between the operating efficiency and the measured optical efficiency. In Figure C-2, the in-focus loss resulted from tests at an average value of 940 W/m^2 insolation. Tests at other insolation values result in different in-focus loss curves. Tests which were done over a large range of incident solar irradiance have shown that the operating thermal loss scales approximately linearly between zero and 1000 W/m^2 insolation (see Ref. 1).

In a thermal loss test where the receiver is shaded from direct sunlight, the receiver surfaces are slightly cooler than the heat-transfer oil inside the receiver pipe. When the collector is in focus, the receiver surfaces are hotter than the oil inside the receiver. This surface temperature difference scales with the value of incident insolation, and since thermal losses depend on the surface temperature , this is the cause of the in-focus loss differences outlined above. We can take advantage of the loss scaling to calculate the performance of the collector at any value of insolation. For an accurate prediction of solar field heat output, solar irradiance changes must be considered, since insolation changes by about a factor of three on nearly every day the field is in operation.

A multiple linear regression of calculated heat gain over the range of insolation from zero to 1100 W/m^2, and temperatures from ambient to 400°C produces a heat gain equation of the following form:

$$Q = A(I) - B(I)(\Delta T) - C(\Delta T) - D(\Delta T^2) \quad (2)$$

Where:

Q = Operating heat gain (W/m^2) at zero incident angle

ΔT = Average fluid temperature (°C) above ambient air temperature

I = Direct normal insolation (W/m^2)

Equation (2) is valid only at zero incident angle. An incident angle modifier term must be added to obtain collector heat gain at any other incident angle. Since the end effect of incident angle is to reduce the value of insolation arriving at the receiver absorber surface, the incident angle modifier K, can be applied to the insolation in the first two terms of equation (2):

$$Q = K[A(I) - B(I)(\Delta T)] - C(\Delta T) - D(\Delta T^2) \quad (3)$$

When the heat gain from equation (3) is divided by the incident insolation, an efficiency equation for the collector results, which should be valid over the full expected range of operating temperature, insolation, and incident angles.

$$\eta = K[A - B(\Delta T)] - C(\Delta T/I) - D(\Delta T^2/I) \quad (4)$$

Equations (2), (3), and (4) are not complete physical models of the collector; rather they are empirical fits to experimental data. Equations like (4) have been used to predict all-day, steady state thermal output from small solar collector fields to within about 1% (see Ref. 2 and 3). Note that the equation is valid only for steady state operation; other calculations must be made to include the thermal mass and heat capacity of the collector field and other equipment, if the result is to correctly reflect the collector field during warmup and the temperature variations of a typical intermittently cloudy day.

Figure C-3 illustrates Equation (4) as derived from the test data for the LS-2 cermet/vacuum receiver,for several values of direct normal insolation. For temperatures up to about 200°C, the drop in operating

efficiency is reasonably small as insolation is reduced. For normal LS-2 operating temperatures near 400°C, the change in efficiency with decreasing insolation becomes increasingly important.

Figure C-4 shows another way to plot the complete range of Equation (4) for the SEGS LS-2 collector, with a cermet and vacuum receiver, at a zero incident angle. Collector efficiency decreases along a hyperbolic path as insolation is reduced, and along a quadratic polynomial path with increases in temperature. A small "floor" area is visible, where heat gain is zero or negative. The floor defines combinations of temperature and insolation where positive heat gain in not possible.

Figure C-5 illustrates the same collector equation, but now for an incident angle of 55 degrees, which would occur in mid-December for the SEGS collector fields. At this incident angle, the heat gain available from the collector is marginal for almost all combinations of temperature and insolation.

References:

Dudley, V. E., and Workhoven, R. M., 1982. SAND81-0984, *Performance Testing of the Solar Kinetics T-700 Solar Collector.* Albuquerque, N.M.: Sandia National Laboratories.

Cameron, C. P., and Dudley, V. E., 1986. SAND85-2316, *Acurex Solar Corporation Modular Industrial Solar Retrofit Qualification Test Results.* Albuquerque, N. M.: Sandia National Laboratories.

Cameron, C. P., and Dudley, V. E., 1986. SAND85-2320, *Solar Kinetics, Incorporated Modular Industrial Solar Retrofit Qualification Test Results.* Albuquerque, N. M.: Sandia National Laboratories.

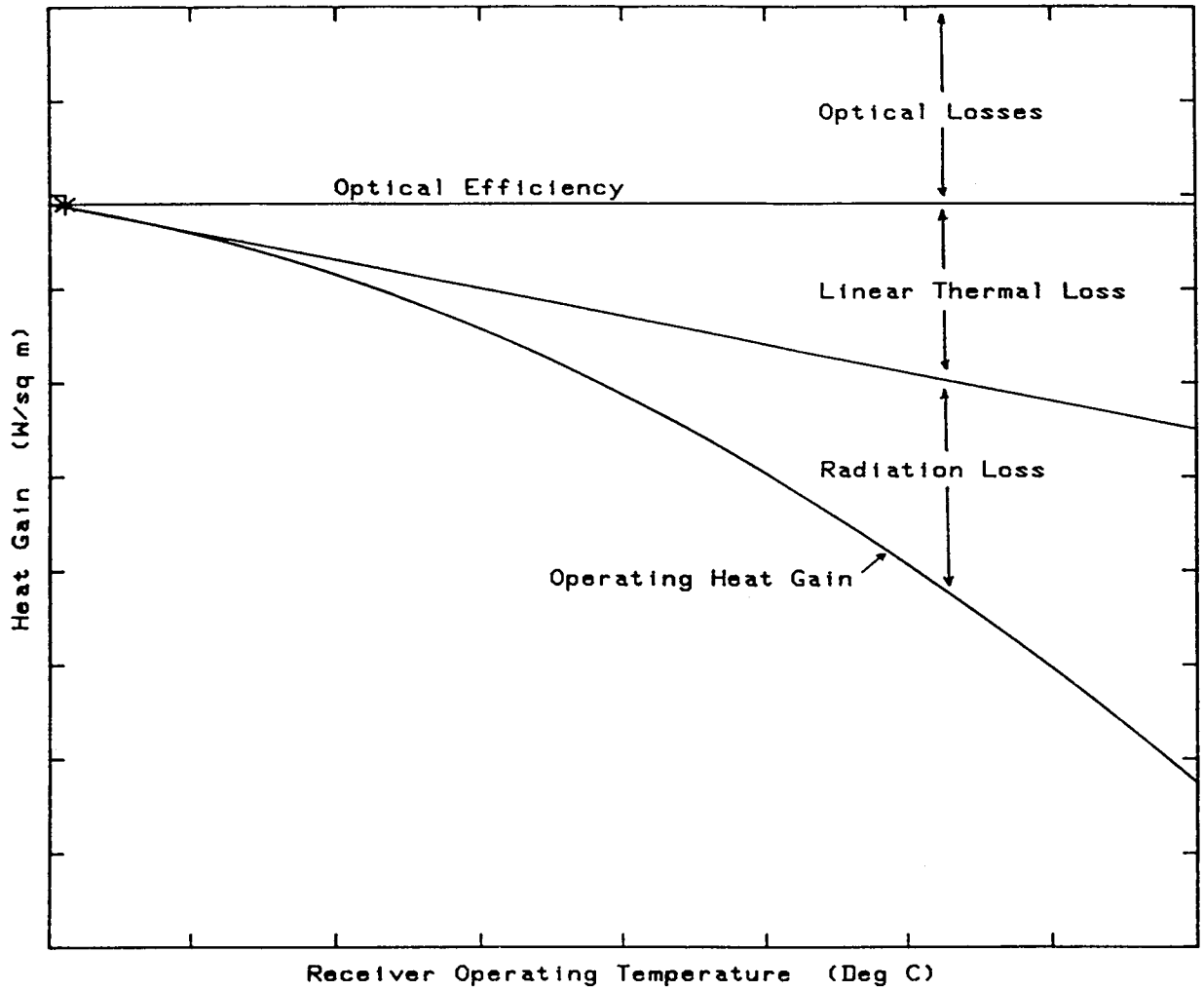

Figure C-1. Ideal Receiver Heat Gain and Losses

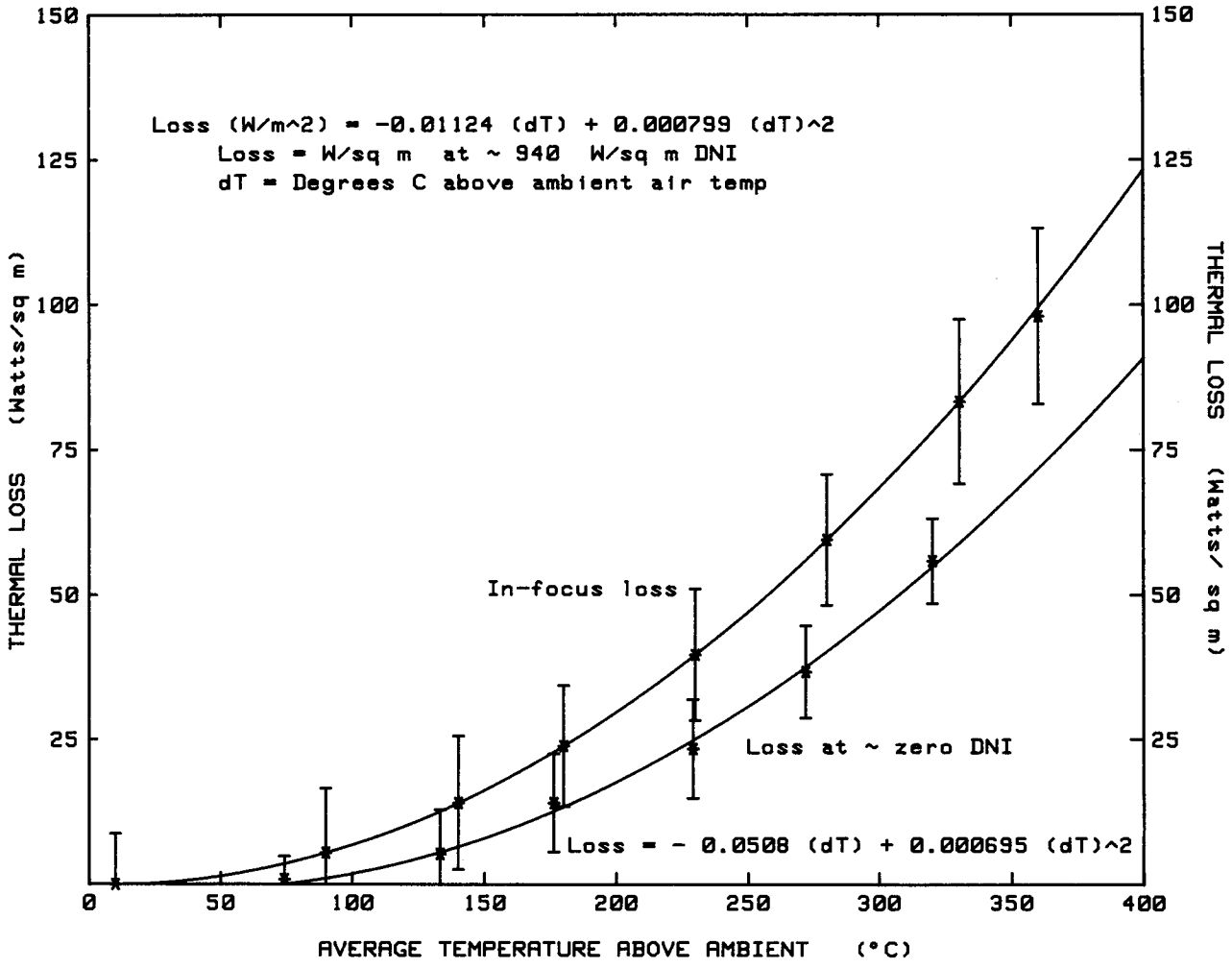

Figure C-2. LS-2 Cermet/Vacuum Receiver Thermal Loss.

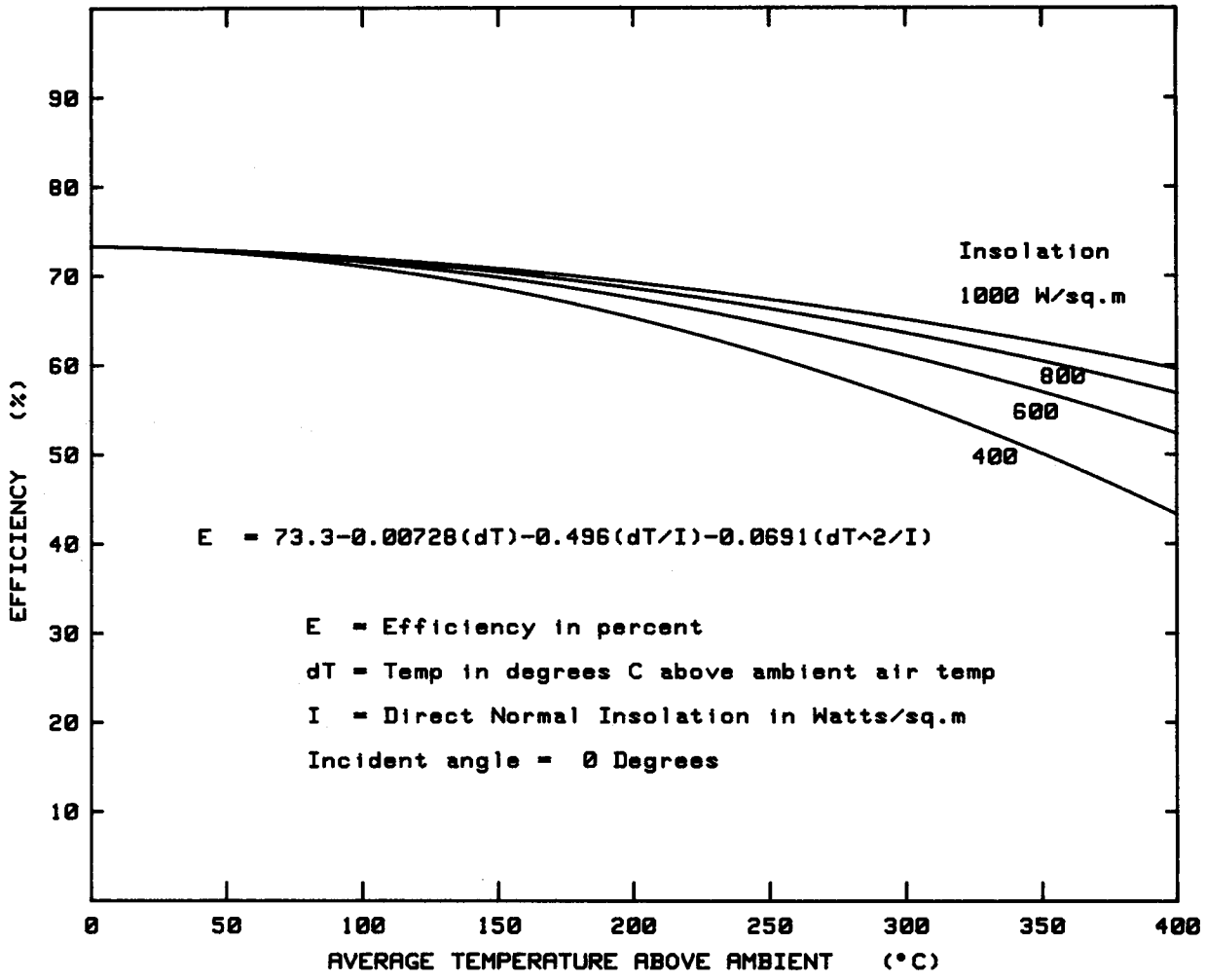

Figure C-3. SEGS LS-2 Cermet/Vacuum Receiver vs. Temperature and Insolation.

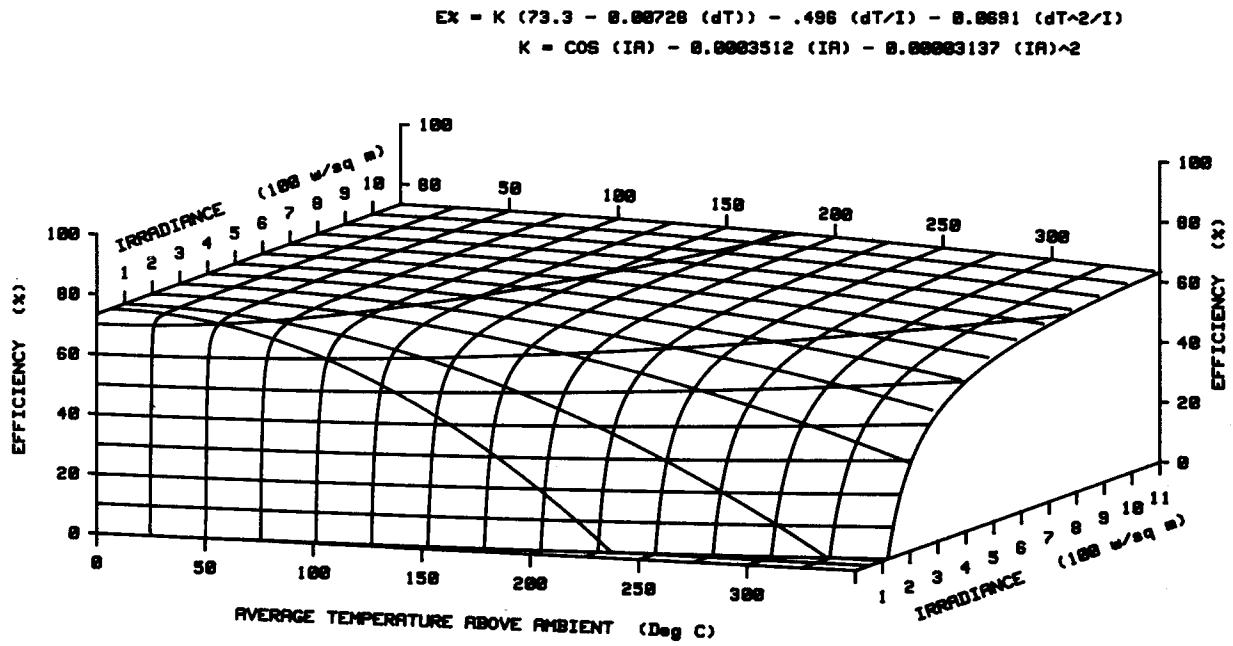

Figure C-4. SEGS LS-2 Cermet/Vacuum Efficiency at Zero Incident Angle.

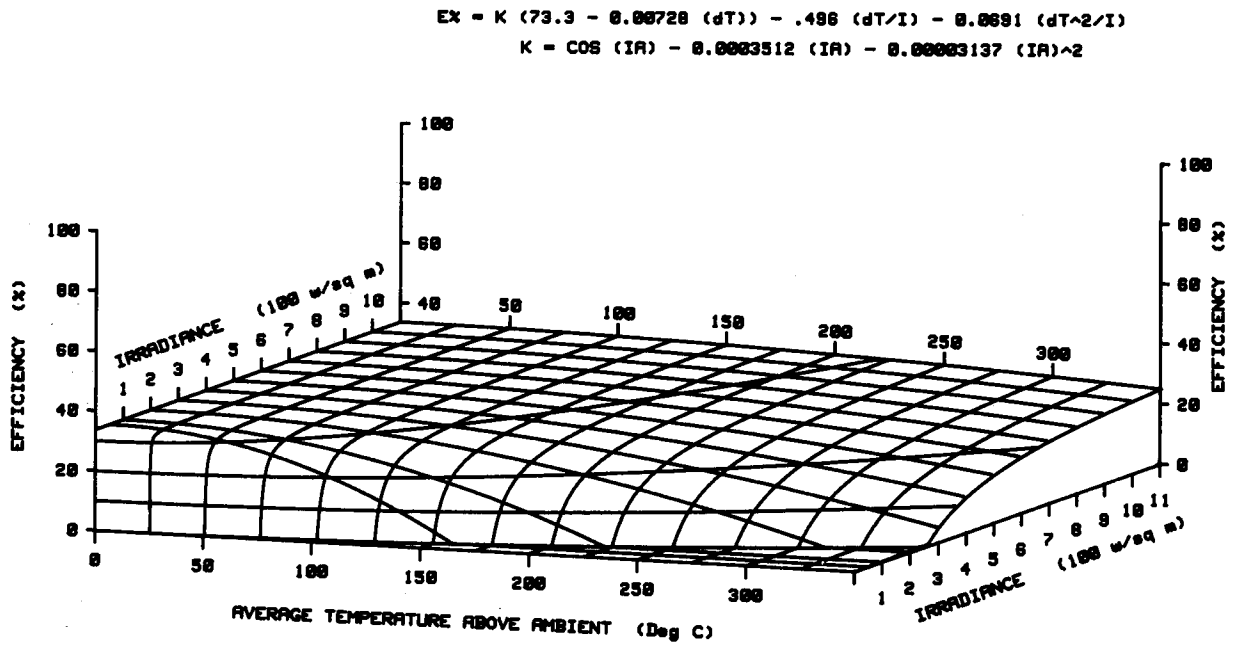

Figure C-5. LS-2 Cermet/Vacuum Efficiency at 55 Deg Incident Angle.

APPENDIX D

TEST RESULTS

Contents for Appendix D

Figures

Tables

APPENDIX D: TEST RESULTS

Introduction

Initial testing of the SEGS LS-2 collector module was done with a receiver which had previously been used for some tests at the Kramer Junction Solar Electric Generating Station (SEGS). The hot oil fluid loop and AZTRAK rotating platform at Sandia Laboratories had not been used for several years; the first receiver was used to check out all the equipment, calibrations, and test procedures. This previously used receiver also had a number of thermocouples welded to the heated receiver surface; we had hoped to obtain some surface temperatures while the receiver was in concentrated sunlight. Unfortunately, the receiver was installed in such a way that many of the surface thermocouples were partly shaded; little useful surface temperature data was obtained. This receiver did enable us to bring the test system back to operational status and to confirm that our test results were similar to those previously obtained at Kramer Junction.

As used in the SEGS fields, the heat-transfer fluid flow-rate is much higher than is possible with the fluid system available at the Sandia test site. To promote turbulent flow within the receiver with our maximum 50 liters/minute flow rate, a closed-end plug tube was installed within the SEGS LS-2 receiver. This confined the fluid flow to a narrow annulus next to the heated surface. Figure D-1 shows the Reynolds numbers attained with the test setup as a function of the fluid temperature.

Figure D-2 shows the results of a time-constant test performed with cold water as the heat transfer fluid. The test was performed by operating the system until temperatures were stable, then suddenly placing the reflector into focus. Data collection was continued until temperatures were again stable. The test was also done by defocusing the collector, and observing the time required for the temperatures to fall to the original values. Both tests produced approximately the same result; we used a value of about 3 minutes as one time constant. The values shown in the data tables in this report are the mean values of measured data over a time interval of 3 time constants, while observing the data stability criteria outlined in Appendix C.

Efficiency and Thermal Loss—Cermet Receiver—Vacuum Annulus

The initial receiver was removed on 1 June, 1992, and a new receiver with a cermet selective coating was installed. This receiver had been evacuated during manufacture, and the annulus between the steel receiver pipe and the glass envelope was under vacuum during the test series discussed below. Any gas (usually air) present in the annulus causes increased thermal losses from the receiver due to convection currents in the gas and heat conduction through the gas to the glass envelope. An evacuated envelope significantly reduces thermal loss by eliminating conduction and convection losses.

Initial testing was done with cold domestic water as the heat transfer fluid. These tests were made to obtain the approximate optical efficiency of the collector, and the change in performance of the collector as the incident angle was increased from zero to 60 degrees. The near-optical efficiency was 72.63%, measured with the average receiver fluid temperature at 11.6°C above ambient-air temperature. The incident angle modifier data points and a least-squares curve fit to the data are shown later in Figure D-23. The optical efficiency data point is included with other efficiency data in Table D-1.

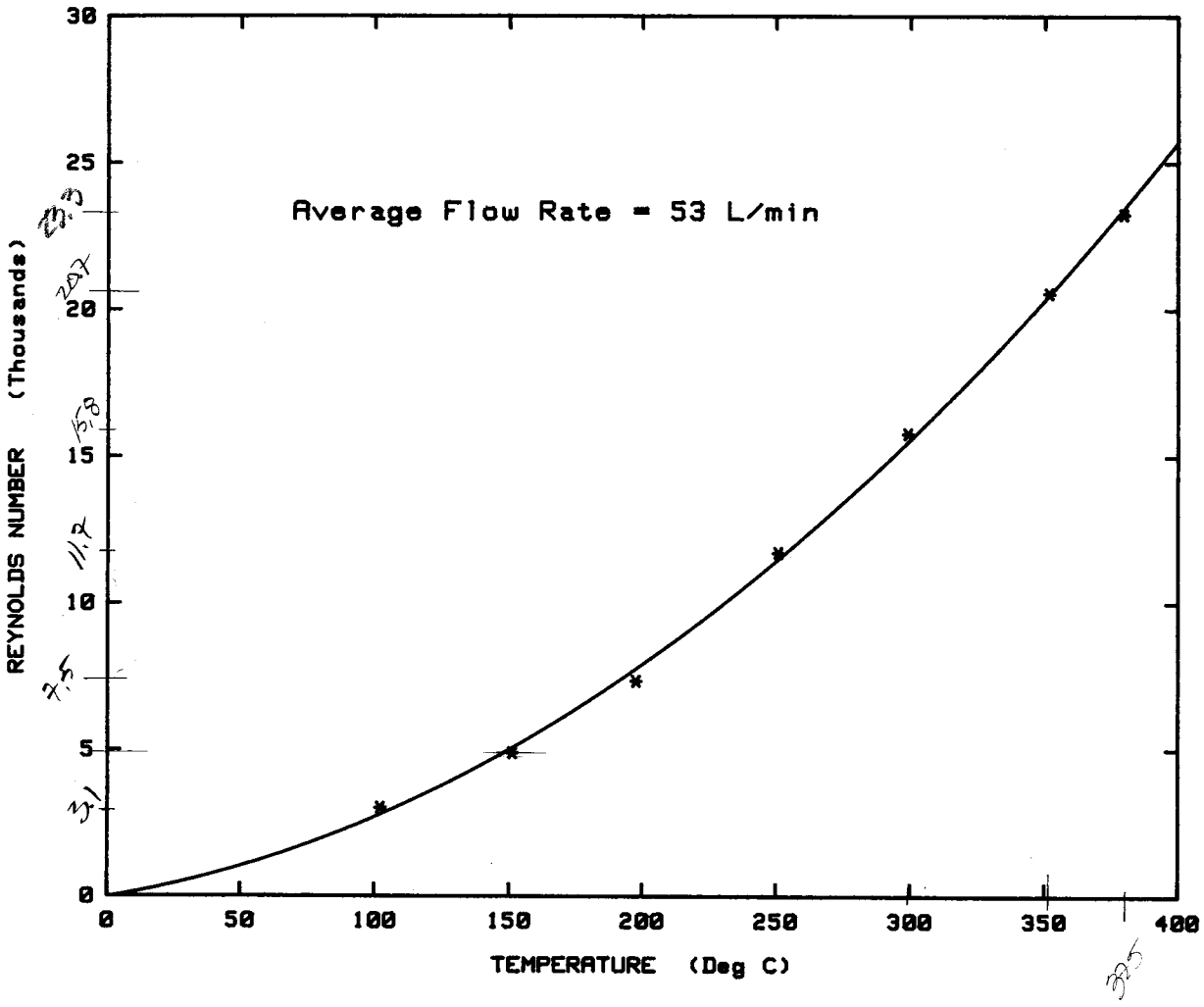

Figure D-1. Reynolds Number vs. Temperature During Sandia Testing.

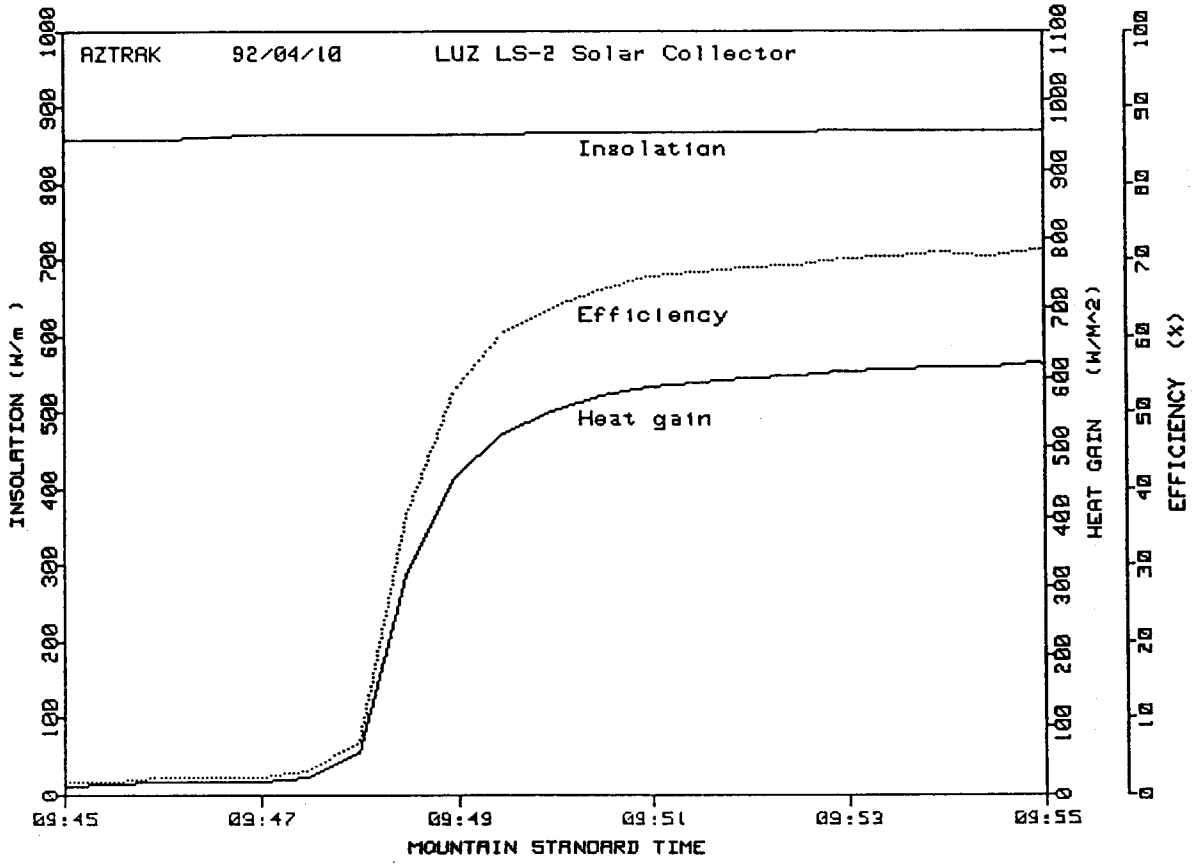

Figure D-2. SEGS LS-2 Receiver Time Constant Test.

On 16 July, 1992, cold water was removed, and the system was replumbed to the high-temperature oil fluid loop for elevated temperature testing. Eight test points were obtained in 5 days of testing, covering the temperature range from approximately 100°C to nearly 400°C. These test data are included in Table D-1, and are shown in graphical form in Figure D-3. The decrease in heat collection efficiency with increasing operating temperature for this collector/receiver combination was the lowest ever measured at this test facility.

An equation for the efficiency curve is also shown in Figure D-3; the equation was obtained from a least-squares regression of the data from Table D-1. Note that the efficiency equation is valid only at the average insolation present during the tests, as noted in the figure.

Table D-1. Measured Efficiency Test Data

Cermet Selective Coating - Vacuum Annulus

Test Date 1992	Direct Normal Insolation W/m^2	Wind speed m/sec	Air Temp °C	Temp In °C	Temp Out °C	Delta Air °C	Flow rate L/min	Meas Effic %	Est Error ±%
02/06	807.9	1.0	15.8	18.34	36.17	11.6	18.4	72.63	1.91
17/06	933.7	2.6	21.2	102.2	124.0	91.9	47.7	72.51	1.95
17/06	968.2	3.7	22.4	151.0	173.3	139.8	47.8	70.9	1.92
17/06	982.3	2.5	24.3	197.5	219.5	184.3	49.1	70.17	1.81
22/06	909.5	3.3	26.2	250.7	269.4	233.9	54.7	70.25	1.90
22/06	937.9	1.0	28.8	297.8	316.9	278.6	55.5	67.98	1.86
25/06	880.6	2.9	27.5	299.0	317.2	280.7	55.6	68.92	2.06
26/06	920.9	2.6	29.5	379.5	398.0	359.4	56.8	62.34	2.41
29/06	903.2	4.2	31.1	355.9	374.0	334.1	56.3	63.82	2.36

Concurrently with efficiency testing at elevated temperatures, heat losses from the receiver assembly were also measured. Seven test points were obtained. The complete set of measured thermal loss data is shown in Table D-2, and a graph is shown in Figure D-4. A least-squares regression of the data in Table D-2 produced the equation shown in Figure D-4.

At each temperature in Table D-1, we can calculate the thermal loss required to lower the measured efficiency from the optical efficiency (first point in Table D-1) to the observed value. These calculated "in-focus loss" points are also plotted in Figure D-4. Because the receiver surface temperatures are higher when concentrated sunlight is focused on the receiver, the in-focus losses are higher than the measured losses with no light on the receiver. Note that the in-focus losses are valid only at the value of insolation present during the efficiency tests. See Appendix C of this report for a discussion of in-focus losses and their use in deriving a general performance equation for the collector.

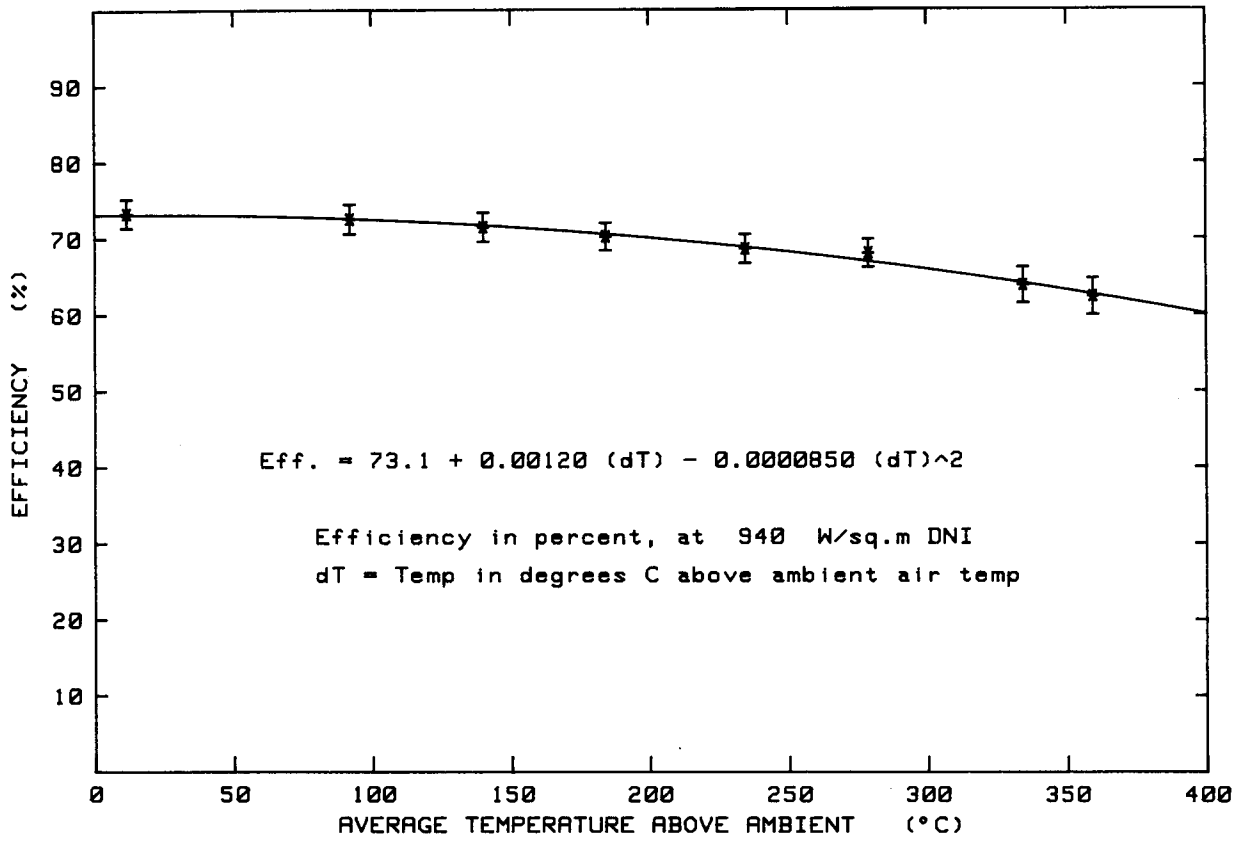

Figure D-3. Efficiency of Cermet Receiver with Vacuum Annulus.

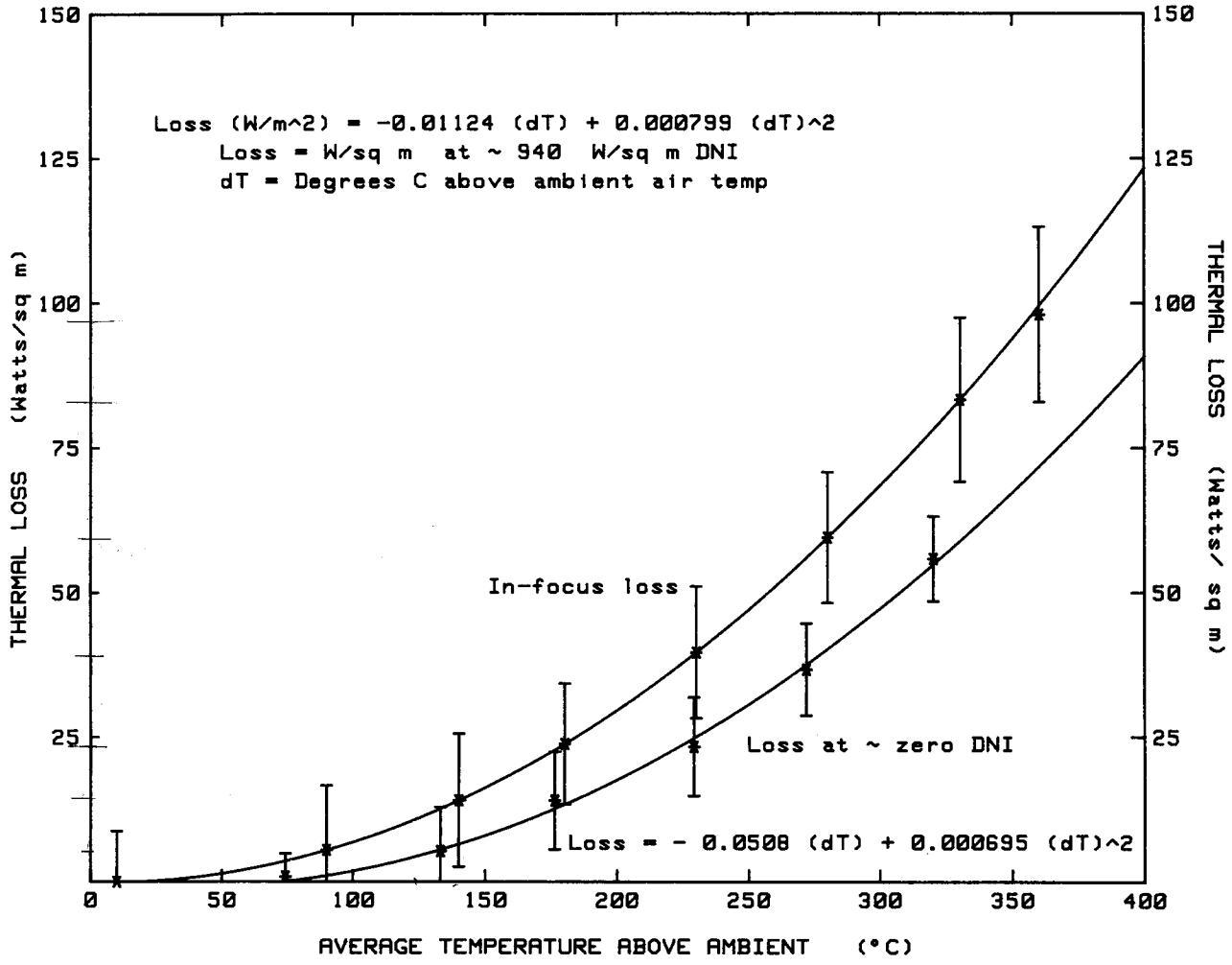

Figure D-4. Thermal Loss from Cermet/Vacuum Receiver.

Table D-2. Measured Thermal Loss Data

Cermet Selective Coating, Vacuum Annulus

Test Date 1992	Wind speed m/sec	Air Temp °C	Temp In °C	Temp Out °C	Delta Air °C	Flow rate L/min	Meas Loss W/m2	Est Error W/m2
24/06	3.2	26.3	99.55	99.54	74.2	27.4	0.3	3.7
24/06	2.9	25.4	100.02	99.97	74.6	27.4	0.85	4.0
25/06	0.1	22.5	199.4	199.0	176.3	54.7	14.04	8.5
25/06	2.0	26.7	299.0	297.9	271.9	56.0	36.7	8.0
26/06	1.1	19.9	153.4	153.3	133.1	53.6	5.3	7.6
26/06	1.5	24.2	253.8	253.1	229.2	55.6	23.4	8.5
29/06	0.6	27.6	348.3	346.6	319.9	56.8	55.8	7.3

Cermet Receiver with Air in Annulus

On completion of the test series with the receiver under vacuum, a #60 hole was drilled in the metal bellows at one end of the receiver glass envelope, thus filling the receiver annulus with ambient pressure air. At the same time, the system was again replumbed to the cold water supply for a recheck of optical efficiency and incident angle modifier. The presence of air in the receiver annulus was not expected to change either efficiency or incident angle modifier, since at near ambient-air temperatures the thermal losses are small enough that no appreciable conduction or convection occurs in the receiver gas. The optical efficiency measured is the first data point is Table D-3 below, and is the essentially the same as the vacuum efficiency, within the error bounds of the individual measurements. Incident angle modifier data was also unchanged; this data is shown in a later section of this report.

On completion of the cold-water tests, the collector was again plumbed to the oil loop to determine the change in elevated-temperature efficiency and thermal loss with air replacing a vacuum in the receiver annulus. Seventeen test points were obtained in 5 days of testing. The efficiency data set is shown in Table D-3; thermal loss is in Table D-4. Graphs in Figures D-5 and D-6 show that elevated temperature performance is significantly degraded by increased thermal losses when air fills the annulus.

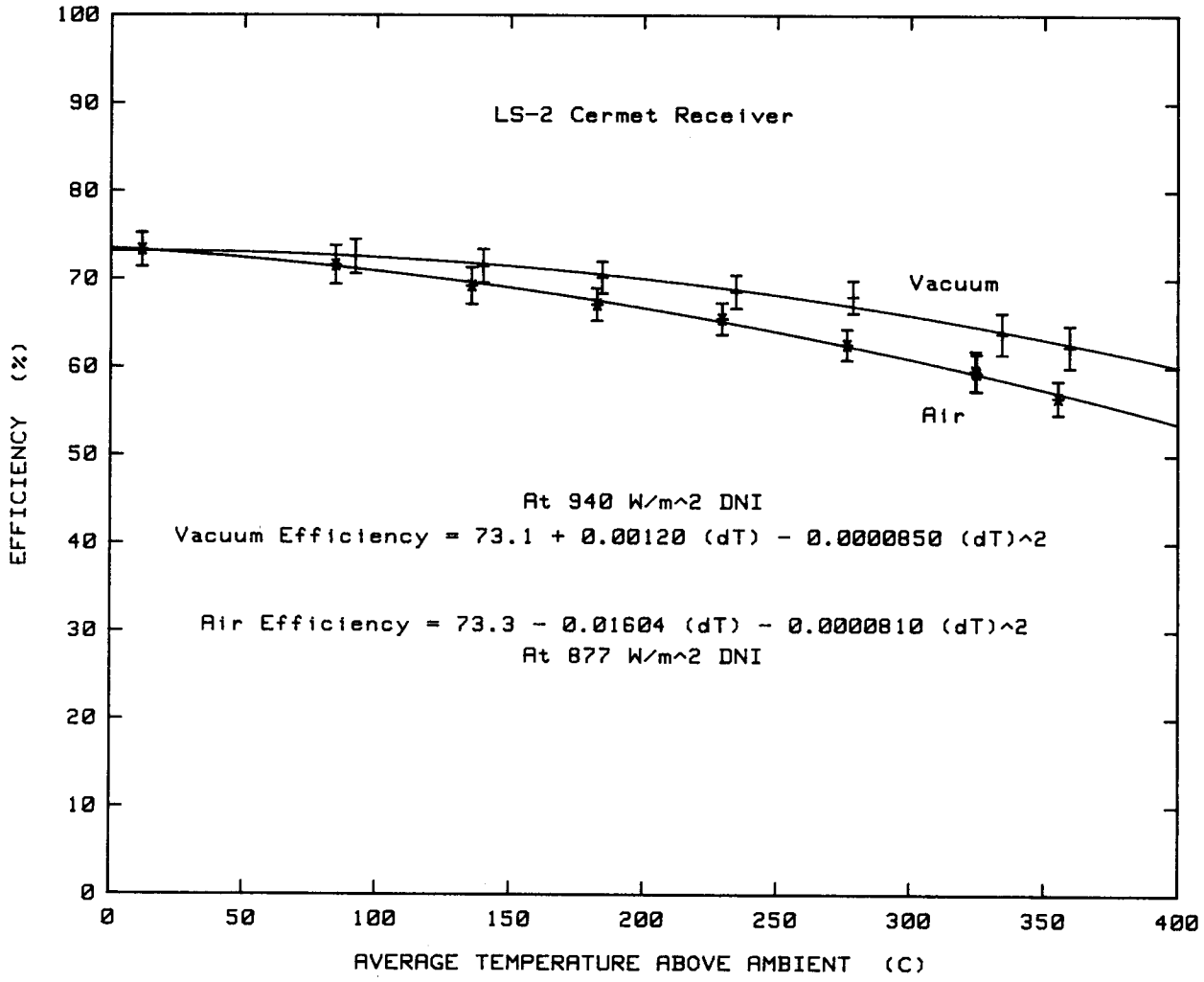

Figure D-5. LS-2 Efficiency Comparison—Vacuum vs. Air in Receiver.

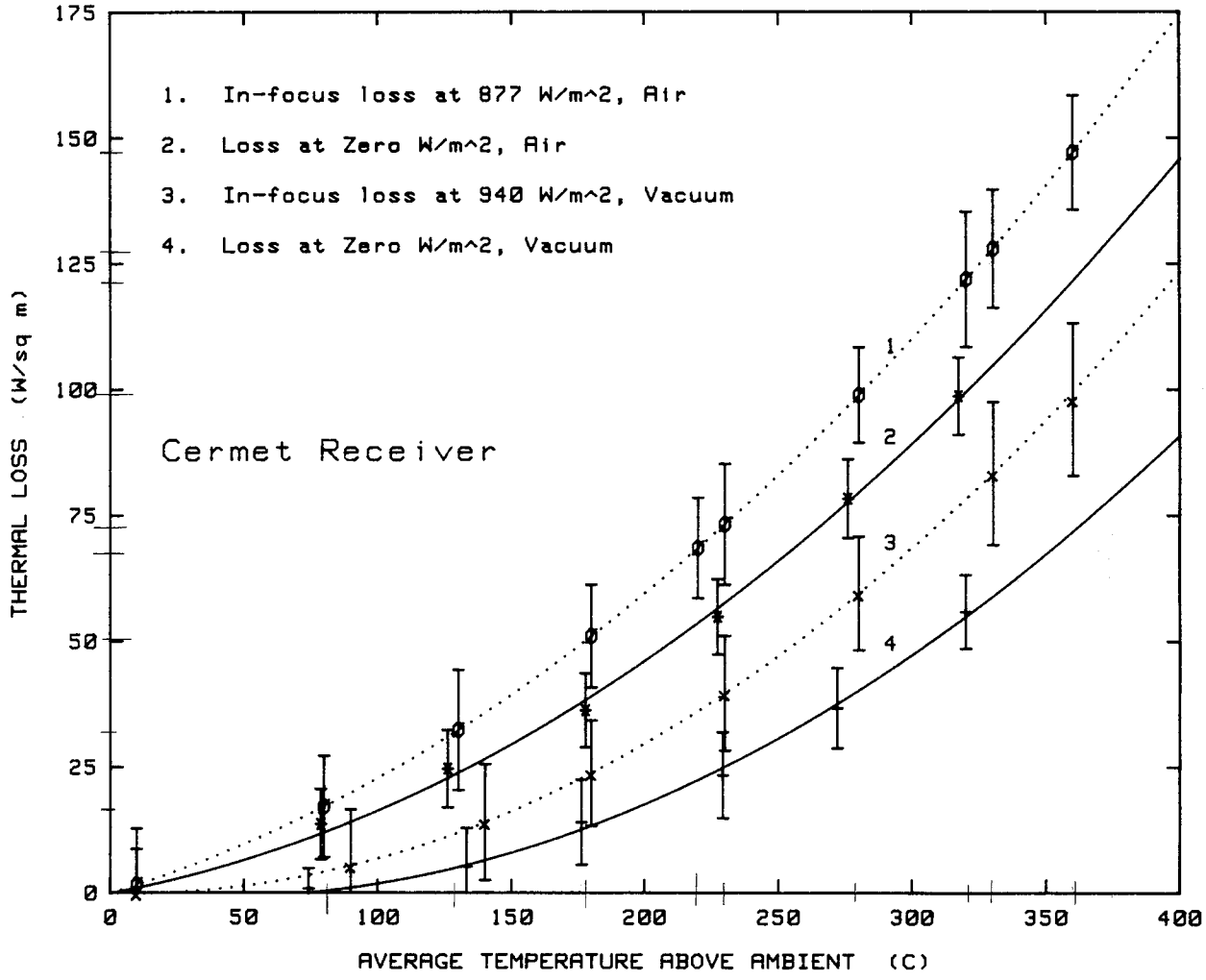

Figure D-6. Thermal Loss Comparison—Vacuum vs. Air in Receiver.

Table D-3. Measured Efficiency Test Data

Cermet Selective Coating - Air in Annulus

Test Date 1992	NIP W/m²	Wind speed m/sec	Air Temp °C	Temp In °C	Temp Out °C	Delta Air °C	Flow rate L/min	Meas Effic %	Est Error ±%
18/08	925.1	3.4	38.4	29.5	47.3	10.0	20.7	73.68	1.96
27/07	889.7	2.8	28.6	251.1	268.3	231.1	55.3	66.61	2.29
28/07	874.1	4.0	28.7	344.9	361.1	324.2	56.2	59.60	2.27
28/07	870.4	0.6	29.1	345.5	361.6	324.5	56.1	59.40	2.12
29/07	813.1	3.6	25.8	101.2	119.0	84.5	50.3	71.56	2.21
29/07	858.4	3.1	27.6	154.3	171.7	135.4	52.9	69.20	2.10
29/07	878.7	3.1	28.6	202.4	219.4	182.3	54.6	67.10	1.88
29/07	896.4	0.9	30.0	250.7	267.8	229.3	55.2	65.5	1.80
29/07	906.7	0.0	31.7	299.5	316.5	276.3	55.4	62.58	1.79
03/08	879.5	1.8	27.4	348.9	365.2	329.6	55.4	58.52	2.02
03/08	898.6	2.8	29.7	376.6	393.1	355.1	56.2	56.54	1.93

Table D-4. Measured Thermal Loss Data

Cermet Selective Coating, Air in Annulus

Test Date 1992	Wind speed m/sec	Air Temp C	Temp In °C	Temp Out °C	Delta Air °C	Flow rate L/min	Meas Loss W/m2	Est Error W/m2
27/07	5.2	19.6	98.7	98.2	78.8	51.4	13.7	7.0
27/07	4.5	22.1	148.5	147.8	126.0	53.8	24.7	7.7
27/07	0.8	23.6	202.0	200.9	177.9	54.6	36.3	7.4
27/07	0.6	24.7	252.5	250.9	227.1	55.4	54.8	7.5
28/07	1.5	23.2	300.3	297.9	275.9	56.5	78.3	7.8
28/07	1.1	26.3	344.8	341.8	317.1	56.7	98.6	7.7

Cermet Receiver with Glass Removed

In an ideal world, once a receiver annulus was evacuated during manufacture, it would remain so forever. But in a practical field installation, degradation occurs. A crack or other leak may introduce air into the vacuum annulus, as in the test described above. Other, more serious accidents may break the glass entirely off the receiver, leaving the bare, heated receiver tube exposed to severe thermal losses because of wind-forced convection. It is difficult and expensive to cut out a receiver section and replace it with a new one; and it may not be possible to always do so promptly. For example, the nine SEGS solar electric plants in California have a combined total of some 56,000 receiver elements like the two under test; inevitably, some are air-filled or broken. Since operation may continue for some time in the damaged condition, knowledge of the degradation in performance can be highly important to a collector field operator. Accordingly, we broke up the receiver glass envelope and removed it entirely. This operation was done carefully to avoid scratching or otherwise damaging the black cermet selective coating on the receiver.

The collector was again plumbed to the domestic cold water supply system for optical efficiency and incident angle modifier testing. The glass envelope was the most transparent available, but the glass still absorbs about 4% of the concentrated light passing through it. Therefore, we expected the optical efficiency would improve slightly when the glass was removed. Test data confirmed this, with the measured cold water efficiency increasing about 4 points, from 73 to 77%.

It is also possible that the presence of a glass envelope would cause some light loss due to reflections, especially at high incident angles. However, the glass envelope on the SEGS receivers is anti-reflection coated on both surfaces, and no significant change in the incident angle modifier was detected in the collector data when the glass was removed. The incident angle test data set obtained in shown later in Table D-13, Appendix D.

The collector was disconnected from the cold water supply and replumbed to the hot oil supply on 20 October 1992. Elevated temperature testing of the bare receiver then began. Variations in wind speed and direction did not cause any appreciable changes in measured efficiency during the cold-water tests, since the receiver temperature was so near the air temperature that no significant thermal losses were occurring. Elevated temperature testing with a bare receiver is much more difficult. For a reliable, accurate measurement of receiver temperature, the receiver must remain at a constant temperature for at least one to three time constants, which for this receiver would be about three to nine minutes. The wind in an outdoor test situation never remains constant for more than a few seconds.

Figure D-7 shows a segment of a test run with the bare receiver at 250°C, showing the variations in collector thermal loss with wind changes. It is obvious that the losses change with wind, but exactly how much is the challenge. For comparison, Figure D-8 shows an earlier test run at approximately the same temperature, while the receiver was still covered by the glass envelope. Note that the measured thermal loss data line shows some scatter due to fluctuations in flow and temperature, but there is no apparent correlation of loss change with wind speed.

We chose to apply running-average smoothing to the data in order to extract more consistent numbers from the data scatter. The time constant of this receiver was about 3 minutes. Figures D-9, D-10, and D-11 show the same thermal losses as Figure D-7, with running-average periods of 1, 2, and 3 time constants (3, 6, and 9 minutes). By plotting an entire day's data in this fashion, we were able to pick out periods when the average wind speed held more or less constant for at least 1 time constant. One time constant (3 minutes) was chosen as a compromise: less time produced data that was too scattered, more averaging seemed to wipe out all the relevant structure.

Similar tests were done to determine efficiency as a function of wind and temperature. A sample of the real-time data is shown in Figure D-12; an example of one-time-constant running-average smoothing is shown in Figure D-13. Efficiency data points obtained are shown in Table D-5, and the data is plotted in Figure D-14. A multiple regression of the data from Table D-5, using temperature, wind speed and efficiency produced the equation shown in Figure D-14. The curves in the figure for different wind speeds were obtained by solving the equation for the specific wind speeds shown. Efficiency curves for the receiver with vacuum and air are also shown for comparison.

Figure D-14 summarizes all the efficiency test results with the cermet receiver. When air is introduced into the receiver annulus, efficiency falls as thermal losses increase, because of increased conduction and convection in the air transferring heat from the receiver surface to the glass. In still air, efficiency decreases by about an equal amount when the glass is removed from the receiver. As wind speed

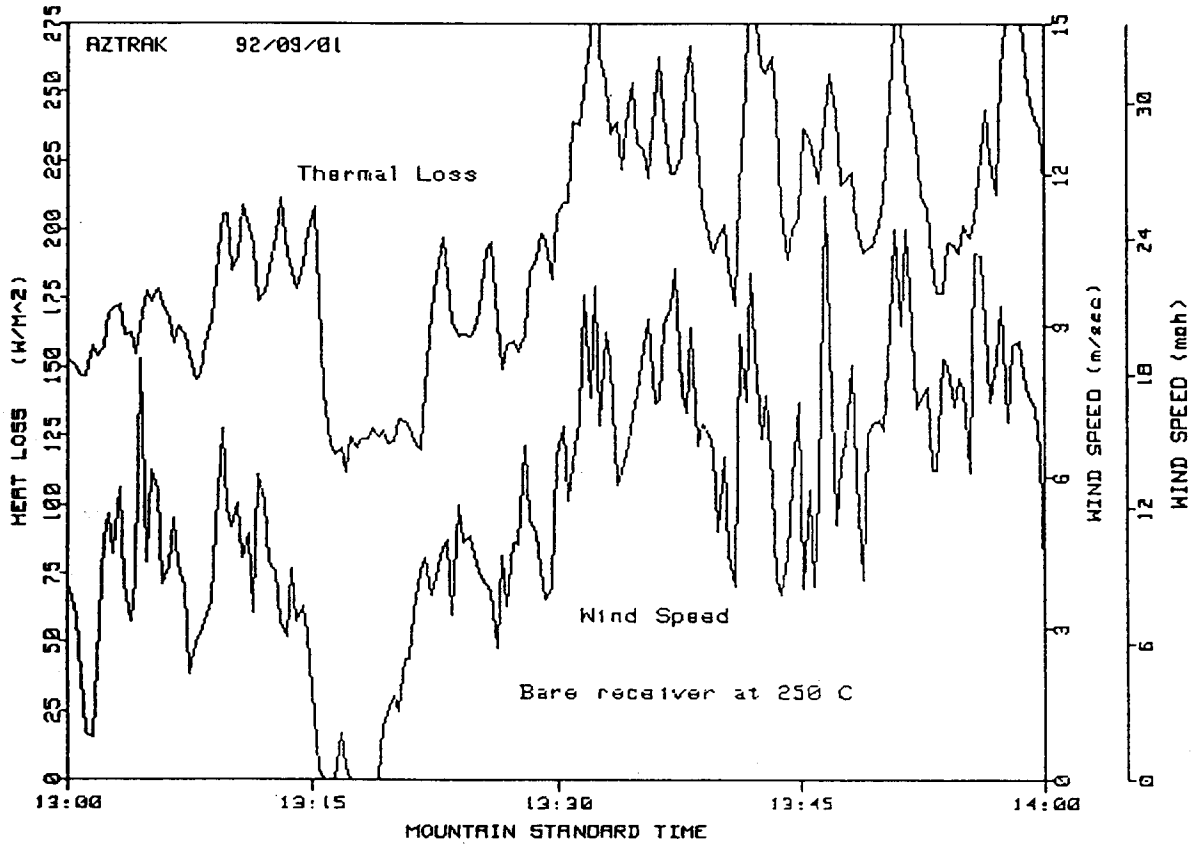

Figure D-7. Wind Speed and Thermal Loss from Bare Cermet Receiver.

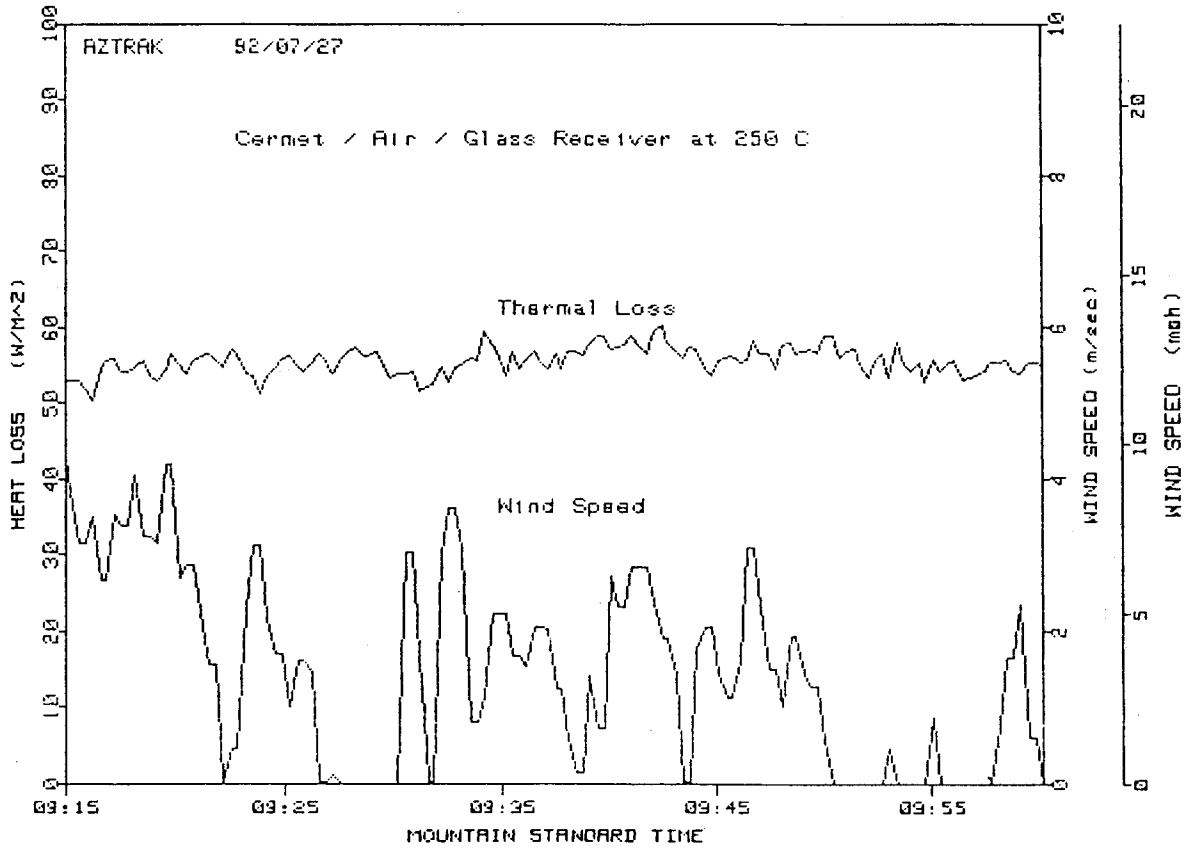

Figure D-8. Wind Speed and Thermal Loss from Receiver with Glass Envelope.

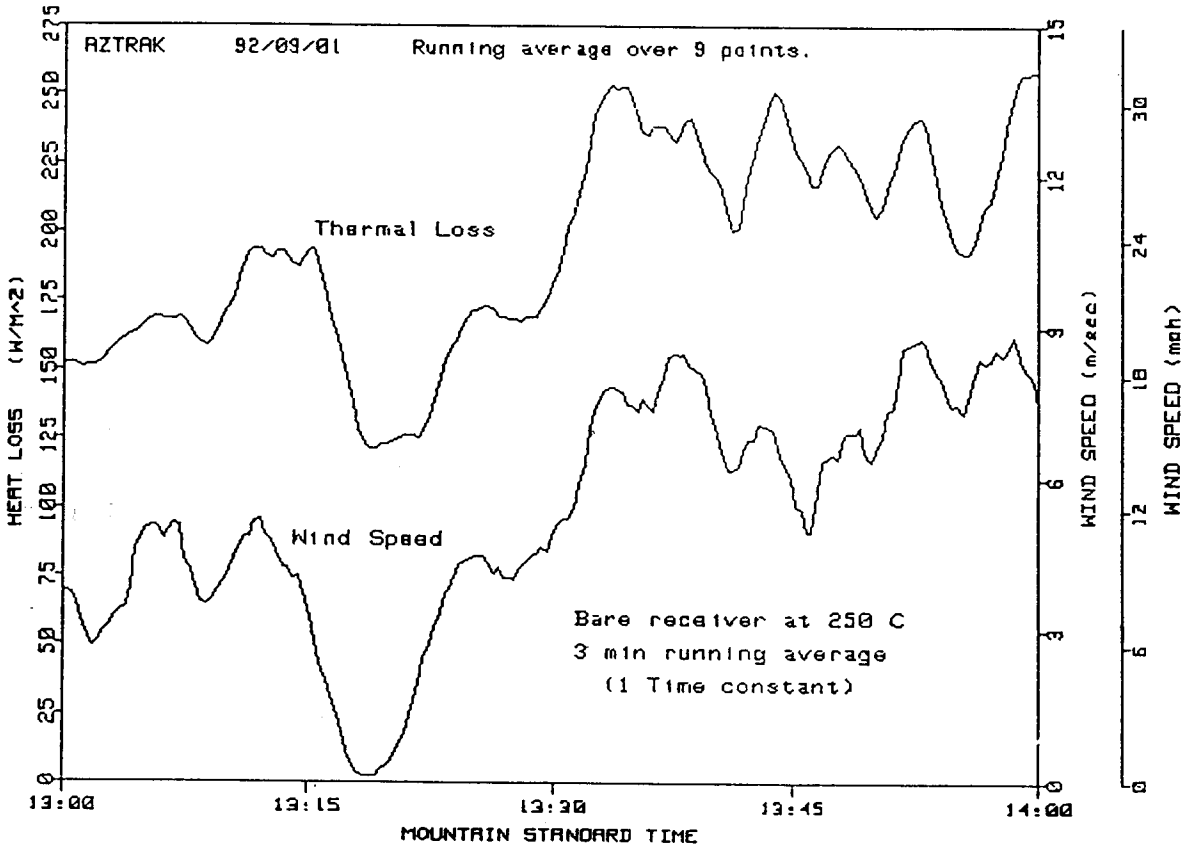

Figure D-9. Wind Speed and Thermal Loss from Bare Receiver.

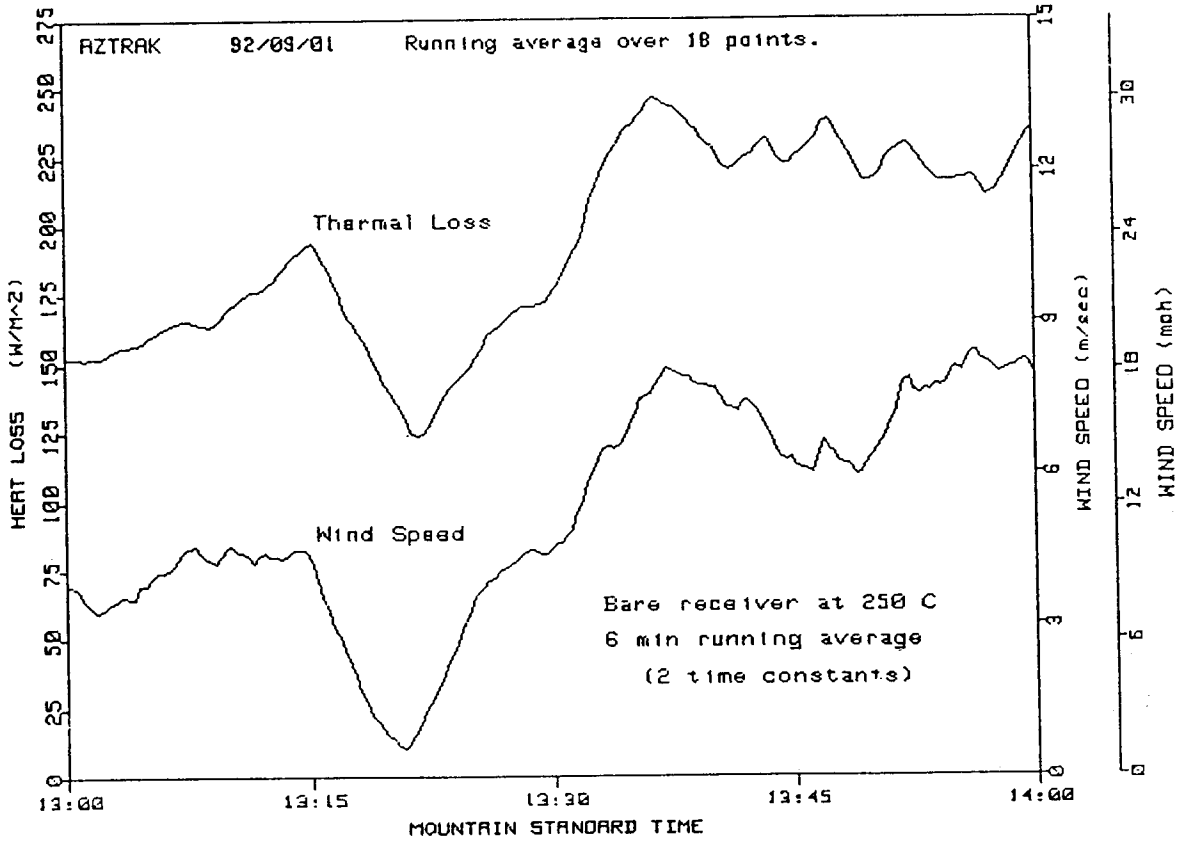

Figure D-10. Wind Speed and Thermal Loss from Bare Receiver.

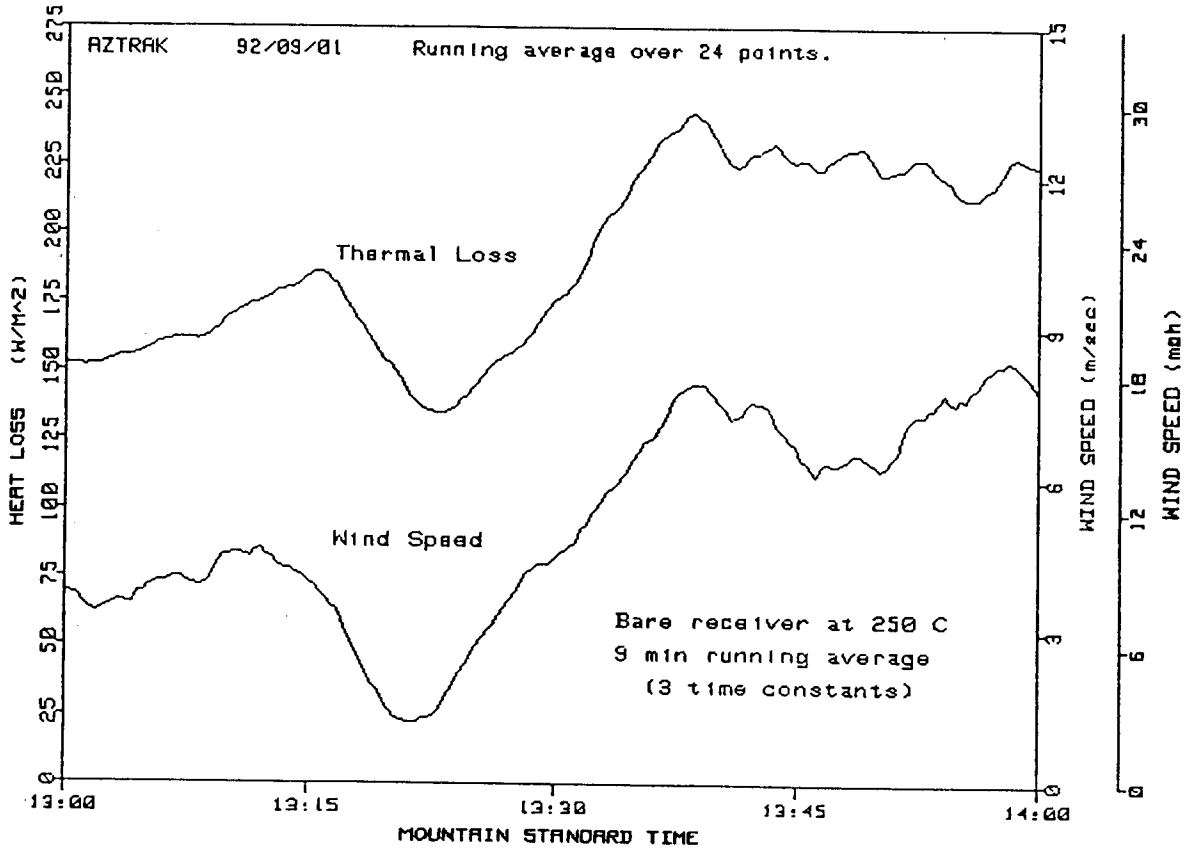

Figure D-11. Wind Speed and Thermal Loss from Bare Receiver.

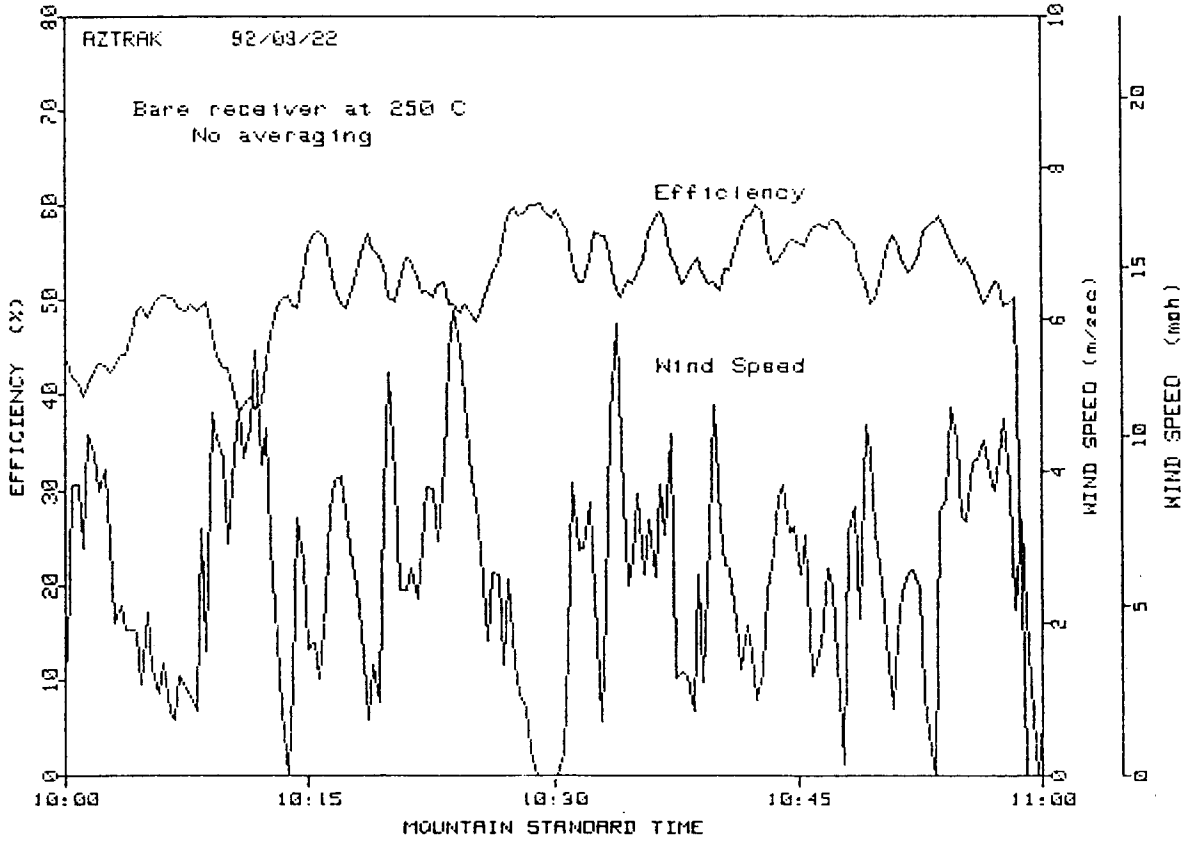

Figure D-12. Efficiency vs. Wind with Bare Cermet Receiver.

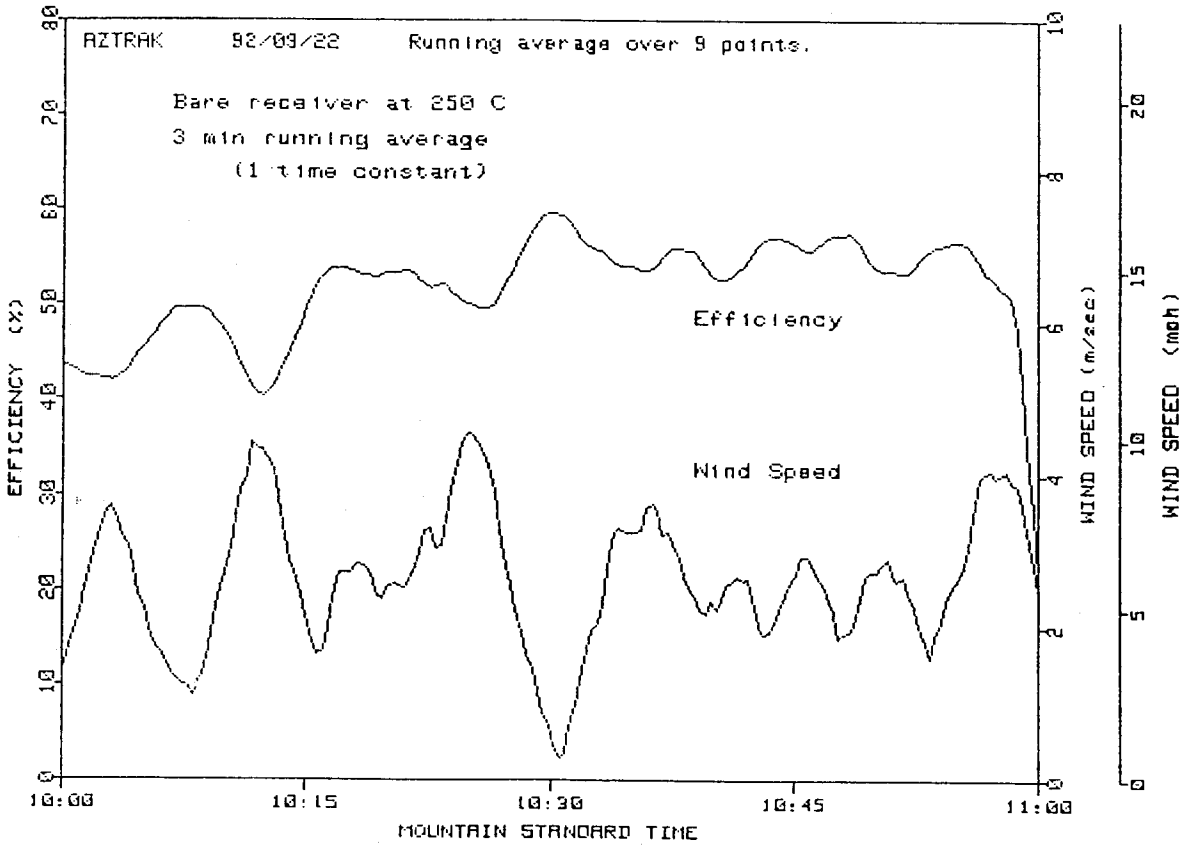

Figure D-13. Efficiency vs. Wind Averaging with Bare Receiver.

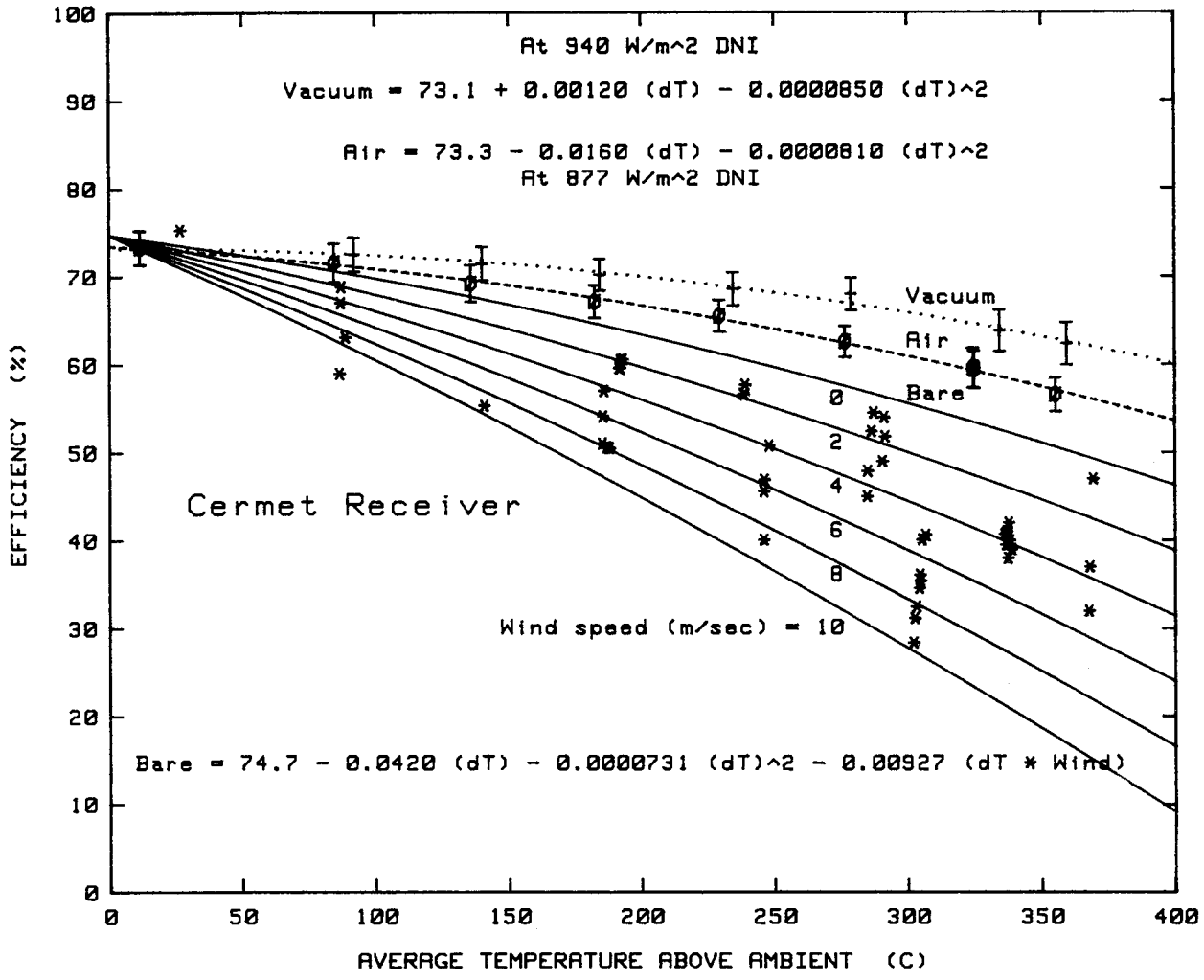

Figure D-14. SEGS LS-2 Efficiency vs. Temperature and Wind - Cermet Receiver.

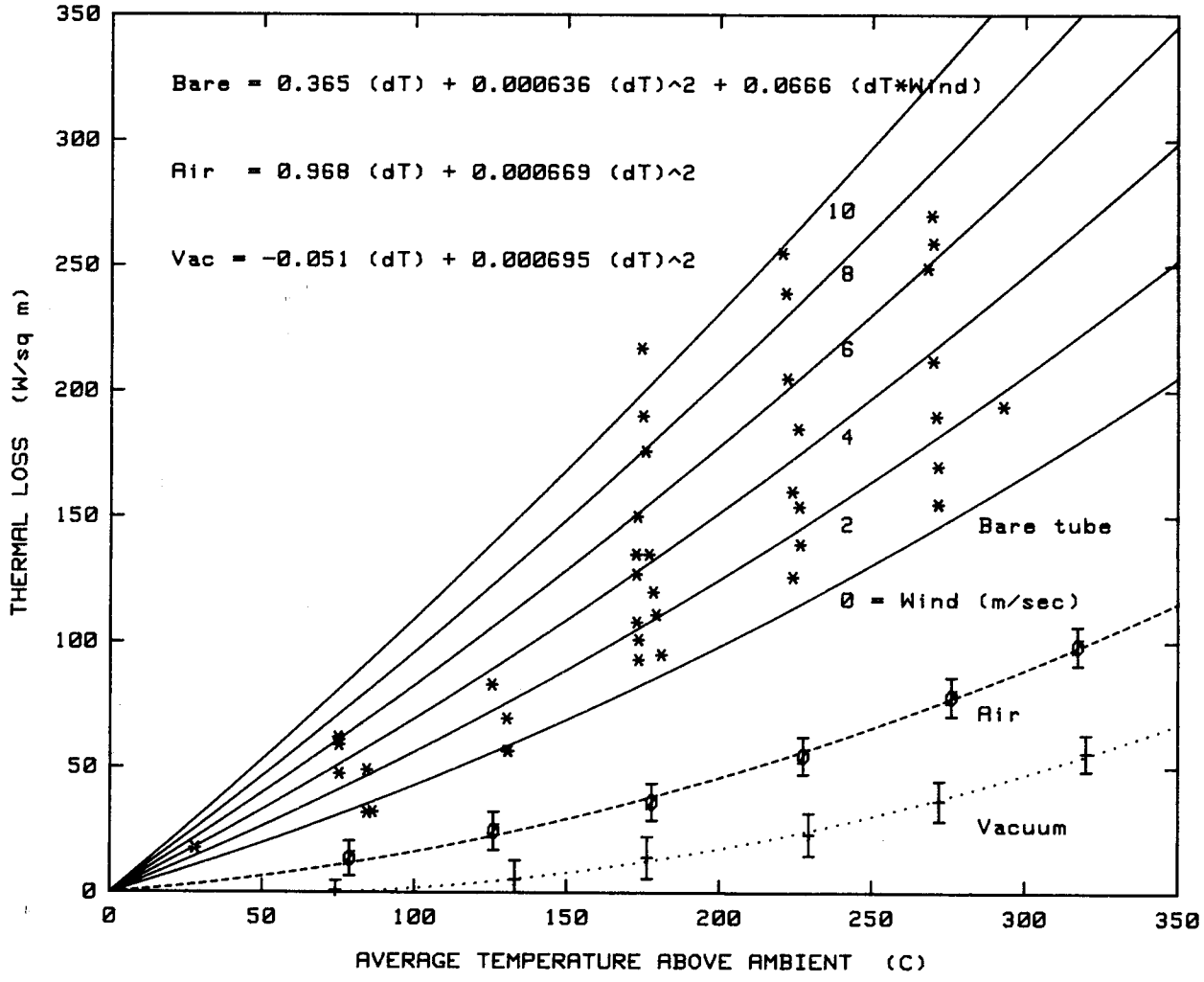

Figure D-15. SEGS LS-2 Thermal Loss vs. Temperature and Wind - Cermet Receiver.

increases, efficiency can be seen to fall to unacceptable levels. The equations shown in Figure D-14 were obtained from a least-squares regression analysis of the measured data points. Note that these equations apply only at the insolation values present during the test, and should not be used for other levels of insolation. The error bars on the data points are the expected worst-case errors caused by the measuring instruments. A discussion of the test errors is shown in Appendix E. Error bars are not included for the bare tube test case, because errors due to temperature instability (caused by variable winds) could not be quantified. The expected uncertainty in the data is certainly larger, but the magnitude is unknown.

Thermal loss data from the receiver as a function of wind and temperature are shown in Table D-6. Figure D-15 is a plot of the loss data and fitted equation lines, along with the curves for vacuum and air losses for comparison. The thermal loss curves reflect the same phenomena as the efficiency test data: increasing losses as the receiver is degraded by allowing air into the vacuum annulus, and significantly worse losses with increasing wind-driven convection and conduction.

The efficiency and thermal loss curves for the bare receiver show that the collector performance is degraded so much by reasonable, average wind speeds that repair of the damaged receiver should be a high priority.

Table D-5. Measured Efficiency Test Data

Cermet Selective Coating - Bare Receiver (No Glass)

Test Date 1992	NIP W/m2	Wind speed m/sec	Air Temp °C	Temp In °C	Temp Out °C	Delta Air °C	Flow rate L/min	Meas Effic %
27/08	954.5		23.5	29.0	47.9	14.9	21.3	77.5
21/09	911.3	5.2	19.5	351.3	363.1	337.8	54.9	40.0
21/09	940.4	5.3	22.0	384.0	395.0	367.6	55.8	32.0
21/09	866.5	2.0	17.6	301.3	315.3	291.0	54.3	54.0
22/09	801.3	7.0	18.2	151.7	166.2	140.6	48.4	55.3
22/09	888.6	4.7	20.2	198.2	215.5	185.2	49.8	51.0
22/09	903.0	4.4	20.8	198.4	214.2	185.8	49.7	54.1
22/09	908.8	3.7	20.8	198.4	214.2	185.8	49.7	57.0
22/09	845.2	2.0	19.0	200.1	213.6	187.8	49.6	50.5
22/09	935.7	2.5	22.3	252.1	268.0	238.4	50.9	56.6
22/09	929.8	1.0	21.8	252.2	269.0	238.9	50.8	57.7
23/09	829.6	2.0	18.0	302.1	315.9	291.3	51.0	51.8
23/09	845.7	4.0	18.6	301.9	315.4	290.3	51.0	49.0
23/09	898.0	3.5	20.7	351.2	363.8	337.3	51.6	42.0
23/09	904.2	4.5	20.9	351.0	364.4	336.7	51.7	41.0
23/09	908.6	4.6	21.2	351.1	363.3	336.4	51.2	39.5
23/09	919.3	3.8	21.9	351.2	364.3	335.9	51.3	40.7
23/09	859.8	4.1	24.0	386.0	397.3	367.9	52.2	37.0
23/09	851.2	2.9	24.2	386.0	400.5	369.2	52.0	47.0
24/09	917.9	4.5	22.5	354.6	367.0	338.4	51.6	39.0
24/09	927.6	4.5	23.6	354.4	367.8	337.1	51.6	38.0
25/09	877.6	6.3	23.0	101.4	122.3	89.0	40.1	62.7
25/09	901.0	8.2	23.8	101.1	122.0	87.4	40.1	57.5
25/09	914.3	8.0	24.6	101.2	121.4	86.9	40.0	58.1
25/09	906.7	6.5	23.8	101.1	121.8	87.9	40.0	60.3
25/09	817.5	4.2	20.8	101.0	120.8	90.3	39.8	64.4
25/09	863.4	5.0	22.3	101.2	122.3	89.2	40.0	61.3

Table D-5. Measured Efficiency Test Data (Continued)

Cermet Selective Coating - Bare Receiver (No Glass)

Test Date 1992	NIP W/m2	Wind speed m/sec	Air Temp °C	Temp In °C	Temp Out °C	Delta Air °C	Flow rate L/min	Meas Effic %
25/09	878.3	4.6	22.9	101.3	123.1	89.3	40.1	64.5
25/09	922.7	7.5	27.2	206.7	221.9	186.8	50.2	50.6
29/09	843.6	1.0	19.5	204.3	220.2	192.9	50.0	60.6
29/09	854.5	2.3	19.6	203.1	219.2	191.5	50.1	59.6
29/09	867.6	0.5	19.8	203.4	219.6	191.9	50.0	60.5
29/09	883.3	2.1	19.9	203.4	220.1	191.9	50.0	59.6
29/09	919.0	0.1	22.6	301.4	318.0	287.0	50.9	54.5
29/09	920.5	3.0	23.4	301.0	314.2	284.6	51.1	45.0
29/09	920.2	1.5	22.9	301.0	316.8	286.2	50.9	52.4
29/09	919.2	2.4	23.7	301.0	315.8	284.7	50.9	47.9
06/10	920.4	4.0	23.8	100.9	120.4	87.0	48.2	67.0
06/10	922.0	1.8	23.7	100.8	121.1	87.2	48.2	68.8
07/10	845.3	3.0	10.8	252.0	264.6	247.8	54.8	50.8
07/10	875.8	7.2	11.0	251.6	263.3	245.8	55.0	40.1
07/10	895.1	7.0	11.2	251.5	262.8	245.8	55.0	45.6
07/10	913.4	6.1	11.5	251.8	264.0	246.0	55.0	46.9
07/10	929.4	5.1	12.6	313.8	324.8	306.4	55.6	40.6
07/10	938.1	7.1	13.3	313.3	320.7	304.5	55.9	35.4
07/10	941.1	8.0	13.5	313.1	322.0	304.1	55.9	34.6
07/10	953.0	7.0	14.0	313.6	322.9	304.3	55.9	36.1
07/10	947.7	6.2	14.0	313.5	323.3	305.0	55.9	40.1
07/10	958.1	9.3	14.5	313.3	321.5	303.0	55.9	32.5
07/10	961.3	9.3	15.1	313.3	320.7	301.9	55.9	28.4
07/10	937.6	7.9	15.2	313.5	321.7	302.3	55.9	31.2

Notes for Table D-5:

1. All entries are 3-minute running averages.
   (Approximately one time constant)
2. Estimated measurement errors were not calculated.

Table D-6. Measured Thermal Loss Data

Cermet Selective Coating, Bare Receiver (No Glass)

Test Date 1992	Wind speed m/sec	Air Temp °C	Temp In °C	Temp Out °C	Delta Air °C	Flow rate L/min	Meas Loss W/m2
01/09	0.1	17.2	102.1	101.1	84.5	49.7	32.0
01/09	2.5	18.4	103.5	101.9	84.4	49.7	49.0
01/09	0.0	16.2	102.9	101.8	86.3	49.7	32.3

Table D-6. Measured Thermal Loss Data (Continued)

Cermet Selective Coating, Bare Receiver (No Glass)

Test Date 1992	Wind speed m/sec	Air Temp °C	Temp In °C	Temp Out °C	Delta Air °C	Flow rate L/min	Meas Loss W/m2
01/09	0.1	19.2	150.8	149.1	130.8	52.6	56.5
01/09	0.2	19.7	150.9	149.3	130.5	52.5	56.6
01/09	1.5	19.4	150.7	148.7	130.3	52.6	69.5
01/09	1.3	21.3	203.4	200.7	180.9	54.4	95.0
01/09	4.0	22.9	202.8	199.3	178.3	54.2	120.0
01/09	2.5	22.0	202.8	199.6	179.2	54.3	111.0
01/09	5.1	24.3	203.0	199.1	176.8	54.0	135.0
01/09	1.1	26.4	252.1	248.5	223.8	55.4	126.0
01/09	4.0	26.3	252.1	247.5	223.5	55.5	160.0
01/09	8.4	26.0	251.2	244.4	221.3	55.5	239.0
01/09	6.5	26.9	251.8	245.9	221.8	55.6	205.0
01/09	8.6	27.6	251.4	244.0	220.2	55.5	255.0
01/09	6.5	28.3	299.8	292.6	267.9	56.7	249.0
01/09	8.2	28.3	301.7	294.1	269.7	56.7	259.0
02/09	2.0	26.9	201.7	198.9	173.4	53.9	101.0
02/09	6.0	26.9	201.4	197.5	172.6	53.9	135.0
02/09	5.2	27.0	201.5	197.8	172.7	53.9	127.0
02/09	0.7	27.1	201.8	199.1	173.4	54.0	93.0
02/09	2.5	29.0	105.0	103.5	75.4	50.4	47.5
18/09	6.0	23.0	51.3	50.6	27.9	40.7	17.7
18/09	1.4	27.8	301.7	296.8	271.4	56.5	170.0
18/09	4.7	28.4	301.4	293.6	269.2	56.6	270.0
18/09	0.1	28.2	301.9	297.5	271.5	56.5	155.0
18/09	5.7	26.4	201.5	197.2	173.0	54.7	150.0
18/09	4.6	27.2	201.5	197.7	172.5	54.6	135.0
18/09	2.5	27.2	201.7	198.3	172.8	54.5	108.0
18/09	6.0	24.6	100.9	98.9	75.3	46.5	59.0
18.09	7.9	24.9	100.9	98.8	75.0	46.4	62.0
18/09	7.0	25.0	100.8	98.7	75.4	46.6	61.0
18/09	4.1	28.9	301.6	295.5	269.7	56.5	212.0
18/09	0.5	28.4	302.0	297.5	271.4	56.4	155.0
18/09	3.0	28.5	301.9	296.4	270.7	56.4	190.0
21/09	2.5	24.6	320.3	314.3	292.7	54.4	194.0
22/09	3.4	25.7	152.4	149.8	125.4	48.7	83.0
22/09	2.5	23.5	251.9	247.1	225.9	51.0	154.0
22/09	3.9	23.7	251.9	246.2	225.4	51.0	185.0
22/09	0.8	23.7	252.1	247.8	226.2	50.8	139.0
25/09	7.5	27.5	205.9	200.4	175.6	50.0	176.0
25/09	8.4	28.0	205.6	199.7	174.7	50.0	190.0
25/09	10.3	28.08	205.6	198.9	174.2	50.0	217.0

Notes for Table D-6:

1. All entries are 3-minute running averages. (Approximately one time constant)

2. Estimated measurement errors were not calculated.

Black Chrome Receiver—Vacuum

On completion of the bare tube tests with the cermet receiver, it was removed and replaced by an identical receiver, except that the selective surface treatment was electroplated black chrome. Initial tests were with the normal vacuum in the receiver, beginning on 9 December 1992. Ten efficiency points were obtained in 7 test days. Data obtained is shown in Table D-7, below, and is plotted in Figure D-16. Also shown in the figure are the cermet receiver vacuum data for comparison. The two are nearly identical, with a small advantage for cermet at the highest temperatures, probably due to lower emittance of the cermet surface.

Thermal losses were also measured, these data are shown in Table D-8, and are compared to the losses using an air-filled receiver in Figure D-20.

Black Chrome Receiver—Air in Annulus

When testing the cermet receiver, the transition from vacuum to air in the receiver annulus was made while the system was shut down between tests. On 4 January 1993, the last black chrome data point with vacuum was obtained in mid-morning. Without taking the collector out of focus, a portable drill was used to drill a #60 hole in each of the receiver's metal bellows. Figure D-17 shows the change in collector efficiency as air filled the receiver vacuum. Increased thermal losses due to convection and conduction in the air-filled receiver annulus causes the drop in efficiency.

Table D-7. Measured Efficiency Test Data

Black Chrome Selective Coating - Vacuum Annulus

Test Date 1992	NIP W/m2	Wind speed m/sec	Air Temp °C	Temp In °C	Temp Out °C	Delta Air °C	Flow rate L/min	Meas Effic %	Est Error %
09/12	850.2	1.3	4.0	14.82	31.81	19.3	20.5	73.1	2.36
11/12	839.8	1.1	3.6	103.4	122.2	109.3	50.6	73.56	3.35
17/12	882.7	2.1	-3.1	253.3	271.3	265.5	54.8	69.58	1.95
17/12	921.5	0.0	-0.7	349.6	367.3	359.2	56.0	61.49	1.82
18/12	902.0	0.0	6.4	154.0	173.3	157.4	52.1	72.1	1.98
22/12	900.7	1.3	0.2	201.6	219.9	207.2	54.0	69.91	3.06
23/12	871.8	4.0	1.6	201.5	219.5	209.1	53.2	69.69	1.86
23/12	884.6	3.0	2.6	303.1	320.6	309.3	54.9	65.36	2.03
1993									
04/01	744.6	1.1	-5.0	100.8	117.2	114.2	50.7	72.47	3.62
04/01	928.4	2.4	-0.9	379.6	397.4	389.4	56.1	57.7	1.91

Interrupted several times by bad weather, seven efficiency points and six thermal loss points were obtained in three more test days. No testing of the black chrome receiver was done with the glass envelope removed, because the relatively small differences between black chrome and cermet selective coatings would probably be completely obscured by the large data jitter caused by wind-forced conduction and convection losses. Testing of the SEGS LS-2 collector was concluded on 20 January 1993.

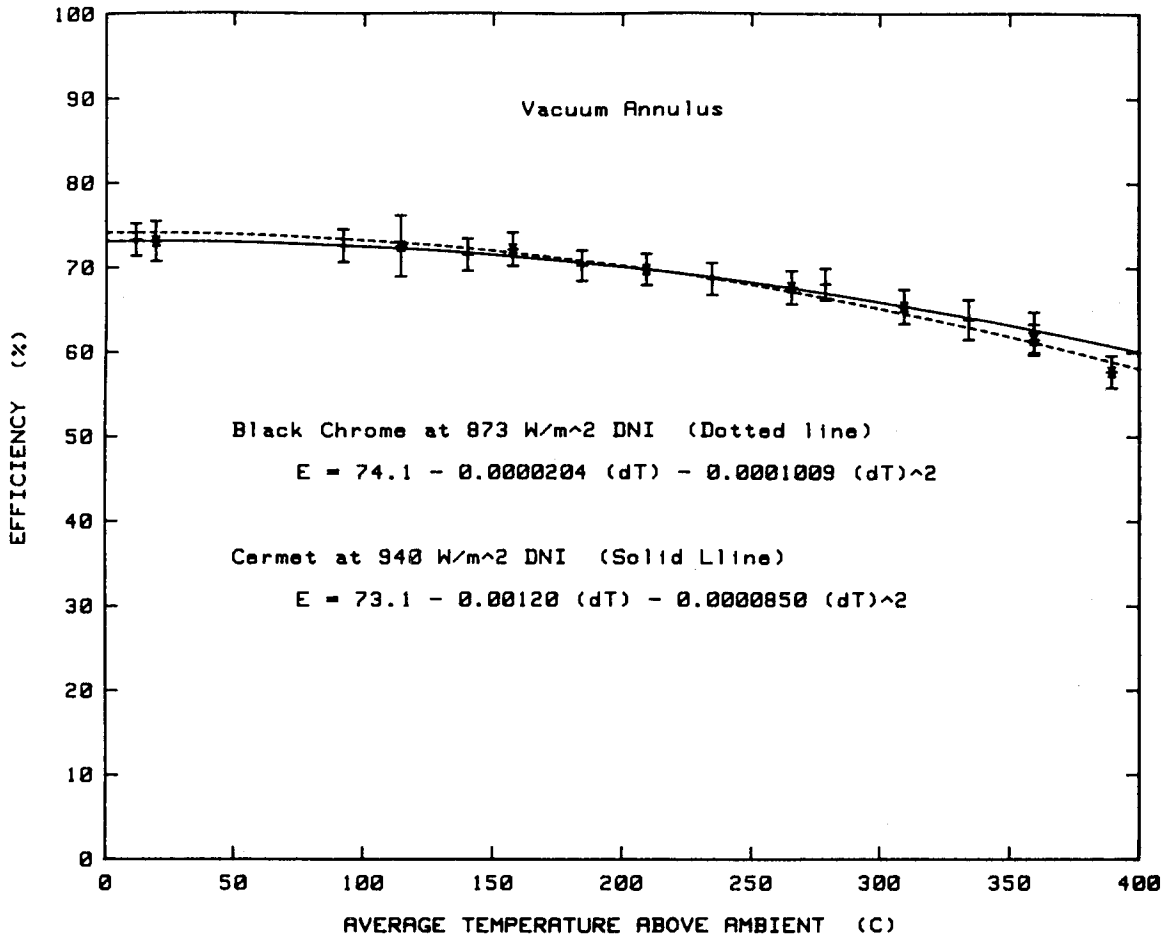

Figure D-16. Efficiency Comparison of Black Chrome and Cermet Receivers.

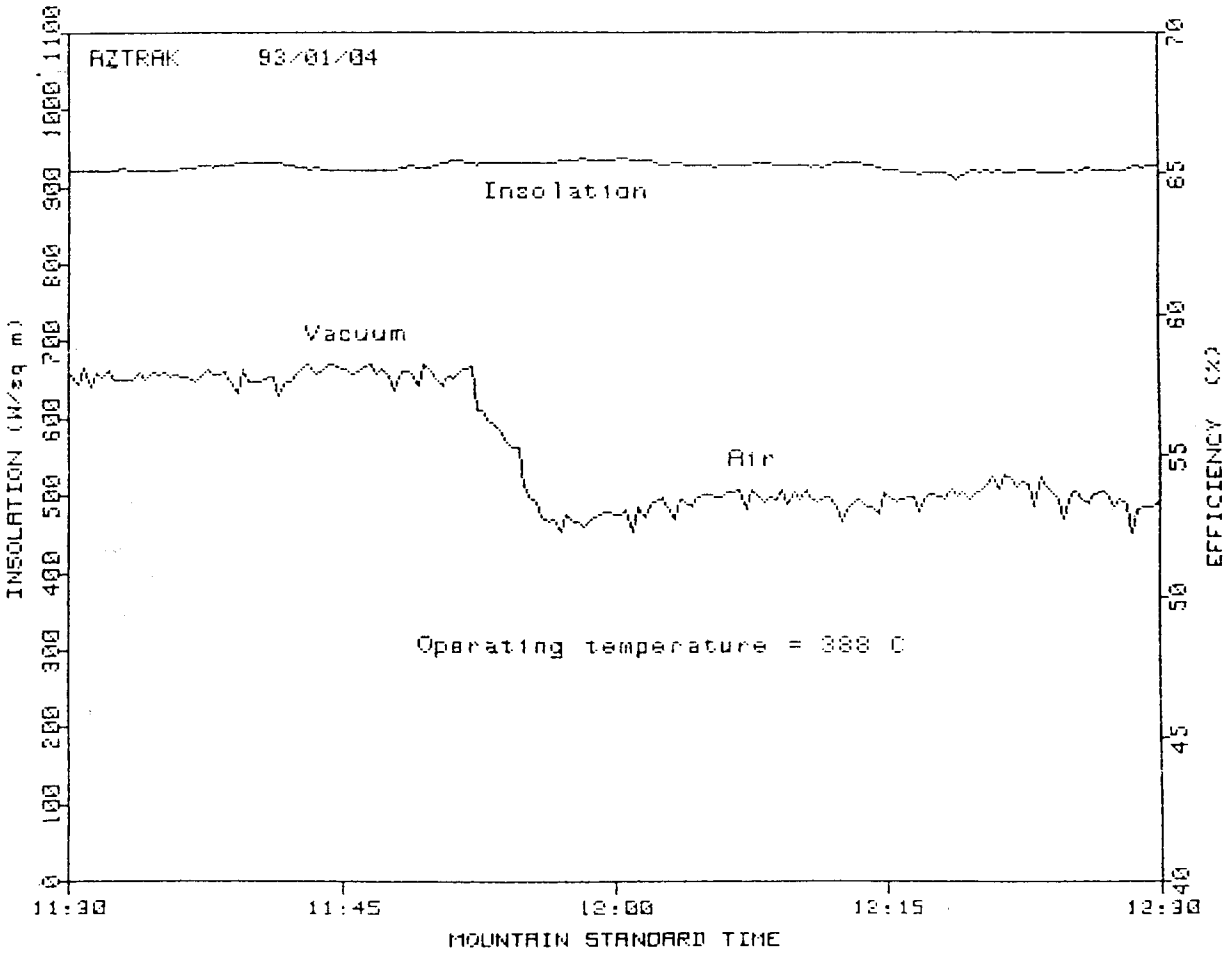

Figure D-17. Efficiency Change with Air Introduced into Receiver.

Table D-8. Measured Thermal Loss Data

Black Chrome Selective Coating, Vacuum Annulus

Test Date 1992	Wind speed m/sec	Air Temp °C	Temp In °C	Temp Out °C	Delta Air °C	Flow rate L/min	Meas Loss W/m2	Est Error W/m2
11/12	0.6	2.3	103.2	102.9	100.7	50.3	6.82	6.89
11/12	1.0	6.0	204.1	203.4	197.8	54.1	22.0	7.27
11/12	1.7	7.5	300.8	299.0	292.5	55.8	62.0	8.05
11/12	2.5	8.9	351.0	348.2	340.8	56.7	89.1	8.77
17/12	0.3	-5.2	150.9	150.6	156.0	52.5	12.4	7.00
17/12	2.8	1.1	348.5	345.7	346.1	56.7	89.1	9.43
17/12	1.5	1.1	253.9	252.8	252.4	55.1	36.7	7.76

Figure D-18 shows the air efficiency data from Table D-9 in graphical form, along with the equation fitted to the data. Also included is the vacuum receiver data for comparison. Figure D-19 compares the vacuum and air efficiency data for both black chrome and cermet receivers. As shown in the figures, the difference between cermet and black chrome is small, with a much larger difference when air is introduced into the vacuum annulus space.

Measured thermal loss data with the air-filled black chrome receiver are shown in Table D-10. Figure D-20 compares the black chrome thermal loss data for the vacuum and air cases, including the in-focus losses. Finally, Figure D-21 compares the measured thermal losses for the four different receiver configurations tested. As for the efficiency data, the differences between black chrome and cermet coatings are generally smaller than the difference between an air-filled and a vacuum annulus. The larger difference above 300°C between cermet and black chrome for the vacuum case may be mostly due to not having enough loss data above 250°C, leading to a bias in the curve fit at higher temperatures. The larger loss shown by the curves above 250°C is not supported by the efficiency measurements at the same temperatures.

Table D-9. Measured Efficiency Test Data

Black Chrome Selective Coating - Air in Annulus

Test Date 1993	NIP W/m2	Wind spd m/sec	Amb Temp °C	Temp In °C	Temp Out °C	Delta Amb °C	Flow rate L/min	Meas Effic %	Est Error %
04/01	919.5	1.4	0.1	379.7	395.8	387.6	56.2	53.71	2.97
12/01	755.0	5.5	-1.0	101.9	117.9	110.9	50.3	69.07	4.38
12/01	850.9	4.7	-0.6	203.2	219.0	211.7	54.3	64.14	1.98
12/01	899.7	4.4	0.5	301.6	317.6	309.1	56.2	60.08	2.23
12/01	909.6	1.2	1.3	251.8	268.7	259.0	55.0	63.32	1.76
20/01	908.1	5.9	5.9	350.2	366.3	352.3	55.6	56.17	2.02
21/01	902.6	1.7	5.1	154.2	172.4	158.3	52.1	67.88	1.89

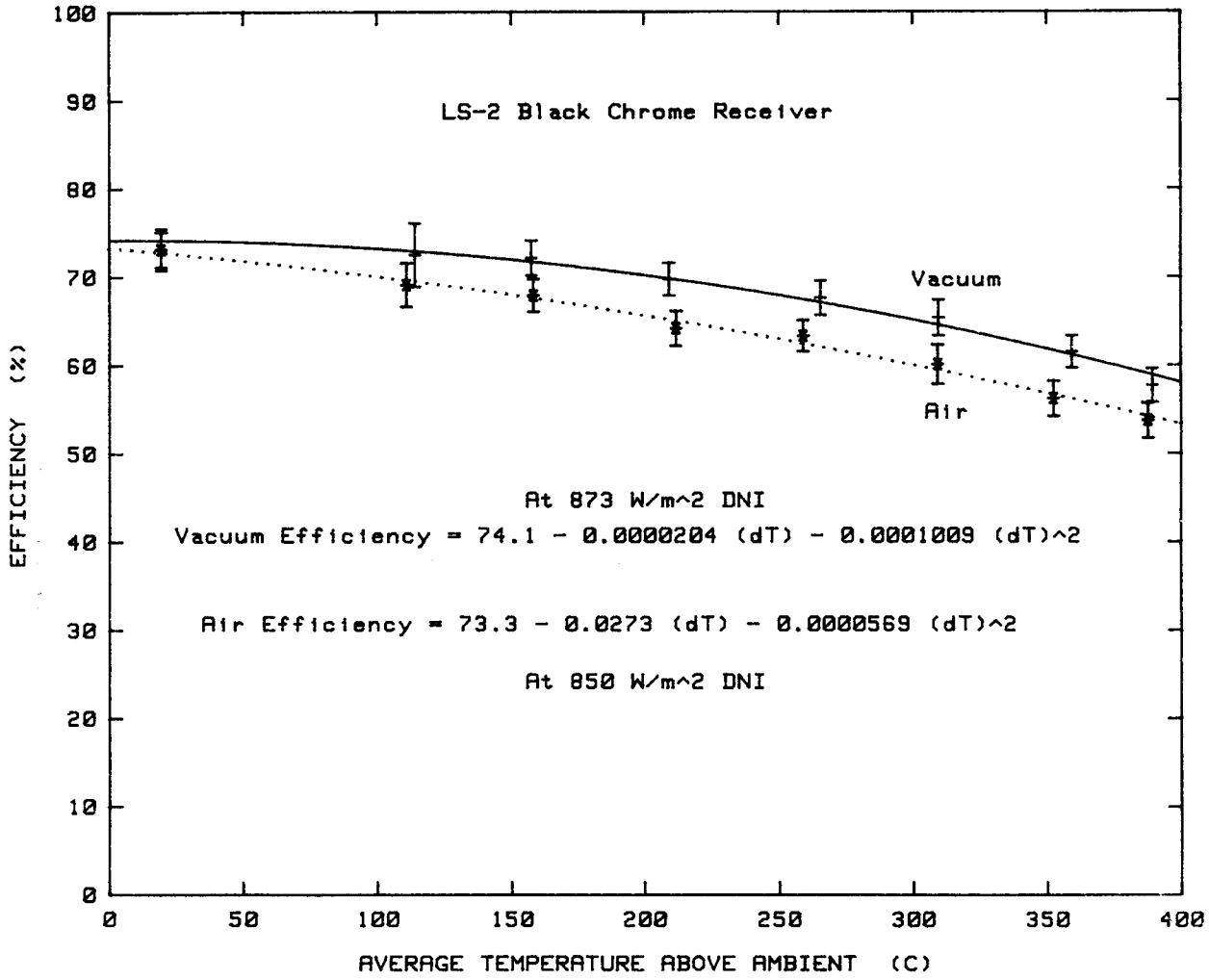

Figure D-18. Efficiency Comparison of Black Chrome Vacuum and Air Receivers.

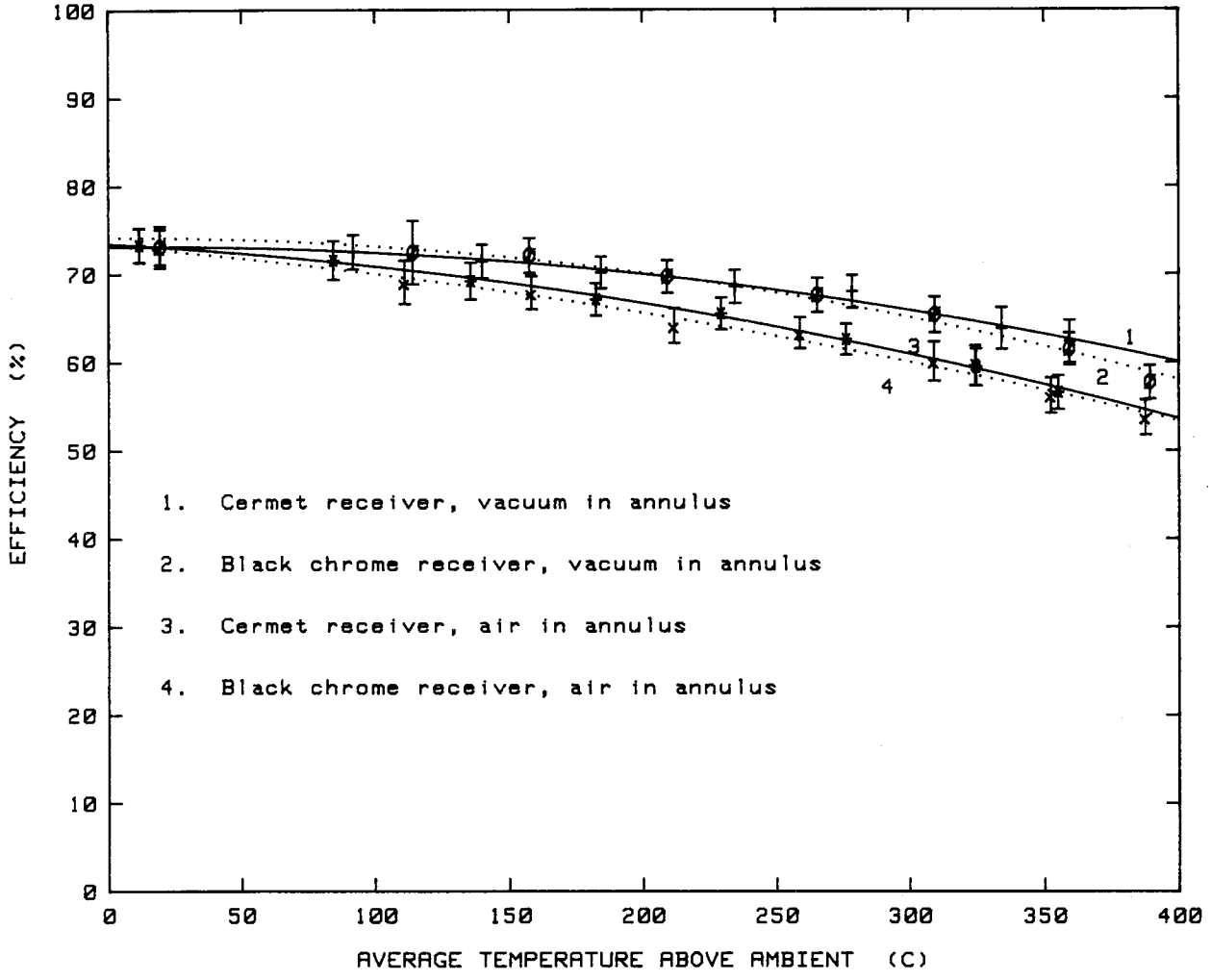

Figure D-19. Efficiency Comparison of Black Chrome and Cermet Receivers.

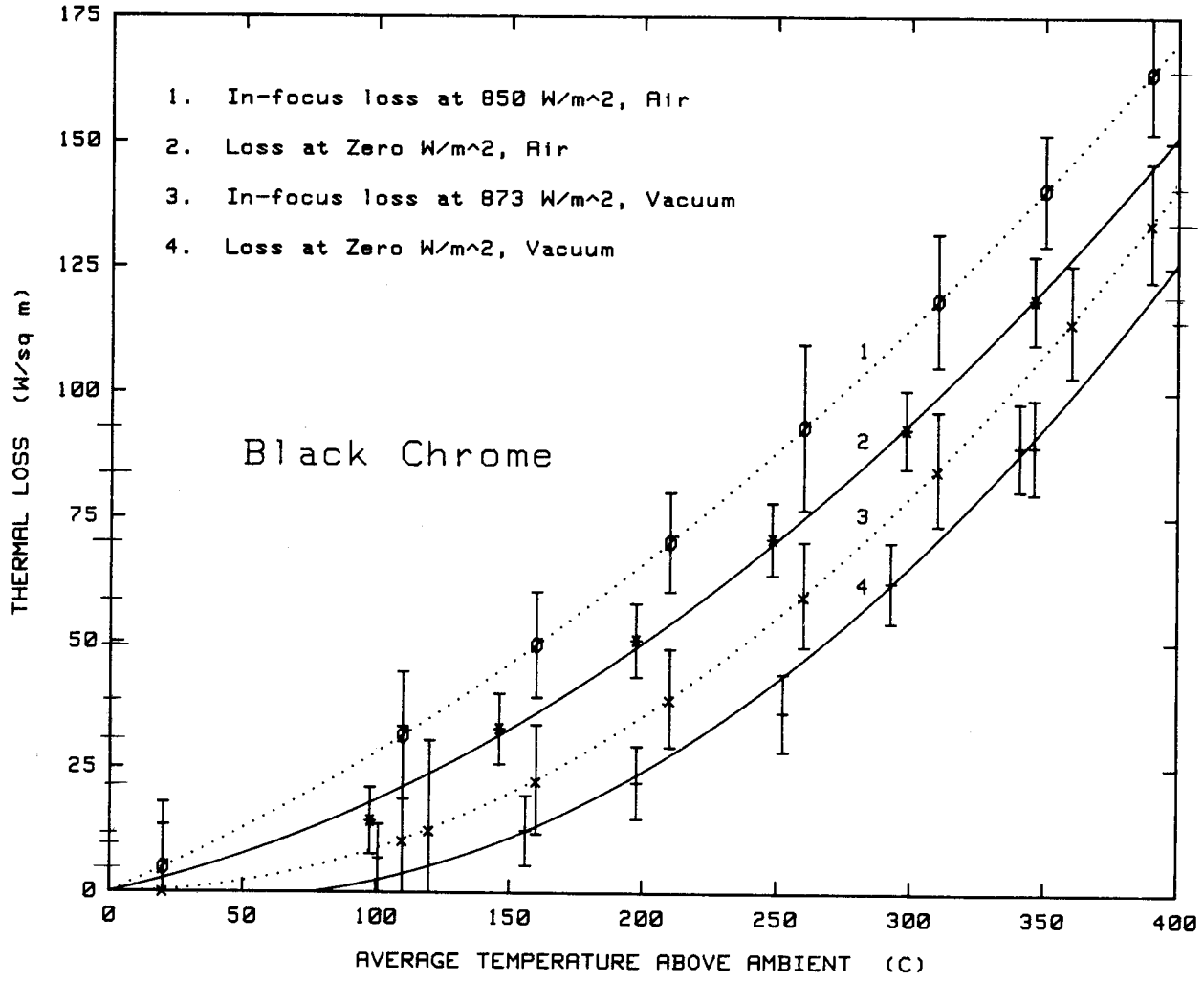

Figure D-20. Thermal Loss Comparisons—Vacuum & Air—Black Chrome.

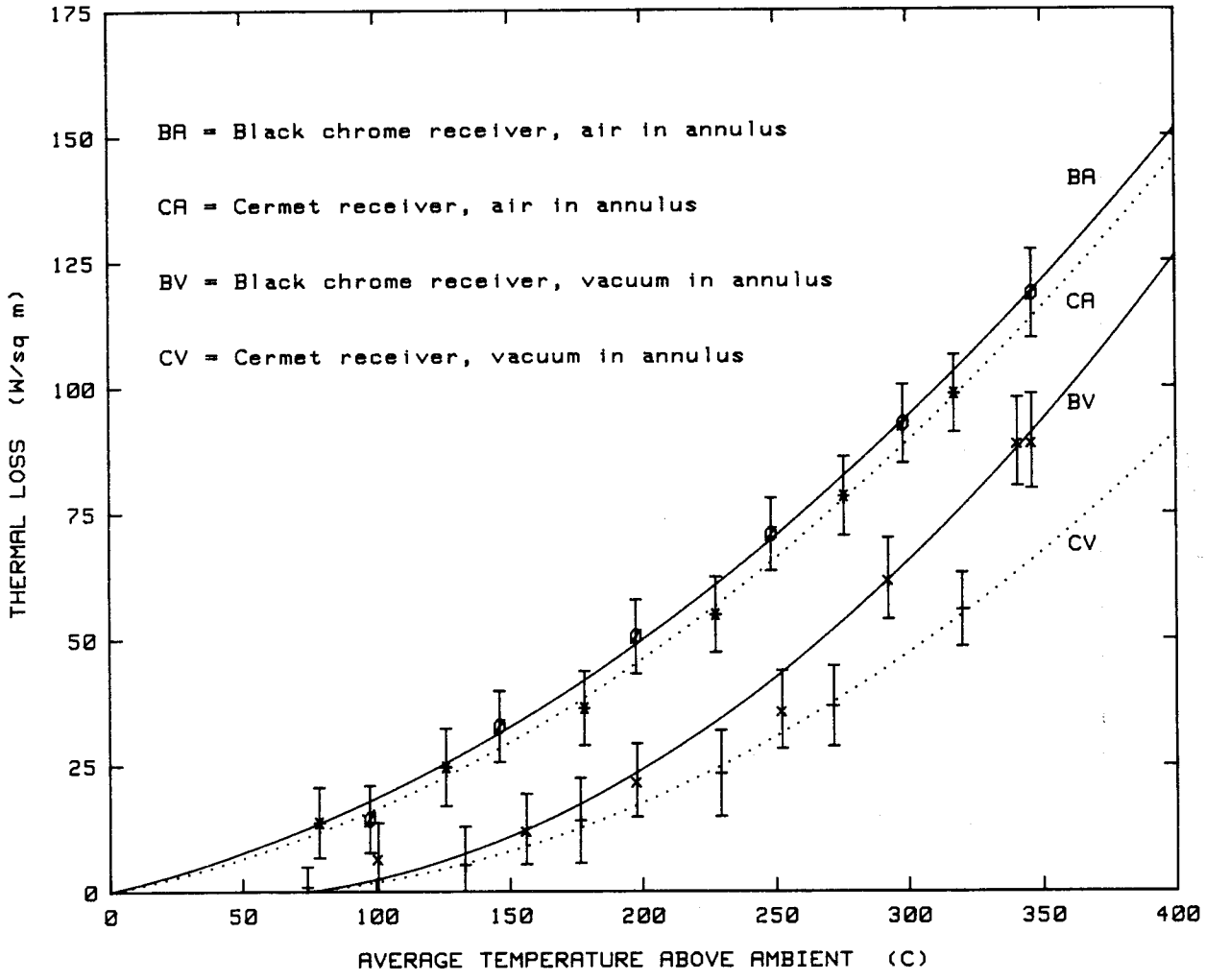

Figure D-21. Thermal Loss Comparisons—Black Chrome and Cermet Receivers.

Table D-10. Measured Thermal Loss Data

Black Chrome Selective Coating, Air in Annulus

Test Date 1993	Wind speed m/sec	Air Temp °C	Temp In °C	Temp Out °C	Delta Air °C	Flow rate L/min	Meas Loss W/m2	Est Error W/m2
04/01	0.6	3.0	302.4	299.7	298.1	55.6	92.6	7.82
04/01	0.6	1.5	349.4	345.7	346.1	56.6	118.5	8.82
12/01	2.5	2.7	251.9	249.9	248.3	54.9	70.7	7.24
12/01	1.7	3.5	201.7	200.2	197.5	53.5	50.5	7.35
12/01	0.8	3.9	150.4	149.4	146.0	52.0	32.7	7.08
12/01		2.9	101.6	100.6	98.2	43.0	14.0	6.67

Incident Angle Tests

These tests were made to determine the change in performance of the collector as the incident angle was increased from zero to 60 degrees. The approximate optical efficiency shown in the earlier data tables was also obtained during these tests when the collector was at zero incident angle. Tests were performed with all three receiver configurations: vacuum annulus, air in annulus, and bare receiver tube. All the testing was done with cold domestic water as the heat transfer fluid.

Since the receiver was operating at very near the ambient air temperature, thermal losses were negligible. No significant differences in peak efficiency of the cermet receiver were expected as a result of changing from a vacuum receiver annulus to an air-filled annulus. A difference in peak efficiency of about 1% was noted between the two receiver configurations, which could be caused by slight differences in reflector cleanliness, and is also less than our measurement error band. The presence of air should also not make any difference in the efficiency measured at various incident angles, and no significant changes in the incident angle modifier ratios were found. The incident angle modifier data points for the cermet/air receiver are listed in Table D-11. The points and a least-squares curve fit to the combined vacuum/air data are shown in Figure D-22

Table D-11. Incident Angle Performance Test Data

Cermet Selective Coating - Air in Annulus

Test Date 1992	NIP W/m^2	Amb Temp °C	Temp In °C	Temp Out °C	Delta Air °C	Flow rate L/m	Incid. Angle °	Calc. Effic %	Effic. Ratio	Ratio Error
18/08	925.1	38.4	29.5	47.3	9.9	20.7	0.0	73.68	1.0	0.0496
18/08	919.9	28.1	29.5	47.6	10.4	20.7	4.73	73.40	0.996	0.0437
18/08	910.0	26.4	29.4	47.0	11.8	20.5	9.72	72.79	0.9879	0.0504
18/08	893.9	24.9	29.2	45.8	12.7	20.5	14.99	71.29	0.9676	0.0473
18/08	888.2	24.4	29.1	44.7	12.5	20.5	20.04	68.91	0.9353	0.0434
18/08	881.0	23.7	28.9	43.5	12.5	20.5	25.01	66.06	0.8966	0.0399
18/08	867.9	24.4	28.8	42.0	11.0	20.5	29.91	62.48	0.8480	0.0391
18/08	851.1	24.3	28.6	40.3	10.2	20.5	34.76	57.88	0.7856	0.0404
18/08	833.8	23.7	28.5	38.6	9.8	20.5	39.94	52.88	0.7177	0.0371
18/08	784.1	22.1	28.3	36.6	10.4	20.4	44.40	47.57	0.6456	0.0584
18/08	737.1	21.7	28.1	34.7	9.7	20.4	49.47	41.50	0.5632	0.0424
18/08	665.6	20.8	27.9	32.6	9.4	20.4	54.71	34.00	0.4615	0.0391
18/08	602.9	20.1	27.7	30.8	9.2	20.2	59.65	27.26	0.3999	0.0253

Removing the glass envelope from the cermet receiver was expected to increase the peak (optical) efficiency, since the glass normally absorbs a small percentage of the light passing through. Measured efficiency did increase, from near 74% to about 77.5%. Test data for the bare tube is listed in Table D-12.

The glass had an anti-reflective coating on both surfaces, which helps reduce glass reflection losses at high incident angles. The glass coating was quite effective: there was little change in the incident angle modifier curve when the glass was removed. Curve fit coefficients for the bare tube incident angle modifier equation are slightly different from those derived from the vacuum/air test case, but the resulting curves (shown in Figure D-22) are identical for all practical purposes. Either equation could be used for calculations of field performance.

Table D-12. Incident Angle Performance Test Data

Cermet Selective Coating - Bare Receiver (No Glass)

Test Date 1992	NIP W/m 2	Air Temp °C	Temp In °C	Temp Out °C	Delta Air °C	Flow rate L/m	Incid. Angle °	Calc. Effic %	Effic. Ratio	Ratio Error
27/08	954.5	23.5	29.0	47.9	14.93	21.3	0.0	77.46	1.0	0.0507
27/08	950.8	23.3	28.8	49.9	15.1	21.3	4.74	77.17	0.9963	0.0507
27/08	944.7	22.9	28.8	47.3	15.2	21.3	9.72	76.43	0.9867	0.0497
27/08	941.4	21.7	28.7	46.3	15.8	21.3	14.72	74.48	0.9615	0.0497
27/08	934.7	21.6	28.6	45.2	15.3	21.2	19.74	71.87	0.9278	0.0473
27/08	922.9	21.3	27.4	43.7	14.3	21.2	24.73	68.18	0.8801	0.0441
27/08	914.5	20.6	28.2	42.1	14.6	21.2	29.70	64.16	0.8283	0.0454
27/08	894.4	20.1	28.0	40.3	14.0	21.2	34.73	59.39	0.7667	0.0469
27/08	881.2	19.3	27.9	38.7	14.0	21.1	39.76	54.69	0.7060	0.0505
27/08	850.1	17.7	27.8	35.5	14.0	21.2	49.67	43.84	0.5660	0.0336
27/08	818.0	17.2	27.8	33.1	13.2	21.2	55.68	34.21	0.4416	0.0422
27/08	786.7	16.9	27.6	31.6	12.7	21.2	59.63	27.93	0.3606	0.0400
27/08	713.1	15.8	27.3	29.7	12.7	21.1	65.09	21.40	0.2763	0.0305

Notes for Tables D-11, D-12, and D-13:

All data taken with cold water as the heat-transfer fluid
Efficiency data corrected for collector end loss, at focal length = 1.84 m

Table D-13. Incident Angle Performance Test Data

Black Chrome Selective Coating - Vacuum in Annulus

Test Date 1992	NIP W/m2	Amb Temp °C	Temp In °C	Temp Out °C	Delta Air °C	Flow rate L/m	Incid. Angle °	Calc. Effic %	Effic. Ratio	Ratio Error
09/12	850.3	4.0	14.8	31.8	19.3	20.5	0.0	73.4	1.0	0.0474
09/12	856.9	3.6	14.7	31.9	19.7	20.5	4.53	73.1	0.996	0.0631
09/12	868.8	3.0	14.5	31.4	20.0	20.5	9.52	73.0	0.995	0.0545
09/12	833.1	2.8	14.4	29.3	18.9	20.5	19.53	70.4	0.959	0.0789
09/12	852.3	2.3	13.8	24.2	16.7	20.6	40.6	53.3	0.736	0.0383
09/12	836.0	1.9	13.9	21.5	15.8	21.0	48.0	43.5	0.593	0.0509
09/12	811.4	1.8	13.8	17.6	13.9	21.5	59.5	27.1	0.369	0.0322

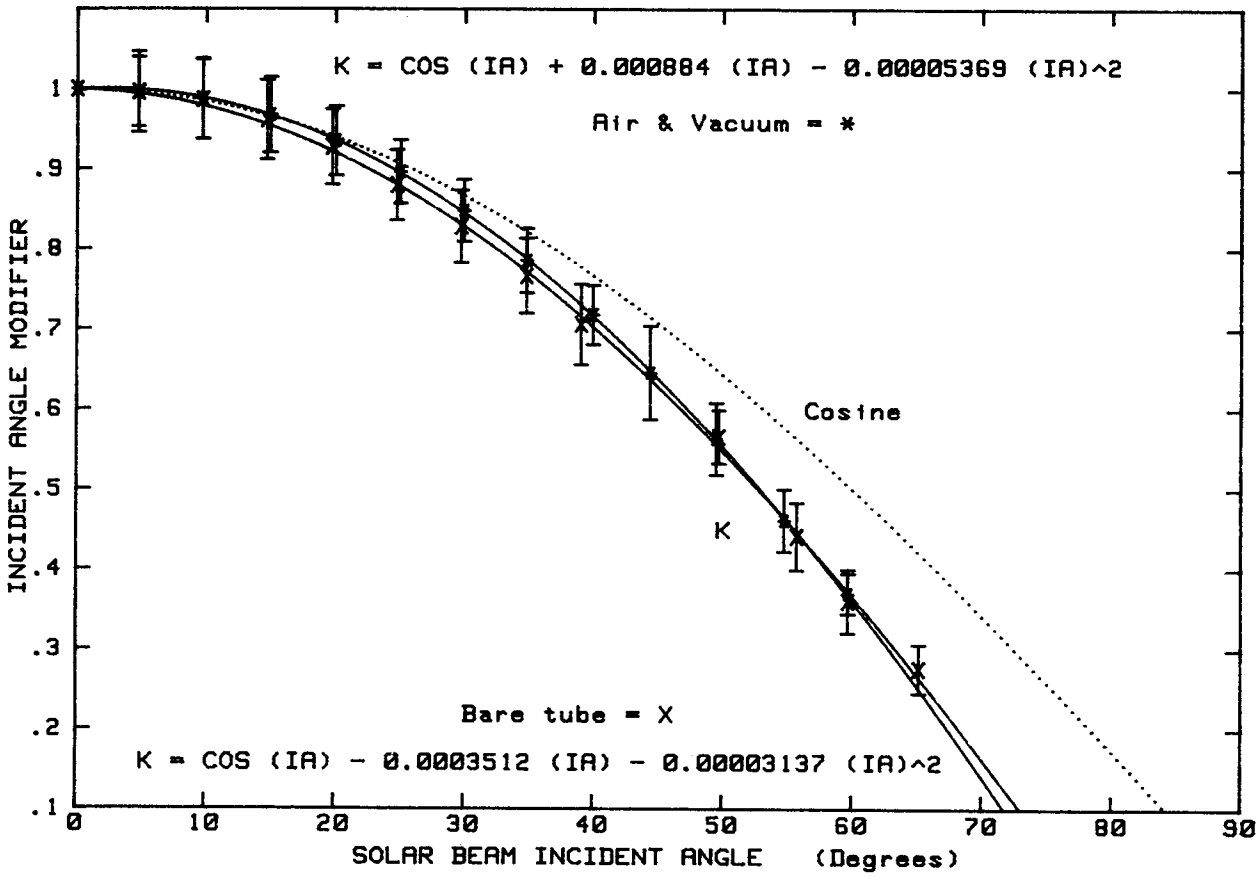

Figure D-22. Incident Angle Modifier—SEGS LS-2 Receiver.

Data Analysis

By linear scaling of thermal losses between the in-focus loss (high value of insolation on receiver) and the measured thermal loss (zero insolation) we can derive the collector efficiency for any desired incident solar irradiance. This procedure (see Appendix C) was performed for a matrix of insolation and temperatures. A multiple regression of the data matrix then produced a performance equation for the collector which should predict performance over the temperature range from ambient to 400°C, and for insolation from zero to about 1100 W/m^2. The incident angle modifier K is also included as a factor in the performance equation. Repeated for each of the receiver configurations tested, except for the bare tube, four equations resulted, as shown in Table D-14. These equations are also shown in the introduction to this report. A plot of one of these performance equations, for the Cermet/air receiver at zero incident angle, is shown in Figure D-23. The shape of the plot changes significantly with incident angle; for an example at 55 deg incident angle, see Appendix C, Figure C-4. The equation can also be plotted in a different format for selected values of insolation; see Appendix C, Figure C-3.

Table D-14. LS-2 Collector Performance Equations

Cermet with vacuum annulus

$$\eta = K\,[73.3 - 0.007276\,(\Delta T)] + 0.496(\Delta T/I) - 0.0691\,(\Delta T2/I) \quad (1)$$

Cermet with air in annulus

$$\eta = K\,[73.4 - 0.00803\,(\Delta T)] - 9.68\,(\Delta T/I) - 0.0669\,(\Delta T2/I) \quad (2)$$

Black chrome with vacuum annulus

$$\eta = K\,[73.6 - 0.004206\,(\Delta T)] + 7.44\,(\Delta T/I) - 0.0958\,(\Delta T2/I) \quad (3)$$

Black chrome with air in annulus

$$\eta = K\,[73.8 - 0.006460\,(\Delta T)] - 12.16\,(\Delta T/I) - 0.0641\,(\Delta T2/I) \quad (4)$$

Incident Angle Modifier, K (For all receiver configurations)

$$K = \cos(Ia) - 0.0003512\,(Ia) - 0.00003137\,(Ia)2 \quad (5)$$

In performance equations (1) through (5):

η = Collector efficiency, in percent
K = Incident angle modifier
ΔT = Receiver fluid temperature above ambient air temperature, °C
Ia = Solar beam incident angle, in degrees

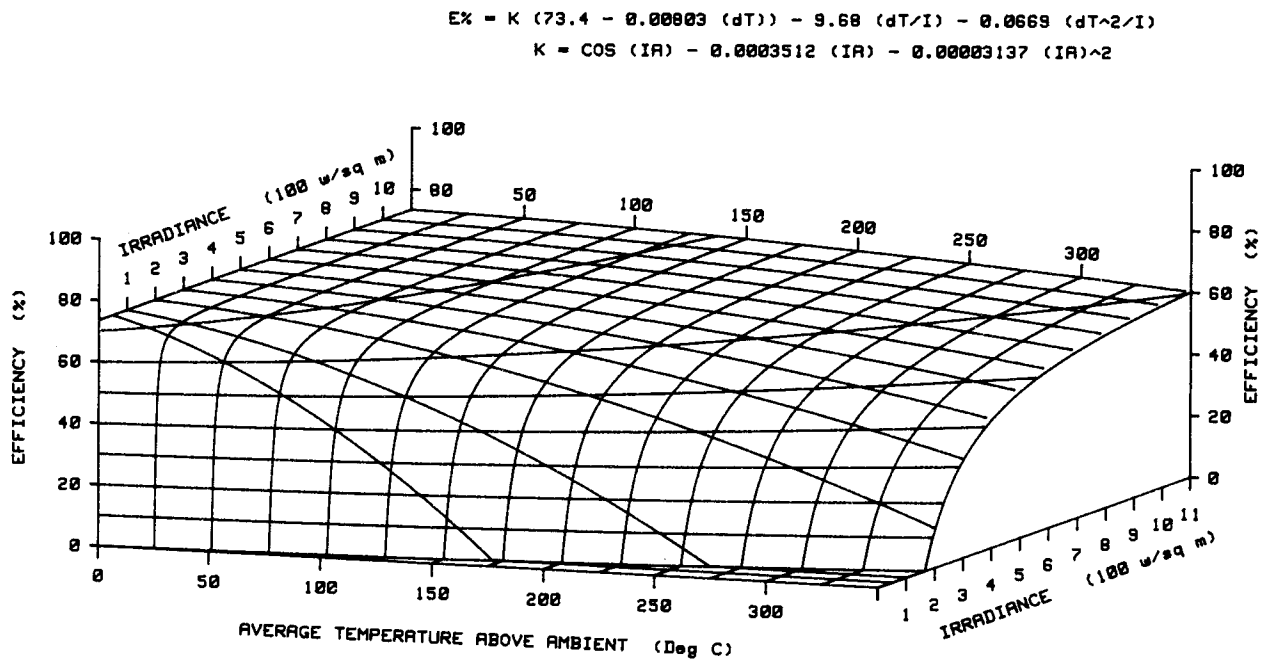

Figure D-23. SEGS LS-2 Cermet/Air Efficiency at Zero Incident Angle.

APPENDIX E

ERROR ANALYSIS

Contents for Appendix E

Appendix E

Error Analysis

Introduction

An error analysis was carried out for measurements of collector efficiency, thermal loss, and incident angle modifier. These measurements all include a combination of fluid mass flow, specific heat and temperature. Insolation was also included for efficiency and incident angle modifier measurements. Both measuring instrument error and statistical data variability were considered in this analysis. There is some uncertainty in the equations for Syltherm® heat-transfer fluid properties (Dow-Corning, 1982); the magnitude of these is unknown, and was not considered in this analysis. The effect of temperature measurement error on fluid properties was included.

Instrument errors apply to a single measurement set, i.e., a computer data scan. These measurement sets were repeated at 15-20 second intervals during each test. In the analysis of the data to obtain a value such as efficiency, the measured data was averaged over a period of several minutes. To determine the length of the averaging period for each data point, receiver time constants were measured at the beginning of the test series, see Figure D-2. The SEGS LS-2 receiver time constant was found to be about three minutes; data averaging time was then set at a minimum of two time constants, or about 6 minutes. Most data point averaging was longer than the minimum, usually about 10 minutes.

Even though the system was operated at each temperature for a long time (usually an hour or more) to obtain maximum system stability of flow and temperature prior to an averaging period, there is always some scatter in the data during the averaging period due to measuring instrument electrical noise and remaining instabilities in flow, temperature or insolation. In estimating the errors of the averaged data points, the errors associated with each point in the average are assumed to be correlated, since instrument calibration errors are not expected to vary over such short periods of time.

A sample of data from a thermal loss test with the black chrome / vacuum receiver is shown in Table E-1, the mean data values are reported as a thermal loss point in Table D-8, line 5. A sample of data from an elevated temperature efficiency test is shown in Table E-2, the mean data values are reported as an efficiency point in Table D-3. All the data points in Appendix D data tables were obtained from calculated mean values similar to those shown in Tables E-1 and E-2. Again note that the system was operated at a constant temperature and flow rate for about an hour before the time periods shown in the sample data tables.

For each averaging period, such as those shown in the sample data tables, the population standard deviation of each measurement was calculated as a check on the stability of the system under test. Also, the data range from minimum value to maximum value during the averaging period had to be within the stability criteria outlined in the Test Plan, Appendix C. For example, in Table E-1, the input and output temperature range of about 0.1°C (± 0.05°) is our usual requirement for a stable data point, and is also about the best the fluid supply system can maintain, and the best we can reasonably measure with current equipment. Operation for less than an hour at a given temperature produces less stable temperatures, operation for longer times results in little improvement.

An important stability requirement for the data averaging period is that there be no trend of temperatures (or flow rates, insolation, etc.) toward higher or lower values, which would indicate that energy is being stored in (or removed from) the mass of the system under test. Even a stringent ± 0.05°C temperature stability requirement is not as good as would be desirable; as the result is a 22% scatter in the measured

thermal losses shown in Table E-1. The low temperature thermal losses with the vacuum receiver configuration (shown in Table E-1) were the worst case for data scatter and total error because of the very small temperature drop across the receiver during the test (only about 0.4 °C). Table E-2 is more typical, where the scatter in measured efficiency is about 0.8%.

Data measurement errors were calculated using the root-sum-square method, defined as: (Doebelin, 1983; Bevington, 1978):

$$E_{rss} = \sqrt{\left[\Delta\mu_1\left(\frac{\partial F}{\partial \mu_1}\right)\right]^2 + \left[\Delta\mu_2\left(\frac{\partial F}{\partial \mu_2}\right)\right]^2 + \cdots + \left[\Delta\mu_n\left(\frac{\partial F}{\partial \mu_n}\right)\right]^2} \qquad (1)$$

Where:

Erss	=	root-sum-square error
u_i	=	measured quantity
Δu_i	=	error in measured quantity
$\partial F/\partial u_i$	=	partial derivitive of the calculated function with respect to the measured quantity.

Two error sources should be considered: the instrument calibration (bias) errors, and statistical errors due to scatter in repeated measurements of the same quantity. Instrument calibration errors were as follows:

Temperature	Et =	0.5°C	(Type T thermocouples)
Delta-temperature	Edt =	0.2°C	(Matched type T thermocouples)
Flow rate	E*f* =	1% of flow	(Liters/minute)
Insolation	Ei =	2% of DNI	(Watts/m^2)

Statistical error was calculated by using the measurement standard deviation multiplied by the Student's T statistic for the measurement degrees of freedom (n measurements -1). The two errors can then be combined using the root-sum-square method for a final error estimate.

For this report, both types of errors were calculated and included in the data, except for the bare receiver test. Statistical errors for the performance data with the bare receiver would have been larger because of the increased measurement variability caused by changing wind velocity.

Heat Gain Errors

The following equation was used in calculating heat gain (or loss):

$$Q = (\text{flow rate}) * (\text{density}) * (\text{specific heat}) * (\text{delta-temperature}) \qquad (2)$$

Density of the heat transfer fluid:

$$\rho = A + B\,(\text{temperature}) + C\,(\text{temperature})^2 + D\,(\text{temperature})^3 \qquad (3)$$

For water, coefficients A, B, C and D were obtained from an equation fitted to data from Keenan and Keys (Ref. 4); for Syltherm®, the coefficients were from Dow Corning (Ref. 1). In each case, the temperature used was the temperature of the fluid at the flow meter. For density, the coefficients are:

	Water	Syltherm oil
A	0.99971 kg/L	954.0 kg/m^3
B	-1.42399 x 10^{-4}	-0.919

C	-2.69909×10^{-6}	4.25×10^{-4}
D	0.0	-1.67×10^{-6}

For specific heat of the heat transfer fluid, the equation is:

$$Cp = E + F\,(\text{temperature}) + G\,(\text{temperature})^2 \qquad (4)$$

Coefficients for specific heat are from the same sources as for density. The average temperature of the fluid in the collector's receiver tube was used to evaluate the equations. For specific heat, the coefficients are:

	Water	Syltherm oil
E	4.0803 kJ/kg°C	1575 J/kg°C
F	-6.379×10^{-4}	1.708
G	4.487×10^{-6}	0.0

For heat gain Q, the error equation (1) becomes:

$$Eq = \sqrt{\left[E\rho\left(\frac{\partial q}{\partial \rho}\right)\right]^2 + \left[Edt\left(\frac{\partial q}{\partial dt}\right)\right]^2 + \left[Ef\left(\frac{\partial q}{\partial f}\right)\right]^2 + \left[Ecp\left(\frac{\partial q}{\partial cp}\right)\right]^2} \qquad (5)$$

Where:

$\partial q/\partial \rho$	=	Flow * Cp * dt
$\partial \rho/\partial t$	=	B + 2C * Temp + 3D * Temp^2
$\partial cp/\partial t$	=	F + 2G * Temp
$\partial q/\partial dt$	=	ρ * Flow * Cp
$\partial q/\partial f$	=	ρ * Cp * dt
$\partial q/\partial cp$	=	ρ * Flow * dt
ρ	=	fluid density, kg/ m^3
$E\rho$	=	Et * $\partial \rho/\partial t$
Ecp	=	Et * $\partial cp/\partial t$
Flow	=	fluid flow in m^3/sec
Ef	=	flow measurement error, m^3/sec
Temp	=	fluid temperature, °C
Et	=	temperature measurement error, °C
dt	=	receiver fluid delta temperature, °C
Edt	=	delta temperature measurement error, °C
Cp	=	fluid specific heat, J/kg °C
q	=	Heat gain (Loss), Watts

Efficiency Errors

Efficiency is derived from heat gain and input insolation:

η = heat gain / heat input = Q / insolation * collector aperture

For an efficiency measurement, the error equation is:

$$E\eta = \sqrt{\left[Eq\left(\frac{\partial\eta}{\partial q}\right)\right]^2 + \left[Ei\left(\frac{\partial\eta}{\partial i}\right)\right]^2} \qquad (6)$$

Where:

Eq	=	error in heat gain
Ei	=	error in insolation
$\partial_\eta / \partial q$	=	1/ (insolation * aperture)
$\partial_\eta / \partial_I$	=	-q / (insolation^2 * aperture)

Incident Angle Modifier

Incident angle modifier K is the ratio of efficiency performance at some incident angle to the efficiency at zero incident angle:

$$K = \eta^{IA} / \eta^0 \qquad (7)$$

The incident angle modifier error equation is:

$$E_k = \sqrt{\left[E_A\left(\frac{\partial_k}{\partial\eta_A}\right)\right]^2 + \left[E_0\left(\frac{\partial_k}{\partial\eta_0}\right)\right]^2} \qquad (8)$$

Where:

E_k	=	Error in incident angle modifier K
E_A	=	Error in efficiency at incident angle A
E_0	=	Error in efficiency at incident angle zero
$\partial k / \partial\eta_A$	=	$1 / \eta_0$
$\partial k / \partial\eta_0$	=	$-\eta_A / \eta_0^2$

Sample Efficiency Error Analysis

When the equations above are evaluated at 202°C inlet temperature (see Table E-2), the values are:

σ	= Population Standard Deviation	
Inlet temp	= 202.41°C	σ = 0.037°C
Outlet temp	= 219.39°C	σ = 0.032°C
Delta-Temp	= 16.98°C	σ = 0.042°C
Ambient air	= 28.5°C	σ = 0.135°C
Oil flow rate	= 0.00090928 m^3 /sec	σ = 0.00000122 m^3 /sec
Density	= 785.4 kg/m^3 @ 202.4°C	
Specific heat	= 1935.2 J/kg °C @ 210.9 °C	
Insolation	= 878.7 W/m^2	σ = 1.067 W/m^2
Heat gain Q	= 598.7 W/m^2	

Efficiency	= 67.1 %	σ = 0.171 %
Et	= 0.816 °C	
Edt	= 0.231 °C	
Ei	= 17.8 W/m^2	
Ef	= 0.00000971 m^3 /sec	
Ecp	= 1.393 J/kg °C	
Eρ	= -0.777 kg/m^3	
∂q/∂cp	= 12.13	
∂q /∂dt	= 1382.03	
$\partial\rho/\partial$t	= -0.9522	
∂cp/∂t	= 1.708	
Eq	= 10.39 W/m^2 gain error	
∂_η /∂_Q	= 0.0010101	
∂_η /∂i	= -0.00072367	
E_η	= 1.88 % efficiency error	

For the measurement analyzed above, 26 data measurements were made over a period of 8 minutes. The 95% confidence T statistic for 26 measurements is 2.771. Including both statistical and measurement errors, the final error estimate is ±1.88%. If the statistical error is not included, the efficiency error estimate is ±1.27%

The calculations for estimated error outlined above were repeated for each entry in the data tables; the results are listed in the 'Est Error' column of each data table in Appendix D, and are also used to size the error bars shown on the curves.

The critical measurements which have the most effect on error size are fluid flow rate, delta-temperature, and insolation. A large sample size with a small standard deviation is also needed for a small error bound, again reinforcing the requirement for maximum system stability before data measurements begin.

References:

Dow Corning; 1985. *Properties of Syltherm 800 Heat Transfer Liquid.* Midland, Michigan.

Doebelin, E. O., 1983. *Measurement Systems; Application and Design.* New York: McGraw-Hill, Inc.

Bevington, P. R., 1969. *Data Reduction and Error Analysis for the Physical Sciences.* New York: McGraw-Hill, Inc.

Keenan, J H., Keys, F. G., Hill, J. G., Moore, J. G. 1978. *Steam Tables.* New York: Wiley-Interscience.

APPENDIX F

User's Manual for HCE-HTX Computer Program

Contents for Appendix F

Figures

Tables

Introduction

This report is designed to assist users of the SEGS heat collection element (HCE) heat transfer analysis program (HCE-HTX) that was developed to support the Sandia O&M Cost Reduction Program. The code, written under subcontract to KJC Operating Company by M. Sloan of Sloan Solar Engineering, uses MS QuickBasic version 4.5 (DOS language) and is based on analysis provided by T. Mancini of Sandia National Laboratory. The coding is general enough to allow modeling of other non-SEGS type collectors. For example, Sandia has used the code to model heat losses from parabolic trough collectors built by Industrial Solar Technologies (Dudley & Evans). The code is available from Sandia upon request.

This HCE-HTX manual includes a program description and flow chart, sample runs with output, and comments on various program details. Material property data and a program listing are included as addenda.

Program Description

This section describes the current HCE-HTX code through discussion of various program features, program limitations, and a flow chart.

General Description

The HCE-HTX program calculates the one-dimensional, steady-state heat losses and HTF heat gain per unit length (meter) of an HCE as a function of fractional HTF flow rate, HTF bulk temperature, and solar conditions (direct normal insolation, date and time). Intermediate products of the analysis include glass envelope and absorber temperatures. In its current form, HCE-HTX v2.0 is an uncompiled program using MS QuickBasic v4.5 program. Case input data are edited directly into the code; future modifications could include a more convenient user interface if warranted by usage. Hence, a typical program run requires modification to the main module to specify the input data and, occasionally, changes to selected values in subroutines.

The primary program variables — fractional HTF flow rate, HTF bulk temperature, and solar conditions (direct normal insolation, site information, date and time) — are defined in the main module, as are output format and device (screen, file, printer). Supporting material rounding out the problem description is supplied in the *HCE.HTX.Set.Up* subroutine. *HCE.HTX.Set.Up* provides two functions: 1) it supplies material definitions (i.e. absorber = "Cermet"), dimensions, optical properties, and ambient conditions; and 2) it sets up the values for all material property look-up tables.

The heat available at the absorber surface is directly determined within the main module from specified solar conditions and optical properties. Under steady state conditions, some portion of this energy will result in sensible heating of the HTF. The remainder of the heat flow will be given up to the environment through convection and radiation losses.

The routines required to perform the heat transfer analysis are organized in the subroutine *HCE.HTX.Analysis*. The methodology utilized by in subroutine is outlined below.

METHODOLOGY

Given

- Direct normal insolation; site location, date, time, ambient conditions
- Geometric configuration and material property data
- HTF flow rate and bulk inlet temperature

Calculation Method

- Assume an envelope temperature and an absorber temperature

- Iterate for envelope temperature until the net heat flow in the evacuated region of the HCE assembly matches the external heat loss to the environment (Loop 1)
- Calculate the net heat loss from consideration of the available insolation at the HCE absorber and the heat gain of the HTF (Loop 2).
- Compare heat losses from the above two steps and reiterate on these steps as necessary until the two heat loss calculations are equal.

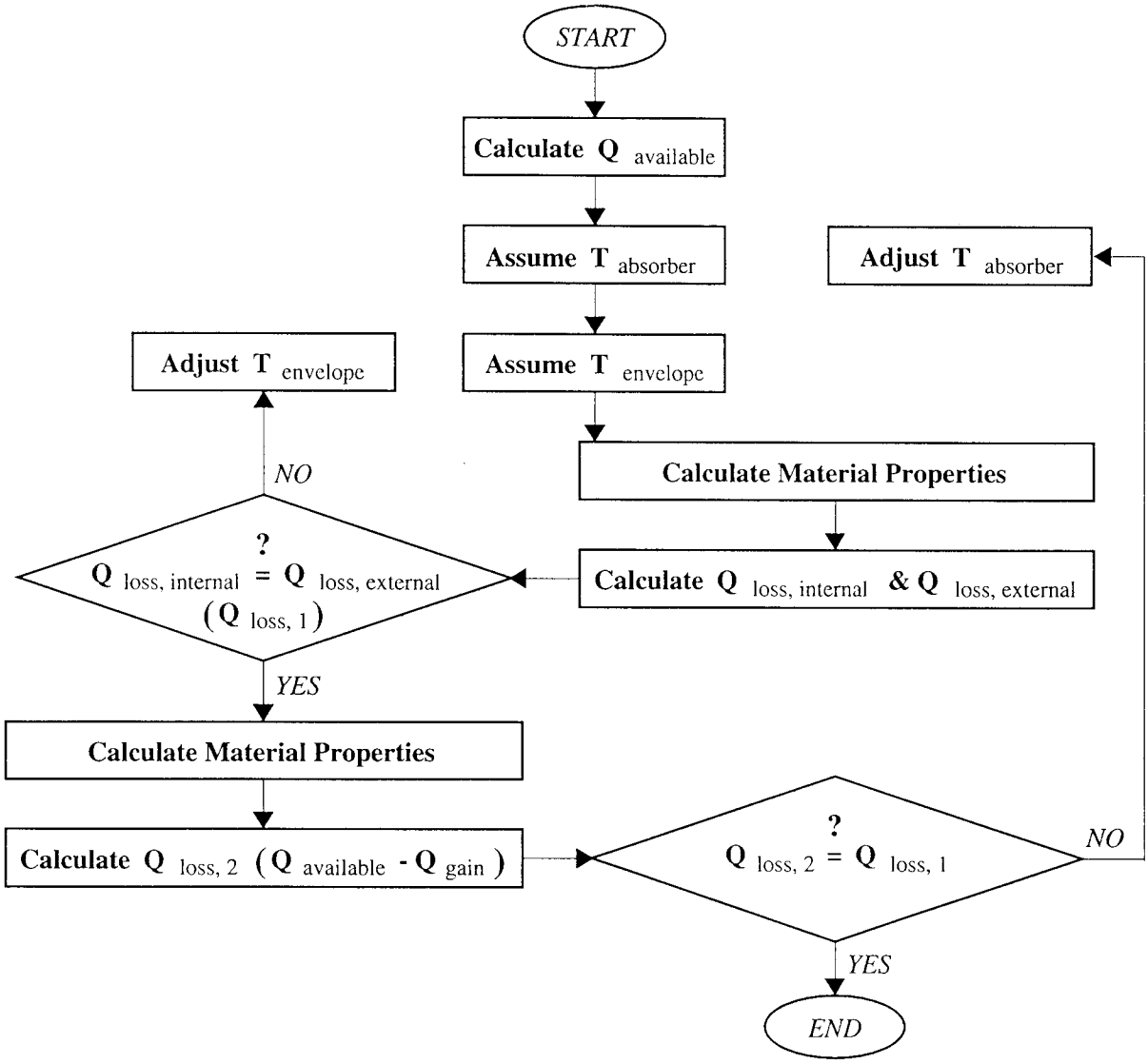

Figure F-1. HCE-HTX program flow chart.

Analytical Basis

The methodology and algorithms that have been incorporated into the HCE heat transfer code were suggested by Dr. Thomas Mancini of Sandia (see description in main body of this report.) As stated previously, the model calculates the one-dimensional, steady-state heat losses and HTF heat gain per unit length (meter) of an HCE of specified dimensions, configuration and material properties. The principal model parameters include fractional HTF flow rate, HTF bulk temperature, ambient solar and weather conditions, and a detailed specification of the HCE. The model accommodates several conditions of the HCE annulus: vacuum intact, lost vacuum (air in annulus), and broken annulus cover (bare tube). Additionally, thermodynamic property data for several materials have been included and are summarized in Table F-1 below.

Table F-1. Available Materials with Property Data in HCE-HTX version 2.0

Region	Material	Information Source
HTF:	1) Therminol VP-1	Manufacturer's data (tables)
	2) Syltherm 800	Manufacturer's data (equations)
Absorber:	1) Stainless Steel w/ Cermet coating	SNL experiment (ε); KJC
	2) SS w/ Black Chrome	KJC
Evacuated Region:	1) Air @ specified pressure	Incropera and DeWitt (tables); ideal gas law
	2) Air @ 1 atm	Incropera and DeWitt (tables)
	3) Hydrogen @ specified pressure	Incropera and DeWitt (tables), ideal gas law
	4) Argon @ specified pressure	Daubert and Danner (equations), ideal gas law
	5) None	
Envelope:	1) Low Iron glass w/ anti-reflective	KJC
	2) None	
Environment:	1) Air @ 1 atm	Incropera and DeWitt (tables)
	2) Air @ reduced pressure	Incropera and DeWitt (tables); ideal gas law

References:
Incropera and DeWitt, *Fundamentals of Heat Transfer*, John Wiley and Sons (1981)
Daubert and Danner, *Physical and Thermodynamic Properties of Pure Chemicals*, Hemisphere Publishers (1989)

The material designation of "None" for the envelope and evacuated region in Table F-1 are applicable to conditions in which the HCE envelope is missing, resulting in a bare absorber, i.e., one exposed to the ambient environment.

Other program features include:

- provision for 2-axis tracking HCE (Sandia experimental set-up)
- provision for obstruction to be placed in flow to increase flow speed (Sandia experimental set-up)
- various code run output options and devices (screen, file, printer)
- LS-2 and LS-3 dimensions and optical efficiencies
- all convection correlations are included in individual subroutines to facilitate modifications.

Additionally, the HCE.HTX main module contains provisions to print various program elements (lines 151-161). Among these are:

- table listing of material property values for any specified material.
- sample solar angle calculations including sunrise, solar noon, and sunset times.
- tabular listing of the modified COS(theta) correction as a function of incidence angle.

Limitations

The following list enumerates some of the limitations and simplifying assumptions inherent in HCE.HTX v2.0. Some items may warrant modification if a more accurate analysis is required:

- The code neglects all conduction effects (axial and radial) in the absorber and envelope. In separate analyses the temperature difference (ΔT) across the glass was calculated in a to be about 4°C, the ΔT across the thickness of the absorber was much smaller.
- The code neglects absorption in the envelope. An independent calculation has shown that inclusion of solar absorption by the glass reduces the temperature difference across the glass by less than 1°C.
- The wind correlation used to determine the convective heat loss of the HCE annulus is for a circular cylinder in cross-flow. This correlation is inadequate for modeling the wind conditions in a parabolic trough solar field. The development of improved wind analyses has been identified as a future task of the overall O&M study.
- The concentrated solar flux that strikes 160° of the outer surface of the absorber is assumed to result in a uniform absorber temperature for calculating heat transfer between the receiver tube and the glass envelope.
- No film temperatures are calculated. The Dittus-Boelter equation, used to calculate the HTF-absorber heat transfer, did not require these quantities. Furthermore, while version 1 of the HCE-HTX code included a provision to switch from the Dittus-Boelter equation to the Sieder-Tate relationship for problems with high ΔT, it was decided that the Dittus-Boelter equation alone would adequately model all expected conditions within the HCE.
- Coded material property data have been partially verified; a few errors may still remain. Based on the material property data that have been examined, interpolation error for all properties and materials is generally less than 2% for temperatures > 0°C. Material property data are summarized in the addendum.

Convergence

Determination of the steady state one dimensional heat transfer of an HCE requires the simultaneous solution to a set of non-linear equations. While this could be achieved through a simultaneous equation solver, the convergence methodology currently employed by the model is based on a simplistic differencing method which requires user-specified exponents in the feedback loops for iteration on both absorber temperature and envelope (glass) temperature. This method could be greatly improved, but to date, has not received attention. Setting the feedback exponents to very small values will generally ensure convergence, but at the expense of longer run time.

In practice, the conditionals included in the HCE-HTX program must often be modified to produce convergence. Convergence problems have been much more prevalent for the second iterative loop (heat gain) since this code section is more sensitive to temperature difference than the heat loss iterative loop ($\Delta T.2 << \Delta T.1$). Sometimes the iterations diverge, other times they set into a recurring pattern which does not satisfy the convergence criterion. A sequence of independent suggestions for dealing with general convergence problems in the HCE.HTX.Analysis[1] subroutine are given below.

Loop 2 convergence problems:

Line #	statement	comment
[125]	X2 = {another value}	change second loop feedback exponent
[123]	{change}	if feedback values are negative
[109]	T.absorber = {another value}	change absorber temperature initial value

[1] The line numbers listed below may vary slightly from those in the current working version of the code.

[116]	DO WHILE Q.difference.2 > {higher value}	loosen loop.2 convergence requirement

Loop 1 convergence problems:

[142]	X1 = {another value}	change 1st loop feedback exponent
[110]	T.absorber = {another value}	change envelope temperature initial value
[137]	WHILE Q.difference.1 > {higher value}	loosen loop.1 convergence requirement

Sample Runs

This section walks through a sample problem, describing the steps required to specify input/output, run the program, and examine output for convergence.

Sample Problem Input (Cermet - No Glass - 15 MPH wind speed)

1) Load MS QuickBasic v. 4.5 (Some problems may be encountered if working with different Basic language software packages)

2) Open HCE-HTX.BAS

3) Edit HCE-HTX.BAS main module to define problem
(statements from lines 101-138 which begin in column 6 are often modified.
The QuickBasic display in the lower right corner of the screen gives the current cursor position as line #:column #, i.e. N 00101:006 = line 101; column 6)

Line #	statement	comment
[101]	print.flag = 3	prints sample 1st loop and all 2nd loop iterations
[109]	output.device$ = "SCRN:"	output to computer screen
[120]	delay.length = .1	slows down output to screen for readability
[118]	case$ = "No Glass - 15 MPH"	define case name
[129-138]	{various}	modify site info, flow, NIP, time as necessary
[178]	FOR xx = 25 to 375 STEP 50	define HTF temperature range

4) Select *HCE.HTX.Set.Up* as the current program item (use the F2 key)

5) Edit the *HCE.HTX.Set.Up* subroutine to complete the problem definition
(statements from lines 28-102 may be modified)

Line #	statement	comment
[35]	evacuated$ = "None"	appropriate for "No Glass" case
[41]	envelope$ = "None"	appropriate for "No Glass" case
[79]	wind.speed = 15 * .44704	set wind speed = 15 MPH; factor converts to m/s

6) RUN (use shift-F5 sequence; use PAUSE key as necessary to examine output)

For "No Glass" cases, the envelope temperature is set equal to the iterative guess for absorber temperature; under "Analysis of HCE Heat Loss Mechanisms," the feedback and evacuated heat transfer terms should be zero. The "HCE Heat Loss derived from Available Insolation - HTF Heat Gain" table shows the results of the second iterative loop. Most convergence problems are easily recognizable from viewing this tabulation — the fifth column, Q.dif, should converge toward a sufficiently small number and exit to the "Summary Results" output section. Suggestions for dealing with convergence and other problems are outlined in section 5.0.

7) If RUN is satisfactory, modify to write summary to file.

Line #	statement	comment
[101]	print.flag = 1	prints summary results only
[109]	output.device$ = "FILE"	output to file
[117]	output.file.name$ = "HTX-6"	assign output file name

8) RUN (shift-F5)

Sample Problem Output (Cermet - No Glass - 15 MPH wind speed, NIP = 940; print.flag = 2)

```
*******************************************************************************
                        HCE Heat Transfer Analysis
*******************************************************************************

CASE: No Glass - Wind = 15                          Site:  Albuquerque, NM
Date of Analysis: 08-12-1993                         Lat:   35.050 N
                                                     Long:  106.620 W
Input Parameters
----------------
   HCE Type:  LS-2
        HTF:  Syltherm 800                          Flow (gpm):  14  ( 10.0%)
   Absorber:  SS - Cermet - as new                 Absorptivity:  .905
                                                Emissivity @ 350C:  .1378
                                                  I.D. / O.D.(mm):  66  /  70
    Annulus:  None                                Pressure (torr):  N.A.
                                                  I.D. / O.D.(mm):  N.A. /  N.A.
   Envelope:  None                                   Absorptivity:  N.A.
                                                  Transmissivity:  N.A.
```

NIP (W/m2)	Solar Date	Hour (PST)	Theta (deg)	POA (W/m2)	Wind Speed (m/s)	Ambnt Temp (F)	Sky Temp (F)
940	06-21-1992	12.0	11.6	920.8	6.7	71.6	57.2

```
*******************************************************************************
```

HCE Heat Loss derived from Available Insolation - HTF Heat Gain

# 2	# 1	T.abs (C)	T.env (C)	Q.dif (W/m)	Qloss.2 /Qloss1	Qloss.1 (W/m)	Qloss.2 (W/m)	Q.gain (W/m)	Q.sun (W/m)	DT.2 (C)	DT.1 (C)
1	1	153	153	678	0.284	947	269	3220	3489	31	131
2	1	148	148	84	0.908	909	825	2663	3489	26	126
3	1	147	147	38	0.958	906	868	2621	3489	25	125
4	1	147	147	18	0.980	905	887	2602	3489	25	125
5	1	147	147	9	0.990	904	896	2593	3489	25	125
6	1	147	147	4	0.995	904	900	2589	3489	25	125
7	1	147	147	2	0.998	904	902	2587	3489	25	125
8	1	147	147	1	0.999	904	903	2586	3489	25	125
9	1	147	147	0	0.999	904	903	2585	3489	25	125
10	1	147	147	0	1.000	904	904	2585	3489	25	125
11	1	147	147	0	1.000	904	904	2585	3489	25	125
12	1	147	147	0	1.000	904	904	2585	3489	25	125

Summary Results No Glass - Wind = 15

Temperatures T,blk (C)	T,abs (C)	T,env (C)	Emiss Abs (1)	Opt Eff (1)	Heat Gain (W/m)	Heat Loss (W/m)	Internal rad (%)	Internal conv (%)	External rad (%)	External conv (%)	HTF flow (gpm)	DT (C)
122	147	147	0.071	0.769	2585	904	0	0	2	98	14	57.0

Validation Runs

This section contains the details of the computer runs that were performed to validate the HCE-HTX model with the experimental data. This comparison is further described in the main body of this report.

Computer runs have also been included for a bare absorber subject to various wind speeds. For these modeled wind cases, wind speed is referenced at the absorber surface and assumes cross flow conditions. Although Sandia conducted numerous tests to examine the relationship between wind speed and HCE heat loss, the parameters monitored during experiment were different than the wind modeling parameters included in the HCE-HTX code. That is, the Sandia wind speed is given by an anemometer located 10 m above ground and 30 m west of the test platform, whereas the HCE model is concerned with the wind velocity at the HCE itself. For this reason, it is not meaningful to present a direct comparison between the Sandia test results and the modeled wind cases. If warranted, the correlation between wind and HCE heat loss may be examined in the future.

HCE-HTX output is provided for the following::

CERMET- FULL SUN CASES (Direct Normal Irradiance = 940 W/m^2)

1) Vacuum annulus (Table 2)
2) Ambient air in annulus (Table 3)
3) Bare annulus (Table 4)

CERMET - NO SUN CASES

1) Vacuum annulus (Table 5)
2) Ambient air in annulus (Table 6)
3) Bare annulus; appended with bare annulus cases with wind = 2, 4, 6, 8, and 10 m/s (Table 7)

Table F-2. CASE: Cermet - Vacuum - No Wind - DNI = 940 W/m^2

****
HCE Heat Transfer Analysis
****

CASE: **Cermet - Vacuum - No Wind**
Date of Analysis: 08-12-1993

Site: Albuquerque, NM
Lat: 35.050 N
Long: 106.620 W

Input Parameters

HCE Type: LS-2
HTF: Syltherm 800
Absorber: SS - Cermet - as new
Annulus: Air
Envelope: Low-Iron Glass - AR

Flow (gpm): 14 (10.0%)
Absorptivity: .905
Emissivity @ 350C: .1378
I.D. / O.D.(mm): 66 / 70
Pressure (torr): 1.000D-04
I.D. / O.D.(mm): 109 / 115
Absorptivity: .02
Transmissivity: .95

NIP (W/m2)	Solar Date	Hour (PST)	Theta (deg)	POA (W/m2)	Wind Speed (m/s)	Ambnt Temp (F)	Sky Temp (F)
940	06-21-1992	12.0	11.6	920.8	0.0	71.6	57.2

****

Summary Results Cermet - Vacuum - No Wind

Temperatures T,blk (C)	T,abs (C)	T,env (C)	Emiss Abs (1)	Opt Eff (1)	Heat Gain (W/m)	Heat Loss (W/m)	Internal rad (%)	Internal conv (%)	External rad (%)	External conv (%)	HTF flow (gpm)	Eff NIP (%)
47	90	19	0.053	0.731	3308	7	96	4	143	-43	14	73.0
97	131	22	0.066	0.731	3298	16	98	2	100	0	14	72.7
147	176	27	0.081	0.731	3281	33	99	1	83	17	14	72.4
197	223	35	0.096	0.731	3252	62	99	1	73	27	14	71.7
247	271	46	0.112	0.731	3206	108	99	1	67	33	14	70.7
297	319	60	0.128	0.731	3138	177	100	0	63	37	14	69.2
347	368	78	0.144	0.731	3038	277	100	0	62	38	14	67.0
397	418	100	0.160	0.731	2898	417	100	0	62	38	14	63.9

Table F-3. CASE: Cermet - Air in Annulus - No Wind - DNI = 940 W/m²

```
****************************************************************************
                    HCE Heat Transfer Analysis
****************************************************************************

CASE: Cermet - Air in Annulus - No Wind          Site:  Albuquerque, NM
Date of Analysis: 08-12-1993                      Lat:    35.050 N
                                                  Long:  106.620 W
Input Parameters
----------------
   HCE Type:  LS-2
        HTF:  Syltherm 800                      Flow (gpm):  14  ( 10.0%)
   Absorber:  SS - Cermet - as new            Absorptivity:  .905
                                         Emissivity @ 350C:  .1378
                                          I.D. / O.D.(mm):   66  /  70
    Annulus:  Air                         Pressure (torr): 6.293D+02
                                          I.D. / O.D.(mm):  109  /  115
   Envelope:  Low-Iron Glass - AR             Absorptivity:  .02
                                            Transmissivity:  .95
```

NIP (W/m2)	Solar Date	Hour (PST)	Theta (deg)	POA (W/m2)	Wind Speed (m/s)	Ambnt Temp (F)	Sky Temp (F)
940	06-21-1992	12.0	11.6	920.8	0.0	71.6	57.2

****

Summary Results   Cermet - Air in Annulus - No Wind

Temperatures T,blk (C)	T,abs (C)	T,env (C)	Emiss Abs (1)	Opt Eff (1)	Heat Gain (W/m)	Heat Loss (W/m)	Internal rad (%)	Internal conv (%)	External rad (%)	External conv (%)	HTF flow (gpm)	Eff NIP (%)
47	89	32	0.052	0.731	3262	53	11	89	75	25	14	71.9
97	131	42	0.066	0.731	3221	94	15	85	68	32	14	71.0
147	175	54	0.081	0.731	3168	146	20	80	64	36	14	69.9
197	222	66	0.096	0.731	3103	211	26	74	63	37	14	68.4
247	269	81	0.111	0.731	3022	293	34	66	62	38	14	66.6
297	318	97	0.127	0.731	2920	395	41	59	62	38	14	64.4
347	366	115	0.143	0.731	2790	524	49	51	63	37	14	61.5
397	416	137	0.159	0.731	2624	690	57	43	64	36	14	57.9

Table F-4. CASE: Cermet - Bare Annulus - No Wind - DNI = 940 W/m^2

```
**************************************************************************
                        HCE Heat Transfer Analysis
**************************************************************************

CASE: Cermet - Bare - No Wind                          Site:  Albuquerque, NM
Date of Analysis: 08-12-1993                            Lat:   35.050 N
                                                       Long:  106.620 W

Input Parameters
----------------
   HCE Type:  LS-2
        HTF:  Syltherm 800                          Flow (gpm):  14  ( 10.0%)
   Absorber:  SS - Cermet - as new                Absorptivity:  .905
                                                Emissivity @ 350C:  .1378
                                                  I.D. / O.D.(mm):   66  /  70
    Annulus:  None                                Pressure (torr):  N.A.
                                                  I.D. / O.D.(mm):  N.A. /  N.A.
   Envelope:  None                                   Absorptivity:  N.A.
                                                    Transmissivity:  N.A.

                                                          Wind     Ambnt      Sky
  NIP      Solar Date      Hour     Theta      POA       Speed     Temp      Temp
 (W/m2)                   (PST)    (deg)     (W/m2)     (m/s)      (F)       (F)
 ------  ------------     -----    -----     ------    ------    ------    ------
   940    06-21-1992      12.0      11.6     920.8       0.0      71.6      57.2

**************************************************************************

Summary Results        Cermet - Bare - No Wind
---------------

   Temperatures    Emiss    Opt     Heat     Heat   Internal   External    HTF    Eff
T,blk T,abs T,env   Abs     Eff     Gain     Loss   rad conv   rad conv   flow   NIP
 (C)   (C)   (C)    (1)     (1)    (W/m)    (W/m)   (%)  (%)   (%)  (%)  (gpm)  (%)
----- ----- -----  -----   -----   -----    -----   ---  ---   ---  ---  ----  ----
  47    91    91   0.053   0.769    3389      100     0    0     7   93    14   74.7
  97   131   131   0.066   0.769    3309      180     0    0     9   91    14   73.0
 147   176   176   0.081   0.769    3209      280     0    0    12   88    14   70.8
 197   222   222   0.096   0.769    3090      399     0    0    16   84    14   68.1
 247   269   269   0.111   0.769    2949      540     0    0    20   80    14   65.0
 297   317   317   0.127   0.769    2780      709     0    0    25   75    14   61.3
 347   365   365   0.143   0.769    2577      912     0    0    31   69    14   56.8
 397   414   414   0.159   0.769    2330     1159     0    0    37   63    14   51.4
```

Table F-5. CASE: Cermet - Vacuum - No Wind - No Sun

```
**************************************************************************
                        HCE Heat Transfer Analysis
**************************************************************************

CASE: Cermet - Vacuum - No Sun/Wind                Site:  Albuquerque, NM
Date of Analysis: 08-12-1993                        Lat:   35.050 N
                                                   Long:  106.620 W

Input Parameters
----------------
   HCE Type:  LS-2
        HTF:  Syltherm 800                          Flow (gpm):  14   ( 10.0%)
   Absorber:  SS - Cermet - as new                Absorptivity:  .905
                                                Emissivity @ 350C:  .1378
                                                  I.D. / O.D.(mm):   66  /  70
    Annulus:  Air                                 Pressure (torr): 1.000D-04
                                                  I.D. / O.D.(mm):  109  /  115
   Envelope:  Low-Iron Glass - AR                   Absorptivity:  .02
                                                  Transmissivity:  .95

                                                            Wind     Ambnt     Sky
 NIP      Solar Date        Hour     Theta      POA        Speed    Temp      Temp
(W/m2)                     (PST)    (deg)     (W/m2)      (m/s)     (F)       (F)
------  ------------      -----    -----     ------      ------   ------    ------
     0  06-21-1992        12.0      11.6       0.0         0.0     71.6      57.2

**************************************************************************
```

Summary Results Cermet - Vacuum - No Sun/Wind

Temperatures T,blk (C)	T,abs (C)	T,env (C)	Emiss Abs (1)	Opt Eff (1)	Heat Gain (W/m)	Heat Loss (W/m)	Internal rad (%)	Internal conv (%)	External rad (%)	External conv (%)	HTF flow (gpm)	Eff NIP (%)
47	47	17	0.050	0.731	-2	2	95	5	307	-207	14	0.0
97	97	19	0.055	0.731	-8	8	97	3	130	-30	14	0.0
147	147	24	0.071	0.731	-21	21	98	2	94	6	14	0.0
197	197	30	0.088	0.731	-45	44	99	1	78	22	14	0.0
247	246	40	0.104	0.731	-82	82	99	1	69	31	14	0.0
297	296	52	0.120	0.731	-141	141	100	0	65	35	14	0.0
347	345	69	0.136	0.731	-225	225	100	0	63	37	14	0.0
397	394	89	0.152	0.731	-344	344	100	0	62	38	14	0.0

Table F-6. CASE: Cermet - Air in Annulus - No Wind - No Sun

```
*************************************************************************
                        HCE Heat Transfer Analysis
*************************************************************************

CASE: Cermet - Air in Annulus - No Sun/Wind     Site:  Albuquerque, NM
Date of Analysis: 08-12-1993                     Lat:   35.050 N
                                                 Long:  106.620 W

Input Parameters
----------------
   HCE Type:  LS-2
        HTF:  Syltherm 800                          Flow (gpm):  14  ( 10.0%)
   Absorber:  SS - Cermet - as new                Absorptivity:  .905
                                                Emissivity @ 350C:  .1378
                                                  I.D. / O.D.(mm):   66  /  70
    Annulus:  Air                                 Pressure (torr): 6.293D+02
                                                  I.D. / O.D.(mm):  109  /  115
   Envelope:  Low-Iron Glass - AR                    Absorptivity:  .02
                                                   Transmissivity:  .95

                                                          Wind      Ambnt      Sky
  NIP      Solar Date      Hour     Theta      POA        Speed     Temp       Temp
 (W/m2)                    (PST)    (deg)    (W/m2)      (m/s)      (F)        (F)
 ------  ------------     -----    -----    ------      ------    ------     ------
     0    06-21-1992      12.0      11.6      0.0         0.0      71.6       57.2

*************************************************************************

Summary Results        Cermet - Air in Annulus - No Sun/Wind
---------------

   Temperatures    Emiss    Opt     Heat     Heat    Internal    External    HTF    Eff
T,blk T,abs T,env  Abs      Eff     Gain     Loss    rad conv    rad conv    flow   NIP
 (C)   (C)   (C)   (1)      (1)    (W/m)    (W/m)   (%)  (%)    (%)  (%)    (gpm)  (%)
-----  -----  -----  -----    -----  -----    -----   ---  ---    ---  ---    ---    ----
  47     47     23   0.050    0.731   -18      18     10   90     97    3      14     0.0
  97     96     34   0.055    0.731   -59      59     11   89     73   27      14     0.0
 147    146     46   0.071    0.731  -110     110     16   84     66   34      14     0.0
 197    195     59   0.087    0.731  -173     173     23   77     64   36      14     0.0
 247    245     73   0.103    0.731  -249     249     30   70     62   38      14     0.0
 297    294     89   0.119    0.731  -342     342     38   62     62   38      14     0.0
 347    343    106   0.135    0.731  -459     459     45   55     62   38      14     0.0
 397    392    126   0.151    0.731  -604     604     53   47     63   37      14     0.0
```

Table F-7. CASE: Cermet - Bare Annulus - Various Wind Speeds - No Sun

****
HCE Heat Transfer Analysis
****

CASE: **Cermet - Bare - No Sun/Wind**
Date of Analysis: 08-12-1993

Site: Albuquerque, NM
Lat: 35.050 N
Long: 106.620 W

Input Parameters

HCE Type: LS-2
HTF: Syltherm 800
Absorber: SS - Cermet - as new
Annulus: None
Envelope: None

Flow (gpm): 14 (10.0%)
Absorptivity: .905
Emissivity @ 350C: .1378
I.D. / O.D.(mm): 66 / 70
Pressure (torr): N.A.
I.D. / O.D.(mm): N.A. / N.A.
Absorptivity: N.A.
Transmissivity: N.A.

NIP (W/m2)	Solar Date	Hour (PST)	Theta (deg)	POA (W/m2)	Wind Speed (m/s)	Ambnt Temp (F)	Sky Temp (F)
0	06-21-1992	12.0	11.6	0.0	0.0	71.6	57.2

****

Summary Results **Cermet - Bare - No Sun/Wind**

Temperatures T,blk (C)	T,abs (C)	T,env (C)	Emiss Abs (1)	Opt Eff (1)	Heat Gain (W/m)	Heat Loss (W/m)	Internal rad (%)	Internal conv (%)	External rad (%)	External conv (%)	HTF flow (gpm)	Eff NIP (%)
47	46	46	0.050	0.769	-28	28	0	0	8	92	14	0.0
97	95	95	0.054	0.769	-109	109	0	0	7	93	14	0.0
147	144	144	0.071	0.769	-208	208	0	0	10	90	14	0.0
197	194	194	0.087	0.769	-324	324	0	0	14	86	14	0.0
247	243	243	0.103	0.769	-459	459	0	0	18	82	14	0.0
297	291	291	0.119	0.769	-617	617	0	0	23	77	14	0.0
347	340	340	0.134	0.769	-802	802	0	0	28	72	14	0.0
397	388	388	0.150	0.769	-1022	1022	0	0	34	66	14	0.0

Table F-7. CASE: Cermet - Bare Annulus - Various Wind Speeds - No Sun (Continued)

Bare Annulus: WIND = 2 m/s

Temperatures T,blk (C)	T,abs (C)	T,env (C)	Emiss Abs (1)	Opt Eff (1)	Heat Gain (W/m)	Heat Loss (W/m)	Internal rad (%)	Internal conv (%)	External rad (%)	External conv (%)	HTF flow (gpm)	Eff NIP (%)
47	45	45	0.050	0.769	-83	83	0	0	3	97	14	0.0
97	93	93	0.054	0.769	-250	251	0	0	3	97	14	0.0
147	142	142	0.070	0.769	-421	421	0	0	5	95	14	0.0
197	191	191	0.086	0.769	-598	598	0	0	7	93	14	0.0
247	239	239	0.102	0.769	-785	786	0	0	10	90	14	0.0
297	288	288	0.117	0.769	-992	992	0	0	14	86	14	0.0
347	336	336	0.133	0.769	-1230	1230	0	0	18	82	14	0.0
397	384	384	0.149	0.769	-1498	1499	0	0	22	78	14	0.0

Bare Annulus: WIND = 4 m/s

Temperatures T,blk (C)	T,abs (C)	T,env (C)	Emiss Abs (1)	Opt Eff (1)	Heat Gain (W/m)	Heat Loss (W/m)	Internal rad (%)	Internal conv (%)	External rad (%)	External conv (%)	HTF flow (gpm)	Eff NIP (%)
47	45	45	0.050	0.769	-122	123	0	0	2	98	14	0.0
97	91	91	0.053	0.769	-371	371	0	0	2	98	14	0.0
147	139	139	0.069	0.769	-623	623	0	0	3	97	14	0.0
197	188	188	0.085	0.769	-880	880	0	0	5	95	14	0.0
247	236	236	0.100	0.769	-1144	1144	0	0	7	93	14	0.0
297	284	284	0.116	0.769	-1420	1421	0	0	9	91	14	0.0
347	332	332	0.132	0.769	-1715	1715	0	0	12	88	14	0.0
397	379	379	0.147	0.769	-2031	2031	0	0	16	84	14	0.0

Bare Annulus: WIND = 6 m/s

Temperatures T,blk (C)	T,abs (C)	T,env (C)	Emiss Abs (1)	Opt Eff (1)	Heat Gain (W/m)	Heat Loss (W/m)	Internal rad (%)	Internal conv (%)	External rad (%)	External conv (%)	HTF flow (gpm)	Eff NIP (%)
47	44	44	0.050	0.769	-153	153	0	0	1	99	14	0.0
97	90	90	0.053	0.769	-465	465	0	0	1	99	14	0.0
147	137	137	0.068	0.769	-782	782	0	0	2	98	14	0.0
197	185	185	0.084	0.769	-1103	1103	0	0	4	96	14	0.0
247	233	233	0.100	0.769	-1429	1429	0	0	5	95	14	0.0
297	281	281	0.115	0.769	-1766	1766	0	0	7	93	14	0.0
347	328	328	0.131	0.769	-2116	2116	0	0	10	90	14	0.0
397	375	375	0.146	0.769	-2485	2485	0	0	12	88	14	0.0

Table F-7. CASE: Cermet - Bare Annulus - Various Wind Speeds - No Sun (Concluded)

Bare Annulus: WIND = 8 m/s

Temperatures T,blk (C)	T,abs (C)	T,env (C)	Emiss Abs (1)	Opt Eff (1)	Heat Gain (W/m)	Heat Loss (W/m)	Internal rad (%)	Internal conv (%)	External rad (%)	External conv (%)	HTF flow (gpm)	Eff NIP (%)
47	43	43	0.050	0.769	-178	178	0	0	1	99	14	0.0
97	89	89	0.052	0.769	-544	544	0	0	1	99	14	0.0
147	136	136	0.068	0.769	-917	917	0	0	2	98	14	0.0
197	183	183	0.083	0.769	-1293	1293	0	0	3	97	14	0.0
247	231	231	0.099	0.769	-1674	1674	0	0	4	96	14	0.0
297	278	278	0.114	0.769	-2062	2063	0	0	6	94	14	0.0
347	325	325	0.130	0.769	-2462	2462	0	0	8	92	14	0.0
397	371	371	0.145	0.769	-2876	2876	0	0	10	90	14	0.0

Bare Annulus: WIND = 10 m/s

Temperatures T,blk (C)	T,abs (C)	T,env (C)	Emiss Abs (1)	Opt Eff (1)	Heat Gain (W/m)	Heat Loss (W/m)	Internal rad (%)	Internal conv (%)	External rad (%)	External conv (%)	HTF flow (gpm)	Eff NIP (%)
47	43	43	0.050	0.769	-200	200	0	0	1	99	14	0.0
97	88	88	0.052	0.769	-614	614	0	0	1	99	14	0.0
147	134	134	0.067	0.769	-1036	1036	0	0	2	98	14	0.0
197	181	181	0.083	0.769	-1462	1463	0	0	3	97	14	0.0
247	229	229	0.098	0.769	-1892	1892	0	0	4	96	14	0.0
297	276	276	0.114	0.769	-2327	2327	0	0	5	95	14	0.0
347	323	323	0.129	0.769	-2771	2771	0	0	7	93	14	0.0
397	368	368	0.144	0.769	-3225	3225	0	0	9	91	14	0.0

Model Uses

The HCE model can be used to examine the effect of various operating conditions on the effectiveness of an HCE. In an operating SEGS plant, this knowledge will then permit a trade-off analysis comparing the cost of HCE repair or replacement against the cost of loss revenues if no repair is carried out.

Figures F-2 through F-4 have been generated to illustrate the effects of several parameters. The reference case for all the plots is an LS-3 HCE with a new cermet selective surface (ε = 0.14 at 350°C) and full vacuum in the annulus (i.e., 10^{-4} torr). The plots show the effect on thermal efficiency of higher emissivities, of a degradation in vacuum level within the annulus, and of the presence of different gases in an HCE with lost vacuum (i.e., at 1 atmosphere pressure). The vacuum level in Figure F-3 has been given in atmospheres in order to compare to ambient pressure (for reference, 10^{-4} torr = 1.31 10^{-7} atmospheres).

References

Dudley, V. E. and Lindsey R. Evans, *Test Results: Industrial Solar Technology Solar Collector,* Draft report, To be published.

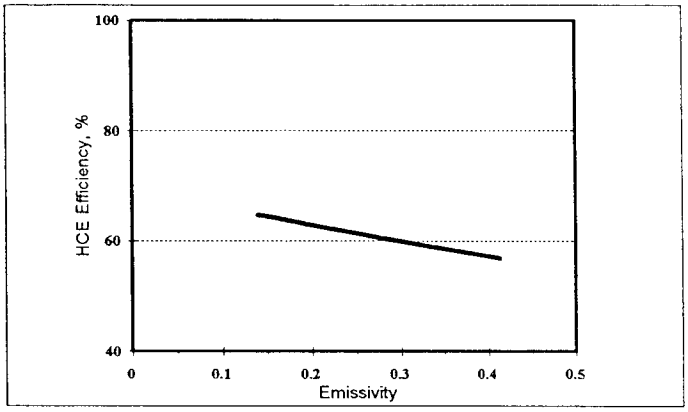

Figure F-2. Effect of emissivity on efficiency of an HCE.

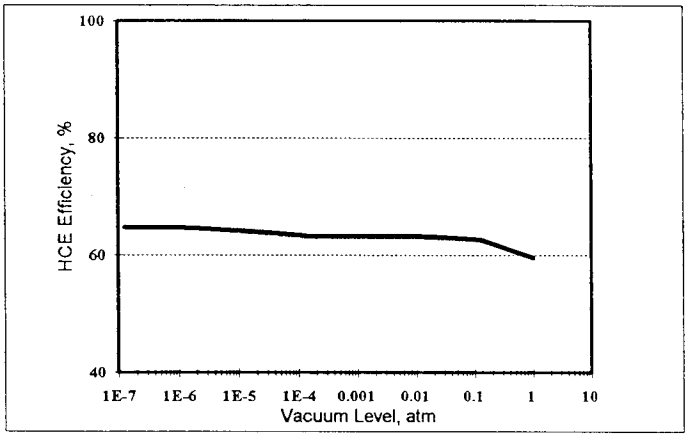

Figure F-3. Effect of vacuum on efficiency of an HCE.

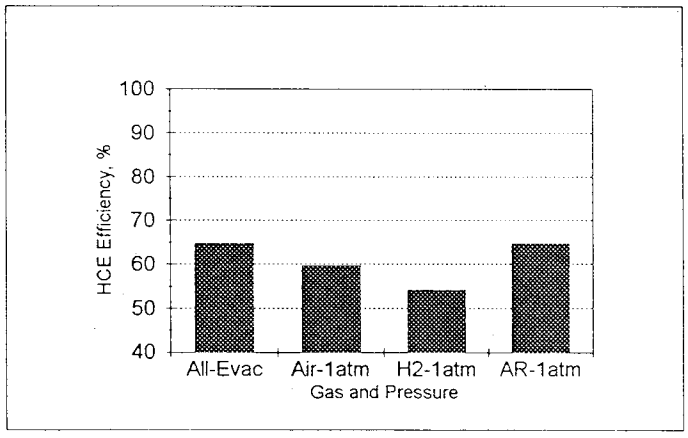

Figure F-4. Efficiency of an HCE with different gases.

Attn: David Hagen
134 Kitchener Street
Garran, ACT 2605, AUSTRALIA

3M - Solar Optics Program
Attn: Paul Jaster
3M Center
Building 225-2N-06
St. Paul, MN 55144-1000

Acurex Corporation
Attn: Hans Dehne
555 Clyde Avenue
Mountain View, CA 94039

Acurex Corporation
Attn: John Schaeffer
555 Clyde Avenue
Mountain View, CA 94039

Advanced Thermal Systems
Attn: Dave Gorman
7600 East Arapahoe Road, Suite 215
Englewood, CO 80112

Arizona Public Service Co.
Attn: Scott McLellan
P.O. Box 53999
MS 1424
Phoenix, AZ 85072-3999

Australian National University
Attn: Stephen Kaneff
R. S. Phy. Sc
Energy Research Centre
Canberra, ACT 2601, AUSTRALIA

Bechtel National, Inc.
Attn: Pat DeLaquil
50 Beale Street
50/15 D8
P.O. Box 193965
San Francisco, CA 94119-3965

Bechtel National, Inc.
Attn: Stuart Fry
50 Beale Street
50/15 D8
P.O. Box 193965
San Francisco, CA 94119-3965

Bechtel National, Inc.
Attn: Bruce Kelly
50 Beale Street
45/26 D8
P.O. Box 193965
San Francisco, CA 94119-3965

Bureau of Reclamation
Attn: Stanley Hightower
Code D-3710
P.O. Box 205007
Denver, CO 80225

California Energy Commission
Attn: Alec Jenkins
Energy Technology Development Div. R&D Office
1516 9th Street
MS-43
Sacramento, CA 95814-5512

California Polytechnic State University
Attn: William B. Stine
Department of Mechanical Engineering
3801 West Temple Avenue
Pomona, CA 91768-4062

Carrizo Solar Corporation
Attn: John Kusianovich
P.O. Box 10239
1011-C Sawmill Road NW
Albuquerque, NM 87184-0239

Central and Southwest Services
Attn: E.L. Gastineau
1616 Woodall Rogers Freeway
MS 7RES
Dallas, TX 75202

Daggett Leasing Corporation
Attn: Bill Ludlow
35100 Santa Fe St.
P.O. Box 373
Daggett, CA 92327

Daggett Leasing Corporation
Attn: Wayne Luton
35100 Santa Fe St.
P.O. Box 373
Daggett, CA 92327

Daggett Leasing Corporation
Attn: Eric Wills
35100 Santa Fe St.
P.O. Box 373
Daggett, CA 92327

DEO Enterprises
Attn: Dave Ochenrider
P.O. Box 2110
Helendale, CA 92342

DLR
Attn: Berthold Obeile
Pfaffenwaldring 38-40
7000 Stuttgart 80, GERMANY

DLR - Cologne, MD-ET
Attn: Manfred Becker
Linder Hohe
P.O. Box 90 60 58
D5000
Koln 90, GERMANY

DLR - Cologne, MD-ET
Attn: Klaus Hennecke
Linder Hohe
P.O. Box 90 60 58
D5000
Koln 90, GERMANY

Electric Power Research Institute
Attn: Doug Morris
P.O. Box 10412
3412 Hillview Avenue
Palo Alto, CA 94303

Electric Power Research Institute
Attn: J. Schaeffer
P.O. Box 10412
3412 Hillview Avenue
Palo Alto, CA 94303

Flachglas Solartechnik GmbH
Attn: M. Geyer
Theodor-Heuss-Ring 1
5000 Koln 1, GERMANY

Florida Solar Energy Center
Attn: Library
300 State Road, Suite 401
Cape Canaveral, FL 32920-4099

Idaho Power
Attn: Jerry Young
P.O. Box 70
Boise, ID 83707

Industrial Solar Technology
Attn: Randy Gee
5775 W. 52nd Avenue
Denver, CO 80212

Institute of Gas Technology
Attn: Library
34245 State Street
Chicago, IL 60616

Jenna Baskets
Attn: Dick Holl
1938 A Avenita Del Oro
Oceanside, CA 92056

Kearney & Associates
Attn: David W. Kearney (5)
14022 Condessa Drive
Del Mar, CA 92014

KJC Operating Company
Attn: Gilbert Cohen (5)
41100 Highway 395
Boron, CA 93516

Kramer Junction Company
Attn: Stuart Lawson
900 19th St. NW
Suite 600
Washington, DC 20006

Los Angeles Dept. of Water and Power
Attn: Daryll Yonamine
Alternate Energy Systems
111 North Hope Street, Rm. 661A
Los Angeles, CA 90012

McDonnell-Douglas Astronautics Co.
Attn: Bob Drubka
5301 Bolsa Avenue
Huntington Beach, CA 92647-2048

Ministry of Non-Conventional Energy Sources
Attn: S.K. Gupta
Block No. 14
CGO Complex
Lodhi Road
New Delhi, 110003 INDIA

Ministry of Non-Conventional Energy Sources
Attn: R.S. Sharma
Block No. 14
CGO Complex
Lodhi Road
New Delhi, 110003 INDIA

Ministry of Non-Conventional Energy Sources
Attn: Narendra Singh
Block No. 14
CGO Complex
Lodhi Road
New Delhi, 110003 INDIA

National Renewable Energy Laboratory
Attn: M. Bohn
1617 Cole Blvd.
Golden, CO 80401-3393

National Renewable Energy Laboratory
Attn: Hank Price (2)
1617 Cole Blvd.
Golden, CO 80401-3393

National Renewable Energy Laboratory
Attn: Tim Wendelin
1617 Cole Blvd.
Golden, CO 80401-3393

National Renewable Energy Laboratory
Attn: Tom Williams
1617 Cole Blvd.
Golden, CO 80401-3393

Nevada Power Co.
Attn: Eric Dominguez
P.O. Box 230
Las Vegas, NV 89151

Plataforma Solar de Almeria
Attn: Manuel Sanchez
Aptdo. 7
Tabernas
Almeria, E-04200 SPAIN

Power Kinetics, Inc.
Attn: W.E. Rogers
415 River Street
Troy, NY 12180-2822

Renewable Energy Training Institute
Attn: Kevin Porter
122 C St. NW, Suite 520
Washington, DC 20001

Rockwell International Corp.
Attn: Bob Musica
Energy Technology Engineering Center
P.O. Box 1449
Canoga Park, CA 91304

Rockwell International Corp.
Attn: Bill Wahl
P.O. Box 7922
6633 Canoga Avenue
Canoga Park, CA 91309-7922

Sacramento Municipal Utility District
Attn: Bud Beebee
Generation Systems Planning
Power Systems Dept.
6201 'S' St.
P.O. Box 15830
Sacramento, CA 95852-1830

Sacramento Municipal Utility District
Attn: Don Osborne
Generation Systems Planning
Power Systems Dept.
6201 'S' St.
P.O. Box 15830
Sacramento, CA 95852-1830

Salt River Project
Attn: Bob Hess
Research and Development
P.O. Box 52025
Phoenix, AZ 85072-2025

Salt River Project
Attn: Ernie Palomino
Research and Development
P.O. Box 52025
Phoenix, AZ 85072-2025

Schlaich, Bergermann & Partner
Attn: W. Schiel
Hohenzollernstr. 1
D-7000 Stuttgart 1, GERMANY

Science Applications International Corp.
Attn: Kelly Beninga
15000 W. 6th Avenue
Suite 202
Golden, CO 80401

Science Applications International Corp.
Attn: Barry L. Butler
Room 2043, M/S C2J
10260 Campus Point Dr.
San Diego, CA 92121

Science Applications International Corp.
Attn: Dave Smith
15000 W. 6th Avenue
Suite 202
Golden, CO 80401

Sloan Engineering
Attn: Michael Sloan
4306 Ramsey Ave.
Austin, TX 78756

Solar Energy Industries Association
Attn: Ken Sheinkopf
122 C Street, NW
4th Floor
Washington, DC 20001-2109

Solar Energy Industries Association
Attn: Scott Sklar
122 C Street., NW
4th Floor
Washington, DC 20001-2109

Solar Kinetics, Inc.
Attn: Gus Hutchinson
10635 King William Drive
P.O. Box 540636
Dallas, TX 75354-0636

Solel Solar Systems, Ltd.
Attn: Har Hotzvim
Science-Based Park
P.O. Box 23577
Jerusalem, 91234 ISRAEL

South Coast AQMD
Attn: Ranji George
21865 Copley Drive
Diamond Bar, CA 91765

Southern California Edison Co.
Attn: Mark Skowronski
P.O. Box 800
2244 Walnut Grove Avenue
Rosemead, CA 91770

Southern California Edison Co.
Attn: Paul Sutherland
P.O. Box 800
2131 Walnut Grove Avenue
Rosemead, CA 91770

Spencer Management Associates
Attn: Byron J. Washom (5)
P.O. Box 724
Diablo, CA 94528-0724

U.S. Department of Energy
Attn: Dan Alpert
2140 L Street, #709
Washington, DC 20037-1530

U.S. Department of Energy
Attn: R. (Bud) Annan (2)
Code EE-13
Forrestal Building
1000 Independence Ave. SW
Washington, DC 20585

U.S. Department of Energy
Attn: Gary Burch (5)
Code EE-132
Forrestal Building
1000 Independence Avenue, SW
Washington, DC 20585

U.S. Department of Energy
Attn: Bob Martin
Golden Field Office
1617 Cole Boulevard
Golden, CO 80401

UC Operating Services
Attn: Dianne Mathis
43880 Harper Lake Road
Hinkley, CA 92347

Union of Concerned Scientists
Attn: Donald Aitken
20100 Skyline Boulevard
Woodside, CA 94062

University of Houston
Attn: Lorin Vant-Hull
Energy Laboratory 5505
4800 Calhoun Road
Houston, TX 77004

University of Nevada at Las Vegas
Attn: Bob Boehm
Dept. of Mech. Engr.
4505 Maryland Parkway
P.O. Box 454027
Las Vegas, NV 89154-4027

Weizmann Institute of Science
Attn: Michael Epstein
P.O. Box 26
Rehovot, 76100 ISRAEL

Weizmann Institute of Science
Attn: Doron Lieberman
P.O. Box 26
Rehovot, 76100 ISRAEL

Zentrum f. Sonnenenergie-und Wasserstoff-Forschung
Attn: Lippke
P.O. Box 801149
Stuttgart, D-705111 GERMANY

Zentrum f. Sonnenenergie-und Wasserstoff-Forschung
Attn: Rheinlander
P.O. Box 801149
Stuttgart, D-705111 GERMANY

Internal Distribution:

MS 0100 (2)	Document Proc. for DOE/OSTI, 7613-2 (2)
MS 0619	Technical Publications, 12613
MS 0702	D.E. Arvizu, 6200
MS 0703	J.R. Anderson, 6216
MS 0703	C.E. Andraka, 6216
MS 0703	C.W. Bennett, 6216
MS 0703	R.B. Diver, 6216
MS 0703	L.R. Evans, 6216
MS 0703	D.R. Gallup, 6216
MS 0703	G.J. Kolb, 6216 (10)
MS 0703	F. Lippke, 6216
MS 0703	T.R. Mancini, 6216
MS 0703	D.F. Menicucci, 6216
MS 0703	J.B. Moreno, 6216
MS 0703	T.A. Moss, 6216
MS 0703	J.E. Pacheco, 6216
MS 0703	M.R. Prairie, 6216
MS 0703	C.E. Tyner, 6216
MS 0704	P.C. Klimas, 6201
MS 0724	D.L. Hartley, 6000
MS 0899	Technical Library, 13414 (5)
MS 1127	J.M. Chavez, 6215
MS 1127	V.E. Dudley, 6215 (2)
MS 1127	Library, 6215 (5)
MS 1127	A.R. Mahoney, 6215
MS 1127	C.W. Matthews, 6215
MS 9014	S. Faas, 5371
MS 9018	Central Technical Files, 8523-2
MS 9402	S. Goods, 8714
MS 9403	B. Bradshaw, 8716